

**ACTIN ORGANIZATION AT INTRACELLULAR
MEMBRANES: TARGETING AND REGULATORY
INTERACTIONS OF THE SPIR/FORMIN ACTIN
NUCLEATOR COMPLEX**

DISSERTATION

zur

Erlangung des akademischen Grades eines Doktors

Doctor rerum naturalium

(Dr. rer. nat.)

vorgelegt der

Mathematisch-Naturwissenschaftlichen Fakultät
der Technischen Universität Dresden

von

Janine Tittel

geboren am 26.07.1984 in Dresden

Dresden, 2014

Gutachter

Prof. Petra Schwille

Prof. Gerhard Rödel

Abstract

Cell biological processes such as migration, proliferation and vesicle transport rely on the organization of the actin cytoskeleton. Important regulators of the actin cytoskeleton are the actin nucleation factors, which initiate the polymerization from actin monomers into filaments. These can be classified into 3 classes: the Arp2/3 complex, formins, and WH2-domain containing nucleators. The class of WH2-domain containing actin nucleators was introduced by the discovery of Spir proteins a decade ago. Spir proteins localize to vesicular structures and form a regulatory complex with the distinct actin nucleators of the formin subgroup. However, the mechanism of targeting and regulation of the Spir/formin complex is almost unknown. Previous sequence studies disclosed a modified FYVE domain at the C-terminus of Spir, which, together with the adjacent Spir-box, mediates the targeting to vesicles in living cells. In this work, it was found that the Spir FYVE domain's membrane binding properties differ from those of canonical FYVE domains. In contrast to canonical FYVE domains, Spir FYVE domains lack phosphatidylinositol-3-phosphate specificity and bind to negatively charged phospholipids with nanomolar affinity, but without preference for a distinct lipid. Also, the Spir FYVE domain occurs in the cytosol as a monomer, while the canonical FYVE-domain is known to dimerize. Nevertheless, just as in the canonical case, a hydrophobic turret-loop is involved in membrane binding, which was observed both in living cells and on artificial membranes.

Furthermore, this work shows that the FYVE domain does not only act as a typical membrane binding domain, but additionally functions as a protein-protein-interaction module. A hitherto unknown intramolecular interaction, which is released upon membrane binding of the C-terminal Spir-2-FYVE domain and the N-terminal Spir-2-KIND domain, was discovered. Competition experiments revealed overlapping interfaces of

the cis-regulatory Spir-2 KIND/FYVE complex and the trans-regulatory Spir-KIND/Fmn-FSI complex. These findings indicate that Spir proteins are regulated by an intramolecular complex that prevents cytoplasmic assembly of the Spir/formin complex. This autoregulatory complex is released upon membrane binding and allows Fmn-FSI to bind to Spir-KIND, establishing the functional Spir/formin actin nucleator complex only on the membrane.

Although a role for Spir actin nucleators in vesicle transport processes of the exocytotic pathway and the transport beyond early endosomes has been described, the function and regulation of Spir in vesicle transport processes are still not well understood, and were addressed in this work. It was shown that Spir-2 acts as an effector of the GTPase Arf1, where, unconventionally, Spir-2 preferentially binds to the GDP-bound form of Arf1. Also, a direct and strong interaction between Spir-2 and the motor protein myosin Vb was revealed, which is mediated by the linker region of Spir-2 and the myosin Vb tail. In this way, Spir-2 is targeted to the vesicle membranes.

To summarize, these results support a model in which the Arf1-GTP organized rigid clathrin coat on vesicles dissociates via hydrolysis of Arf1-GTP to Arf1-GDP, and a dynamic Spir-2/actin/myosin Vb complex is formed on vesicles. By binding of formin, the Spir/formin complex is assembled and polymerizes actin filaments. Myosin Vb moves along these filaments and generates forces which pull protrusions out of the vesicles. These protrusions can then reach and connect to the microtubule network for fast long-range vesicle transport.

Zusammenfassung

Viele zellbiologische Prozesse, wie Zellmigration, Proliferation und Vesikeltransport, beruhen auf der Organisation des Aktin-Zellskeletts. Zu den wichtigen Regulatoren des Aktin-Zellskeletts gehören die Aktinnukleatoren, welche die Polymerisation der Aktinmonomere in Filamente einleiten. Diese lassen sich in 3 Gruppen einordnen: der Arp2/3 Komplex, die Formine und die WH2 Domänen-enthaltenden Aktinnukleatoren. Spir prägte als erstes Mitglied die neue Gruppe der WH2 Domänen-enthaltenden Aktinnukleatoren. Spir ist an vesikulären Strukturen lokalisiert und bildet einen regulatorischen Komplex mit einem weiteren Aktinnukleator aus der Gruppe der Formine. Der Mechanismus der Membranbindung und Regulation des Spir/Formin-Komplexes ist weitgehend unbekannt. Frühere Sequenzstudien zeigten auf, dass Spir-Proteine eine modifizierte FYVE-Domäne am C-Terminus aufweisen, welche zusammen mit der anliegenden Spir-Box-Domäne die Membranbindung an intrazellulären Vesikeln in lebenden Zellen vermittelt. In dieser Arbeit wurde gezeigt, dass die Spir FYVE-modifizierte Domäne, im Gegensatz zur klassischen FYVE-Domäne, keine Spezifität für Phosphatidylinositol-3-Phosphat aufweist, sondern ohne weitere Spezifität für ein bestimmtes Lipid mit nanomolarer Affinität an negativ geladene Phospholipide bindet. Außerdem zeigte sich, dass die Spir FYVE-modifizierte Domäne als Monomer im Cytosol vorliegt, während die klassische FYVE-Domäne bekanntlich dimerisiert. Jedoch ist wie bei der klassischen Domäne eine hydrophobe Loop-Region an der Membranbindung beteiligt, was sowohl an artifiziellen Membranen, als auch in lebenden Zellen untersucht wurde.

Des Weiteren wurde entdeckt, dass die FYVE-Domäne offenbar nicht nur eine typische Membranbindungsdomäne ist, sondern zusätzlich auch als Protein-Protein-Interaktionsmodul fungiert. Eine bis dato unbekannte intramolekulare Interaktion zwischen der C-terminalen

Spir-FYVE Domäne und der N-terminalen Spir-KIND Domäne wurde entdeckt, welche durch die Bindung an die Membran aufgelöst wird. Konkurrenzexperimente zeigten überlappende Bindungsflächen des cis-regulatorischen Spir-2-KIND/FYVE-Komplexes und des trans-regulatorischen Spir-2-KIND/Fmn-FSI Komplexes auf. Diese Resultate deuten darauf hin, dass Spir-Proteine in einem intramolekularen Komplex vorliegen, der den zytoplasmatischen Aufbau des Spir/Formin-Komplexes verhindert. Dieser autoregulatorische Komplex wird jedoch durch Membranbindung aufgelöst und ermöglicht die Bindung von Formin, wodurch ein funktioneller Spir/Formin Aktin-Nukleotorkomplex nur an der Membran ausgebildet wird.

Obwohl schon früher beschrieben wurde, dass Spir sowohl in exozytotischen Vesikelprozessen als auch im Vesikeltransport zwischen den frühen Endosomen eine Rolle spielt, sind der Mechanismus und die Regulation von Spir in Vesikeltransportprozessen bisher noch nicht ausreichend gut verstanden, und wurde näher in dieser Arbeit untersucht. Zunächst wurde gezeigt, dass Spir-2 als Effektorprotein von Arf1 fungiert, wobei Spir unkonventionellerweise an die GDP-gebundene Form von Arf1 bindet. Zudem wurde eine starke und direkte Interaktion zwischen Spir-2 und dem Motorprotein Myosin Vb gezeigt, welche durch die Linker-Region von Spir-2 und der Schwanzregion von Myosin Vb vermittelt wird. Dadurch wird Spir-2 an Vesikelmembranen rekrutiert.

Zusammenfassend unterstützen die gefundenen Ergebnisse ein Modell, bei dem eine von Arf1-GTP organisierte rigide Clathrin-Hülle an den Vesikeln durch Hydrolyse des Arf1-GTP zu Arf1-GDP dissoziiert, wodurch ein dynamischer Spir-2/Aktin/Myosin Vb Komplex aufgebaut wird. Der durch die zusätzliche Bindung von Formin entstandene Spir/Formin-Komplex initiiert die Bildung von Aktinfilamenten. Myosin Vb gleitet entlang der Aktinfilamente und generiert dabei Kräfte, um Ausstülpungen aus den Vesikeln herauszuziehen, die in Kontakt mit Mikrotubuli treten, und dabei einen schnellen, weitreichenden Vesikeltransport einleiten.

Table of contents

Abstract	i
Zusammenfassung	iii
1 Introduction	1
1.1 Actin	2
1.2 Actin nucleation factors	3
1.2.1 Arp 2/3 complex.....	4
1.2.2 Formins	4
1.2.3 WH2 domain containing actin nucleation factors	6
1.3 The actin nucleation factor Spir	6
1.3.1 Domain structures of the Spir-family	7
1.3.2 Spir/formin cooperation.....	9
1.3.3 Spir function.....	10
1.3.3.1 Spir function in vesicle processes.....	11
1.4 Regulation of vesicle transport processes	11
1.4.1 The Ras Superfamily	11
1.4.1.1 The Rab GTPase family.....	12
1.4.1.2 The Arf GTPase family	12
1.4.2 Myosin Superfamily	13
1.4.3 Rab11a/Myosin Vb cooperation.....	14
1.5 Biomembranes.....	15
1.5.1 Functions and structure of cellular membranes	15
1.5.2 Membrane-binding domains.....	16
1.5.3 Model membrane systems	17
1.6 Fluorescence-based techniques.....	18
1.6.1 Principle of Fluorescence.....	18
1.6.2 Fluorescence Correlation Spectroscopy (FCS).....	19
1.6.3 Fluorescence Cross-Correlation Spectroscopy (FCCS).....	22
1.6.4 Fluorescence Lifetime Imaging/ Förster Resonance Energy Transfer (FLIM/FRET).....	23
2 Aim of the work.....	25

3	Material and Methods	27
3.1	Reagents	27
3.2	DNA constructs	27
3.3	Protein Expression and Purification	27
3.3.1	Expression and purification of Spir-2 variants	27
3.3.2	Expression and purification of myristoylated Arf1	28
3.4	Labeling of the proteins	29
3.5	Gel electrophoresis and Western Blot	30
3.6	GST-Pulldown assay	31
3.7	Preparation of model membranes	32
3.7.1	Lipids used in this study	32
3.7.2	Giant Unilamellar Vesicles (GUVs)	33
3.7.3	Large Unilamellar vesicles (LUVs)	33
3.8	LUV Flootation assay	33
3.9	Electrochemiluminescence immunoassay (EIA)	34
3.10	Cell Culture	35
3.11	Cell seeding and transfection	35
3.12	Confocal Laser scanning microscopy	36
3.13	FCS and FCCS Data Acquisition	36
3.14	FCS and FCCS Data Analysis	37
3.14.1	<i>In vitro</i> FCS and FCCS	37
3.14.2	<i>In vivo</i> FCS and FCCS	38
3.14.3	Titration of HisAcGFP-Spir-2-CT and Spir-2-KIND*Alexa ⁶⁴⁷	39
3.15	FLIM-FRET	40
3.16	Statistical analysis	40
4	Results	41
4.1	Characterization of membrane binding of Spir-2	41
4.1.1	Preface	41
4.1.2	Characterization of the membrane binding domains of Spir-2	43
4.1.3	Characterization of the phospholipid interactions of Spir-2	45
4.1.4	Spir-2 is a monomer in the cytosol	49
4.2	Cis-regulatory interactions of Spir-2	51
4.2.1	Preface	51
4.2.2	Identification of an intramolecular Spir-2-interaction	53
4.2.3	Quantification of the intramolecular Spir-2-interaction	55

4.2.4	Membrane binding regulates the intramolecular Spir-2 interaction	57
4.2.5	Fmn-2-eFSI regulates the intramolecular Spir-2 interaction	59
4.3	Trans-regulatory interactions of Spir-2	61
4.3.1	Spir interacts with Arf1 protein.....	61
4.3.2	Spir-Arf1 interaction does not influence their binding properties	63
4.3.3	Spir-2 interacts with myosin Vb	66
4.3.4	Spir-2 linker region mediates the interaction with myosin Vb-tail	72
5	Discussion	75
5.1	Spir-2 possesses a FYVE-related domain.....	75
5.2	Spir-2-FYVE domain is a protein-protein interaction module	77
5.3	Spir-2 is regulated by an intramolecular complex	78
5.4	Spir-2 is an unconventional effector protein of Arf1	84
5.5	Spir-2/myosin Vb interaction regulates vesicle processes	86
6	Future directions	93
7	Bibliography.....	95
8	Appendix.....	109
8.1	List of constructs	109
9	Abbreviations	113
10	Symbols.....	116
11	Acknowledgements.....	117
12	Declaration	119

1 Introduction

“Imagine this Nobel Prize Award Ceremony without any of the beautiful flowers that you can see here around me. These flowers are transported to Stockholm each year from Sanremo in Italy. But imagine if they were missorted and ended up in Copenhagen. Without a functioning transport system, this could easily be a reality. To avoid chaos, we are totally dependent on fine-tuned transport systems, where cargo is loaded into the right vehicle and transported to the right destination at the right time.”¹

In 2013 the Nobel Prize for physiology was awarded to Dr. James E. Rothman, Dr. Randy W. Schekman and Dr. Thomas C. Südhof for their discoveries of the machinery regulating vesicle traffic, the essential transport system in cells. In contrast to prokaryotic cells, eukaryotic cells are compartmentalized in a highly complex way, which improves the efficiency of many cellular processes and protects the cell from dangerous freely roaming molecules. Cells are able to organize complex routing of molecules packaged in vesicles with high specificity and precision to many intracellular destinations as well as to the outside of the cell. Cells are filled with plenty of traveling vesicles, which need to be organized and guided into the right direction. Special motor proteins attach to the cargo vesicle and carry them along filaments and tubes of the cytoskeleton, like trucks on a highway. Without a precise organization and a functional transport system the cells would end up in chaos (1,2).

¹ Excerpt from the Award Ceremony Speech. "The 2013 Nobel Prize in Physiology or Medicine - Presentation Speech" Nobelprize.org Nobel Media AB 2013. Web.26 Apr 2014 http://www.nobelprize.org/nobel_prizes/medicine/laureates/2013/presentation-speech.html

1.1 Actin

Functional cells need to organize themselves and be able to mechanically interact with their environment. To be capable of changing their shape, migrating and arranging their internal structures, cells build up a force generating system of filaments, called cytoskeleton. The cytoskeleton is divided into 3 types of filaments: *Intermediate filaments* for providing mechanical strength, *Microtubules* for positioning organelles and for intracellular transport and *Actin filaments* for determining cell shape and motility (3). The dynamic assembly and disassembly of actin filaments and associated motor proteins of the myosin family generate forces that drive many cellular processes such as migration, vesicular transport and cell division (4,5). The assembly of the 42 kDa globular actin monomers (G-actin) into double stranded helical filaments (F-actin) is highly regulated to control the high concentration of actin monomers in cells. As all actin subunits face the same direction, actin filaments are polar with a dynamic, fast-growing “barbed” end (+ end) and a less active, slow-growing “pointed” end (- end) (6). The actin monomer possesses two binding sites, one for the actin-binding proteins and one for ATP and its associated Mg^{2+} . The ATP-bound actin monomers associate to the barbed end, whereas ADP-bound actin monomers dissociate from the pointed end. This process, called actin filament treadmilling, and the resulting dynamics are caused by ATP hydrolysis due to the enzymatic activity of actin, which regulates the transition between G-actin and F-actin (7,8). However, the assembly of actin dimers and trimers in the initial nucleation phase is kinetically unfavourable due to their instability and impairs spontaneous actin nucleation. In cells the large pool of actin monomers is buffered by actin monomer binding proteins such as profilin. To overcome the kinetic barrier of actin nucleation, actin nucleation factors are required (5,9).

1.2 Actin nucleation factors

To date actin nucleation factors are divided into three major groups: the Arp 2/3 complex, the Formin superfamily and the novel group of nucleation factors containing one or multiple WH2 domains (**Figure 1.1**).

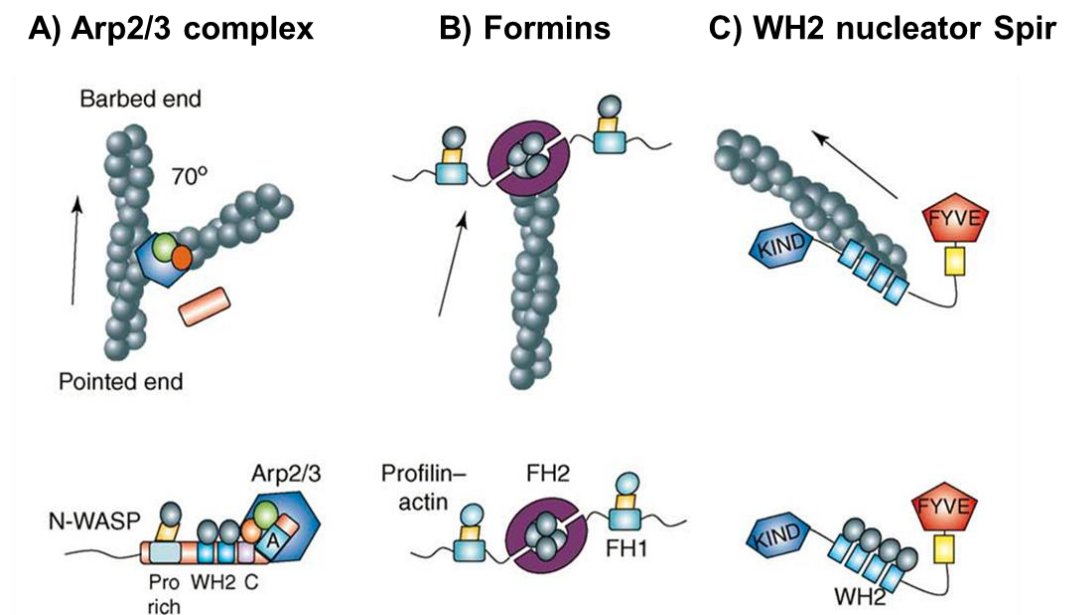


Figure 1.1: Actin nucleation factors

(A) The Arp2/3 complex is a seven-subunit complex, which becomes activated by binding of nucleation-promoting factors such as N-WASP. The proteins Arp2 (orange circle) and Arp3 (green circle) mimic an actin dimer and thereby overcome the kinetic barrier to actin nucleation (10). The Arp2/3 complex binds to the side of preexisting filaments and nucleates new actin filament branches at an angle of 70° (11) (B) Formins contain the formin homology 1 (FH1) domain and formin homology 2 (FH2) domain at the C-terminus. FH1 domain binds Profilin-actin and the FH2 domain forms a ring-like dimer structure, in which each FH2 domain binds two actin monomers (12). Formins remains associated as a dimer with the barbed end of the actin filament (13). (C) Spir as a member of the WH2 nucleator contains a cluster of four WH2 domains to bind four actin monomers. In contrast to the Arp2/3 complex, Formin and Spir proteins nucleate unbranched actin filaments. Picture adapted from (14).

1.2.1 Arp 2/3 complex

The Arp 2/3 complex together with its multiple nucleation promoting factors (NPFs) nucleates a branched network of actin filaments of various cellular structures (8,15). The Arp 2/3 complex contains 7 subunits and its activity is locally increased by nucleation promoting factors (NPFs). Major activators are the Wiskott-Aldrich-syndrome protein (WASP) family (16) which act mainly at the plasma membrane and are linked to dorsal ruffles (WAVE1), lamellipodia (WAVE2) as well as filopodia and podosomes (WASP, N-WASP) (17). More recently discovered activators are WASH, acting in endosome trafficking, WHAMM, functioning in ER-Golgi transport and Golgi-organization and the poorly characterized JMY functioning in cell motility and as regulator of neuritogenesis (18-20).

1.2.2 Formins

Formins are large multidomain proteins that form homodimers. They are named after the mouse *limb deformity* (*ld*) gene, the first formin gene identified (21). While the Arp 2/3 nucleates branched actin filaments, formin nucleates unbranched, linear filaments and beyond that, sustains the barbed-end elongation (22). Formins contain a highly conserved formin homology 2 (FH2) domain and an adjacent prolin rich formin homology 1 (FH1) domain (23). Through phylogenetic analyses of the FH2 domain formins are classified into eight groups: Dia (diaphanous), DAAM (disheveled-associated activator of morphogenesis), FMNL (formin like protein), FHOD (formin homology domain containing protein), WHIF (WH2 domain containing formin), INF (inverted formin), Delphilin and Fmn (formin) (23,24). The FH2 domain binds to the barbed end of actin filaments and moves processively to elongate or depolymerize these barbed ends, whereas the FH1 domain influences the FH2 function via binding to profilin. Profilin provides the cellular pool of ATP-actin for new filament assembly by accelerating the exchange of ADP to ATP on Actin (25). But the FH2 domain is sufficient for actin nucleation and the FH1 domain stimulates filament elongation. While the mechanism for

FH2-mediated actin nucleation is uniform for all formins, the regulation of their activity differs among the formin families and even for individual orthologues within a specific family (26).

Many formins are regulated by the formation of an auto-inhibited complex in the cytosol and must be activated by specific ligands. The best studied mechanism of regulation is the autoinhibitory interactions of the N- and C-terminal halves in Diaphanous-related formin (DRFs), including Dia, DAAM, FRL formins in mammals and Bni1, Bnr1 and SepA in yeast. As pictured in **Figure 1.2**, the Diaphanous auto-regulatory domain (DAD) is located at the C-terminus, adjacent to the FH1-FH2 module. At the N-terminus, the regulatory region encompasses the GTPase binding domain (GDB), Diaphanous inhibitory domain (DID), the dimerization domain (DD) and a coiled-coil region (CC). The C-terminal DAD domain binds to the N-terminal GDB-DID domain, which impedes the actin polymerization activity of the FH2 domain. The auto-inhibition is mediated by the DAD-DID interaction which keeps the protein 'inactive' until a Rho GTPase binds to the GTPase binding domain and disrupts the intramolecular interaction (12,27,28). DID shows a weak binding and inhibition to the isolated FH2 domain, which is extremely increased in the presence of DAD mediating a high-affinity binding to DID. Thus, the DAD functions as an affinity-enhancing motif for auto-inhibition (29).

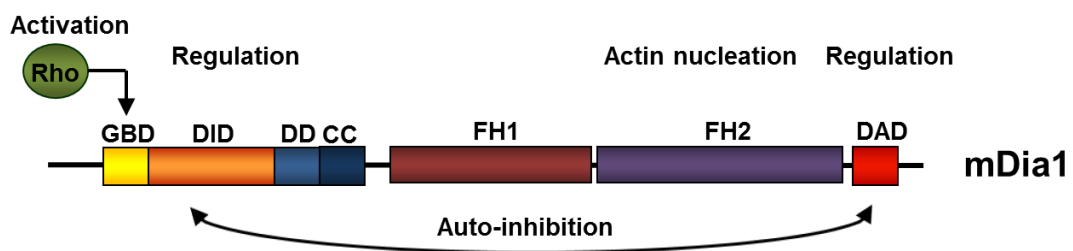


Figure 1.2: Auto-regulation of mDia1

Structural and functional domains of mDia1. Abbreviations: GBD: GTP-binding region necessary for RhoA binding; DID, Diaphanous inhibitory domain; DD, dimerization domain; CC, coiled coil; FH1, formin homology 1 domain; FH2, formin homology 2 domain; DAD, Diaphanous autoinhibitory domain; GDB, GTP-binding domain; picture modified from (22).

Besides the GTPase mediated activation two further mechanisms to regulate the auto-inhibition have been reported. Competitive binding of effector proteins to the DAD domain and DAD modification such as phosphorylation have been shown to open the intramolecular interaction. For WHIF2 formins even a substrate-based regulation has been described, where the autoinhibition has been shown to be sensitive to the concentration of actin. WHIF2 formins contain the actin-binding domain WH2 and actin binding releases the auto-inhibited state. Consequently, the actin acts on the one hand as a competitive binder, and on the other hand as a substrate for actin filament elongation (26).

1.2.3 WH2 domain containing actin nucleation factors

The novel group of actin nucleators is hallmarked by one or multiple Wiskott-Aldrich syndrome protein (WASP) homology 2 domains (WH2) for actin nucleation. Cordon-blue (Cobl), Leiomodin (Lmod) and Spire are the best-studied members of the new group, which serve distinct cellular functions and employ different molecular mechanisms (30). Cobl contains three WH2 domains and fulfills functions in neuritogenesis and dendritic branching, whereas Lmod possesses only one WH2 domain and plays a crucial role in muscle sarcomere assembly (31,32).

1.3 The actin nucleation factor Spir

Vertebrate genomes encode two *spir* genes, *spir-1* and *spir-2*, whereby the corresponding proteins Spir-1 and Spir-2 share a high degree of homology, especially within the conserved domain structures (**Figure 1.3A**). The sea squirt *Ciona Savignyi* and *Drosophila melanogaster* each encode one *spir* gene, *posterior end mark-5* with the corresponding protein pem-5 for the sea squirt, and the *Drosophila* gene *dSpir* where the corresponding protein has two isoforms: p150-Spir and Spir-short (33). Spir proteins have been exclusively identified in metazoans. No *spir* genes have been found in plants and single cell organisms such as yeast.

1.3.1 Domain structures of the Spir-family

Spir proteins encode a cluster of four **WH2 domains** (WH2-A,B,C,D) in the central region which are connected through three conserved linker regions (L-1, L-2 and L-3). WH2-C, WH2-D and L-3 form a stabilized actin dimer to which WH2-B and WH2-A later add the third and fourth actin monomer to form a longitudinal tetramer (**Figure 1.3B**). After formation of the complete nucleus, fast polymerization proceeds (34).

All Spir proteins contain the **KIND domain** at the N-terminus, which was named due to sequence similarity to the C-lobe of the protein kinase fold (35). Spir proteins possess the entire C-lobe without the essential catalytic residues, naming the region Kinase non-catalytic C-lobe domain. Hence, in Spir the KIND domain evolved from a functional kinase and turned into a protein-protein interaction module, which mediates the interaction with formin proteins (36).

Spir proteins localize to intracellular membrane structures which is attributed by the C-terminal located **modified FYVE domain** and the adjacent **Spir-Box (SB)**. The Spir-Box is highly conserved among Spir proteins of different species and shares sequence homology with a α -helical domain of rabphilin-3A, which mediates the interaction of rabphilin-3A with the GTP-bound form of the GTPase Rab3A (37).

The FYVE zinc finger domain is a widespread protein-lipid interaction module, which is named after the first four proteins in which it was found: **Fab1p**, **YOTB**, **Vac1p** and **EEA1** (38). The zinc finger is a small structural motif in several proteins, characterized by particular sequences of cysteines that coordinate bound zinc ions. The zinc ions are structurally crucial, and avoid the need of a hydrophobic core by nucleating the protein structure (39). The FYVE domain contains eight cysteines coordinating two zinc ions. Moreover, FYVE domains are characterized by a specificity to phosphatidylinositol-3-phosphate (PI(3)P) and contain a hydrophobic ‘turret loop’ which penetrates the lipid bilayer (38,40). However, the Spir FYVE domain lacks the basic consensus

sequence, which mediates the specific binding to PI(3)P, suggesting that Spir proteins feature different phospholipid binding properties. Furthermore, the Spir FYVE domain has a loop insertion between cysteine 6 and 7. Thereby, the Spir FYVE domain represents a modified version of the canonical FYVE domains.

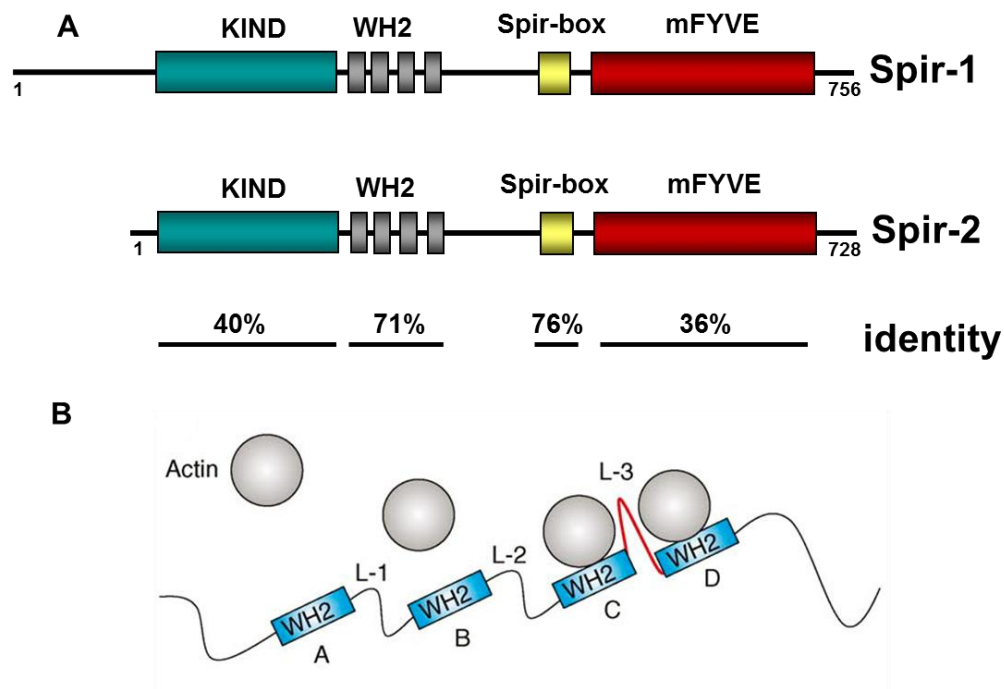


Figure 1.3: The actin nucleator Spir

(A) Domain architecture of Spir-1 and Spir-2. The conserved regions share a high similarity. The KIND domain acts as a protein-protein-interaction module and the four WH2 domains function for actin nucleation. The Spir-Box and modified FYVE domain mediate the localization to intracellular membranes. Picture modified from (41) **(B)** Mechanism of actin nucleation by Spir proteins. The domains WH2-C and WH2-D bind two actin monomers to form an initial actin dimer, which is stabilized by the linker 3 region (red). Subsequently two further actin monomers bind to WH2-B and WH2-A to form a trimer and tetramer. Picture adapted from (14).

1.3.2 Spir/formin cooperation

Spir proteins were discovered in a screen for female sterile mutants in *Drosophila melanogaster* (42). The *spire* gene affects both the dorsal-ventral and anterior-posterior axes of the *Drosophila* egg and embryo. In the same genetic screen a second mutant with an identical phenotype to *spire* was found - *cappuccino*. The Cappuccino protein is an actin nucleation factor of the formin family. During *Drosophila* oogenesis the two distinct actin nucleators work in concert to organize an ooplasmic actin mesh, which represses premature microtubule-based cytoplasmic streaming. During early to middle oogenesis (stage 5-10A), the actin mesh suppresses kinesin-dependent motility, which allows the formation of a polarized microtubule cytoskeleton. Once the polarization factors are correctly targeted to the oocyte cortex, the actin mesh is disassembled at stage 10B and relieves the inhibition of kinesin-dependent organelle movement and activates rapid ooplasmic streaming (43). A direct interaction of Cappuccino and Spir was revealed by biochemical approaches (44,45).

The interaction of the mammalian homologs Spir-1, Spir-2 with formin-1 (Fmn-1), formin-2 (Fmn-2) was characterized by biochemical and crystallography studies (36,46). The interaction is mediated by an acidic cluster of the KIND domain at the N-terminus of Spir and basic residues at the C-terminal end of the FMN formin, which was then named the formin-Spir-interaction (FSI) motif (36,45,46). It was shown that both Spir proteins, Spir-1 and Spir-2 are able to interact with both formins, Fmn-1 and Fmn-2, with nanomolar affinity (36). *In vitro* pyrene actin polymerization assays found an inhibition of the formin nucleation activity, but an enhanced Spir nucleation activity by the Spir/formin complex formation (44). The formin FH2 dimer binds two KIND domains to form a hetero-tetrameric complex (44), where a 1:1 ratio of KIND:FSI complex formation was seen in the crystal structure, indicating a possible dimerization of Spir, which is still an open question (45,46).

A further functional cooperation in mammals has been found by gene expression analysis of *spir-1* and *formin-2* during mouse

embryogenesis and in adult mouse tissues (47). *Spir-1* and *formin-2* are highly expressed in the oocytes, testis, in the developing nervous system and neuronal cells of the adult nervous system (47,48).

Later, the first mechanistic evidence for the Spir/formin cooperation in mammals came from studies in mouse oocytes. In these, an actin-dependent mechanism of long-range vesicle transport was uncovered which is driven by the cooperation of Spir-1, Spir-2 with formin-2 to nucleate an actin network from Rab11-positive vesicles to connect the vesicles with each other and the plasma membrane. In a myosin Vb-dependent manner the vesicles moves along their own tracks to converge and reach the plasma membrane (49). Later, a vesicle-based mechanism of actin network modulation by clustering Spir and formin proteins was described to drive the asymmetric spindle positioning of the meiotic spindle in mouse oocytes, which is a vital step for mammalian reproduction (50).

1.3.3 Spir function

Both *spir* genes, *spir-1* and *spir-2*, are highly expressed in mouse oocytes, testis and brain. *Spir-2* displays a much broader expression pattern than *spir-1*. *Spir-1* is mainly found in the nervous system, whereas *spir-2* is expressed in the digestive tracts as well (41). Recently generated *spir-1* mutant mice have been found to show enhanced fear expression (51). Furthermore, a crucial role of Spir proteins in the dendrite patterning has been reported, which is important for neurons to receive sensory and synaptic input. Spir has been identified as a Lola effector in *Drosophila* involved in motor axon guidance (52). Lola (Longitudinals Lacking), as a transcription factor in *Drosophila*, controls the expression of Spir as an actin nucleator and thus shapes the dendrite architecture. It does so by controlling the formation of branches and the abundance and spatial arrangement of F-actin in those branches (53). A connection of Spir-1 to human disease was found by detecting anti-Spir-1 antibodies in the blood sera of human breast cancer patients. The reason of the immunoreactivity against Spir-1 has not been found yet (54).

1.3.3.1 Spir function in vesicle processes

The FYVE domain of Spir proteins, which target Spir proteins to vesicular structures, is a domain typically found in proteins involved in membrane trafficking (55,56). Spir proteins have been found to colocalize with the small G-protein Rab11, which is located at the trans-Golgi network, post-Golgi vesicles and recycling endosomes (57,58). A possible role for Spir-1 in the endocytic pathways has been described, where dynamic actin patches on early endosomes depends on Annexin A2 and Spir-1, which interact with each other. By knocking-down the *spir-1* gene, the transport of dextran to late endosomes and the formation of actin patches on early endosomes was inhibited (59). Furthermore, a role in the secretory pathways has been reported, where a N-terminal truncated variant Spir-1-CT, lacking the KIND and WH2 domains, inhibits the transport of vesicular stomatitis virus G protein (VSV G) to the plasma membrane (57).

1.4 Regulation of vesicle transport processes

1.4.1 The Ras Superfamily

The Ras superfamily of small guanosine triphosphatases (GTPases) is divided into five major subfamilies: Ras, Rho, Rab, Ran and Arf. The Ras family proteins function as monomeric G proteins (60). The function of the small G proteins is based on the same mechanism. They act as GDP/GTP-regulated molecular switches, which cycle between two distinct states, the GTP bound state and the GDP bound state. In general, the GTP bound conformation represents the active state and allows high affinity interactions with their effector proteins (61). GTPases exhibit high-affinity binding for GTP and GDP and show low intrinsic GTP hydrolysis as well as GDP/GTP exchange activities. The low intrinsic nucleotide exchange activity of the GDP-bound GTPase is increased by interaction with Guanine nucleotide exchange factors (GEFs). Membrane associated GTPases are recruited to the membrane in

the GTP-bound state. Due to GTP hydrolysis, the GTPase is inactivated and redistributed to the cytosol. The low intrinsic GTP hydrolysis rate is accelerated by GTPase-activating proteins (GAPs), which are recruited from the cytosol by active GTPases. Thus, the activity of the GTPase relies on the interplay of the GEFs and GAPs, which are triggered by interactions with regulatory proteins (62).

1.4.1.1 The Rab GTPase family

The Rab family was first described as Ras-like proteins in brain and is the largest family within the Ras superfamily. In humans the Rab family comprises more than 60 members (63). In the GTP bound form the Rab proteins recruit effector proteins to the membrane to regulate vesicle formation, membrane fusion and actin- and tubulin-dependent vesicle movement. Some Rab proteins are expressed ubiquitously and others are tissue-specific (64). Within cells Rab proteins localize to intracellular membranes to function as membrane organizers, compartment identifiers and regulators of specific intracellular traffic pathways (65). The membrane localization is mediated by a posttranslational modification of a cysteine motif, which carries one or two geranylgeranyl groups (64).

Rab11 exists in three isoforms in mammals: Rab11a, Rab11b and Rab11c (also known as Rab25). Rab11a is ubiquitously expressed, whereas Rab11b expression is restricted to brain, heart, testis and Rab25 occurs in lung, kidney and the gastric tract (66,67). Rab11 is localized to the trans-Golgi network (TGN), post-Golgi vesicles and recycling endosomes and is involved in endocytic, exocytic and lysosomal pathways (64,68).

1.4.1.2 The Arf GTPase family

Members of the ADP ribosylation factor (Arf) GTPases family are involved in membrane trafficking by regulating the cytoskeleton dynamics and recruitment of coat proteins. Originally, Arf proteins were named after their function as cofactors for cholera-toxin-catalysed ADP-ribosylation of the α -subunit of heterotrimeric G proteins. Later they were found to regulate membrane trafficking pathways. All Arf proteins

are myristoylated at the second glycine of the N-terminus, which is important for their membrane localization. Mammalian genome encodes six members of Arf proteins which can be classified into three groups based on amino-acid sequence identity: class I (Arf1, Arf2, Arf3), class II (Arf4, Arf5) and class III (Arf6) (69). Arf1 and Arf6 are the best characterized Arf proteins. Arf1 regulates the secretory pathways from the Golgi apparatus to the endoplasmatic reticulum (ER) and between Golgi cisternae by the recruitment of the coat protein complex I (COPI) to budding vesicles. In addition, Arf1 regulates the formation of clathrin-coated vesicles on the trans-Golgi network (TGN) and endosomes by recruitment of the heterotetrameric adaptor protein complex (AP-1, AP-3 and AP-4) and Golgi-localized γ -ear-containing Arf-binding proteins (GGA). Arf6 localizes to the plasma membrane and endosomal compartments, where it plays a role in clathrin-mediated endocytosis and actin remodeling at the cell surface (70).

1.4.2 Myosin Superfamily

Eukaryotic cells use molecular motors to transport and distribute organelles. Motor proteins are divided into three groups: kinesins, dyneins and myosins. In general, long-range transport is mediated by the microtubule-dependent motors kinesin and dynein and short-range transport by the actin-based motor protein myosin. The myosin superfamily is a large and diverse superfamily, which is separated into at least 35 classes (71).

Myosin V belongs to the group of unconventional myosins, in contrast to the conventional myosin II, which is essential for muscle contraction. There are three isoforms in mammals: myosin Va, myosin Vb and myosin Vc (72). In general, myosins are composed of three domains: The motor domain or head, which binds ATP and actin, is connected to the α -helical neck domain and the tail domain, which can contain a coiled-coil structure for dimerization. The two-headed motor allows the molecule to walk along the actin filaments by alternating the positions of the leading and trailing heads. Whereas the catalytic heads share

conserved elements, the tail regions of various classes are highly diverse. Specific regions in the tail domain are able to undergo interactions with adaptors and other binding proteins to fulfill the distinct cellular functions (71-73). One important connection is the interaction of myosin V with members of the Rab family through adaptor proteins.

1.4.3 Rab11a/Myosin Vb cooperation

Myosin V motor proteins have been implicated in organelle tethering and organelle transport along actin filaments. To ensure the selection of the right specific vesicle or organelle, Rab proteins have been identified as important regulators of myosin V recruitment. Myosin Vb has been found to be involved in the plasma membrane recycling system. A direct interaction of the myosin Vb tail, lacking the motor domain, with all members of the Rab11 family (Rab11a, Rab11b and Rab25) has been identified (74). Furthermore, the recycling of the G-protein-coupled receptors (GPCRs) has been shown to be mediated through a Rab11a/myosin Vb pathway (75). In addition, myosin Vb has been shown to interact with the Rab11 effector protein FIP2. FIP2 belongs to the family of Rab11 interacting proteins and binds specifically to the GTP-bound form of Rab11. FIP2 is assumed to act as an adaptor protein to stabilize the Rab11/myosin Vb interaction within the ternary Rab11/FIP2/myosin Vb complex (76). Recently, myosin Vb has been discovered to be associated to schizophrenia in the Chinese Han population (77). Myosin Vb is enriched in the hippocampus (78) and the Rab11/FIP2/myosin Vb plays a role in synaptic AMPA receptor trafficking during neuronal signaling. The ternary Rab11/FIP2/myosin Vb complex is required for the AMPA receptor insertion, the dendritic spine growth and hence for the synaptic long-term potentiation (79).

1.5 Biomembranes

1.5.1 Functions and structure of cellular membranes

Cells are literally packed with membranes. In humans, which composed of 10^{14} cells, the total surface of membranes has to be estimated to cover an area of 100 km² (80). This amount is justified by the fact that cell membranes possess several important functions in cells. First and foremost, the plasma membrane presents a selective barrier to the outside of the cell, enabling the cell to gather nutrients from the environment, retaining the products it synthesizes for its own use and excreting its waste products. Furthermore, cells are highly compartmentalized to improve the efficiency of many cellular processes. There are a number of intracellular membranes creating barriers to define different organelles. The two main constituents of membranes are proteins and lipids. Lipid molecules constitute about 50% of the mass of the most animal cell membranes, where the most abundant membrane lipids are the phospholipids. Phospholipids have a polar headgroup and two hydrophobic hydrocarbon tails, usually fatty acids of different lengths (3). The lipids in the membrane are arranged into a bilayer which is 3-5 nm thick. The cell membranes vary in the lipid and proteins compositions to gain characteristic functional properties. The lipid composition of membranes is highly complex, since besides the variations of the head groups, hydrocarbon tails and desaturation of the phospholipids, membranes contain also structurally distinct minor lipids such as inositol phospholipids. Inositol phospholipid can undergo reversible phosphorylation at multiple sites on the inositol head group. They occur only in small amounts in some membranes, but fulfill crucial functions in membrane trafficking and cell signaling (3).

1.5.2 Membrane-binding domains

Membrane proteins can be associated with the membrane in different ways. Besides transmembrane proteins, where hydrophobic regions pass through the membrane, other membrane proteins are located in the cytosol and can associate with the cytosolic side of the lipid bilayer. Association of protein with membranes is essential for various cellular functions such as membrane anchoring of the cytoskeleton, membrane traffic and signaling. These proteins contain globular domains which either bind highly specifically by stereospecific recognition of particular membrane components or non-specifically to a general physical property of the membrane such as charge, amphiphilicity or curvature (81). At least 11 membrane-binding domains have been identified. For membrane binding they use to a different extent a combination of specific headgroup recognition, delocalized electrostatic interactions with negatively charged phospholipids and penetration into the hydrophobic milieu. The **PH (pleckstrin homology) domain** specifically binds to phosphatidylinositols, especially PIP(3,4,5)P₃ and PIP(3,4)P₂ (82), While the **C1 domain**, named after the first region of protein kinase C (PKC), is a zinc finger, the **C2 domain**, named after the second region of PKC, is a 8-stranded antiparallel β -sandwich. C1 domains bind to diacylglycerol and phorbol ester and some C2 domains can bind Ca²⁺ and phosphatidylserin. Like C1, **FYVE domains** are zinc finger domains which contain two zinc-ions and a conserved basic motif (RR/KHHCR) which specifically binds to PI(3)P. Furthermore, **PX (Phox-homology) domains** are widespread and usually bind to the preferred lipid PI(3)P, but some members prefer PI(3,4)P₂ or PI(4,5)P₂. **ENTH** and **ANTH** (Epsin N-terminal homology and AP180 N-terminal homology) domains comprise superhelical folds which can bind all phosphoinositides, preferentially PI(4,5)P₂ (39). Besides membrane-binding domains, there are many basic and amphipathic sequences, often with covalent lipid modifications, involved in membrane targeting (83).

1.5.3 Model membrane systems

Artificial model membrane systems provide an important tool for the investigation of the properties of cellular membranes, the functions of membrane proteins and membrane-binding proteins and lipid-lipid interactions. In model membranes, the chemical composition as well as the environment can be easily controlled. Due to their reduced complexity, they allow the determination of parameters of membrane functions which are difficult to investigate in highly complex native membranes. An artificial lipid bilayer can be made by synthetic and natural lipids of one or several types. There are various types of model membranes systems (84). Liposomes are the most commonly used model membrane systems. They are water-filled vesicles, which can be multi- and unilamellar and can differ in sizes. Whereas **large unilamellar vesicles (LUVs)** have a size of 100-1000 nm, **small unilamellar vesicles (SUVs)** are 20-50 nm in diameter and have a very large curvature. **Giant unilamellar vesicles (GUVs)** have a diameter on the order of 1-300 μm . Thus, they can be observed by confocal microscopy. GUVs are suitable systems for studying membrane deformations such as tubulation by specific proteins (85,86). **Supported-lipid bilayers (SLBs)** are planar bilayers which are deposited on a support, such as glass or mica. The support can also contain holes to obtain free-standing membranes (87). They can be used for imaging by total internal reflection fluorescence microscopy, atomic force microscopy and confocal microscopy combined with fluorescence correlation spectroscopy. Moreover, **nanotubes** can be pulled from vesicles, which are about 100-300 nm in diameter. They are attractive for studying protein-membrane interactions, where membrane fission and fusion are involved (88). **Lipid monolayers** are one of the first model membrane systems. The lipids, which spread at the water-air interface, form a one-molecule thick layer over the surface, where the hydrophilic headgroup of the molecule faces the water phase and the hydrophobic tail sticks out to the air. (84).

1.6 Fluorescence-based techniques

1.6.1 Principle of Fluorescence

Fluorescence is the emission of a photon which occurs as a result of molecule relaxation from an electronically excited state to the ground state. The main way of excitation is the absorption of light, but molecules can be also excited by thermal and chemical energy. The process of fluorescence is usually depicted in the Jablonski diagram (**Figure 1.4**). Upon absorption of light, the molecule goes from a singlet ground state (S_0) to a higher electronic state (S_1 or S_2) in 10^{-15} s. At each electronic state the molecule can exist in a number of vibrational energy levels, denoted as 0, 1 and 2. The molecule is usually excited to some higher vibrational level of S_1 or S_2 . By vibrational relaxation and internal conversion the molecule relaxes to the lowest vibrational level of S_1 within 10^{-13} s. From there the molecule returns to the ground state S_0 under emission of a photon in 10^{-8} s. This process is called fluorescence and the corresponding relaxation time fluorescence lifetime. The energy of the emission is less than the energy of the absorption, which leads to a shift of the fluorescence emission to longer wavelengths. This so-called Stokes-shift enables the separation of the emitted light from the excitation light by dichroic mirrors. Molecules in the S_1 state can also undergo a spin conversion to the first triplet state T_1 , which is called intersystem crossing, and occurs with a much lower probability than fluorescence. In this case, the molecule returns from T_1 into the ground state S_0 under emission of a photon within more than 10^{-4} s, a longer lifetime than fluorescence, which is called phosphorescence (89).

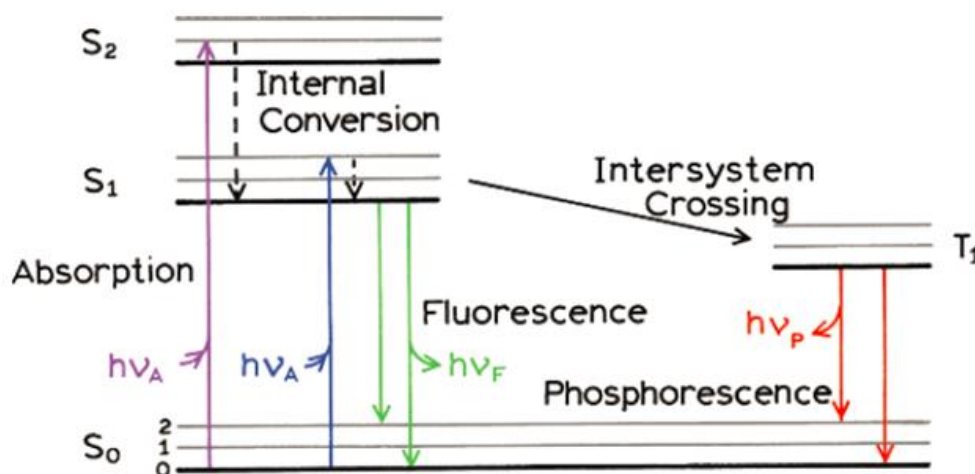


Figure 1.4: Jablonski diagram. Adapted from (89).

1.6.2 Fluorescence Correlation Spectroscopy (FCS)

Fluorescence correlation spectroscopy (FCS) is a highly sensitive and versatile technique to study the dynamics and interactions of fluorescently labelled molecules in solution and in living cells. The standard FCS setup consists of an inverted microscope equipped with a high numerical aperture objective, dichroic mirrors, emission filters, excitation lasers and single-photon sensitive detectors, so called avalanche photodiodes (APDs). FCS provides accurate information about diffusion coefficients, concentrations, molecular brightness and molecular interactions. For FCS measurements the laser focus is positioned to the area of interest such as the membrane or solution. The emitted fluorescence of the diffusing molecules is collected by the objective. The fluorescent light is then separated from the excitation light by dichroic mirrors and emission filters and focused through a pinhole. The pinhole confines the detection volume. The fluorescence signal F is detected for a certain time by a sensitive photo detector, which give rise to a fluctuating intensity trace $F(t)$. Fluorescence intensity fluctuations can be caused by diffusion of the molecules through the observation volume or by fluorescence brightness changes of the molecules due to chemical reactions or photophysical processes (90). FCS performs statistical analysis of the fluctuations. Thus, it correlates a signal at a certain time t

with the same signal after a lag time $t + \tau$ and takes the temporal average. Thus, the self-similarity of the signal in time is tested to generate a temporal decay function of average fluctuations, which is represented by the autocorrelation function (Eq. 1.1), where the fluorescence intensity $F(t)$ is the sum of the average fluorescence $\langle F \rangle$ and their fluctuations $\delta F(t)$ (Eq. 1.2), and $\langle \rangle$ denotes the temporal average and τ the lag time.

$$G(\tau) = \frac{\langle \delta F(t) \cdot \delta F(t + \tau) \rangle}{\langle F(t) \rangle^2} \quad (1.1)$$

$$F(t) = \langle F \rangle + \delta F(t) \quad \text{with} \quad \langle F \rangle = \frac{1}{t_{meas}} \int_0^{t_{meas}} F(t) dt \quad (1.2)$$

The experimental autocorrelation curve is fitted to an appropriate mathematical model to obtain important values of diffusion time, concentration and molecular brightness. The basic mathematical models for fitting the autocorrelation curves for the molecules diffusing in 3D (solution) or in 2D (membranes) are the following models:

$$G_{3D}(\tau) = \frac{1}{N} \cdot \frac{1}{1 + \frac{\tau}{\tau_D}} \cdot \frac{1}{\sqrt{1 + \frac{\tau}{S^2 \tau_D}}} \quad (1.3)$$

$$G_{2D}(\tau) = \frac{1}{N} \cdot \frac{1}{1 + \frac{\tau}{\tau_D}} \quad (1.4)$$

$$S = \frac{\omega_z}{\omega_0} \quad (1.5)$$

S is the structural parameter, which describes the ratio of axial ω_z and radial ω_0 dimensions of the detection volume.

Most fluorescent dyes exhibit blinking dynamics from a bright to a dark state due to intersystem crossing. In particular, they show an increased long-lived triplet state, which can be seen in an additional shoulder in the correlation curve for lag times in the μs range. Thus, the

fluorescent molecules can be divided into a fluorescent fraction and a non-fluorescent fraction T in the dark triplet state with an average duration of $\tau_{triplet}$.

$$G_{triplet} = 1 + \frac{T}{1-T} e^{-\frac{\tau}{\tau_{triplet}}} \quad (1.6)$$

Since the triplet blinking is much faster and independent from the diffusion time of the molecule, the autocorrelation function is multiplied by this fraction.

$$G_{3D+T}(\tau) = G_{triplet}(\tau) \cdot G_{3D} \quad (1.7)$$

$$G_{2D+T}(\tau) = G_{triplet}(\tau) \cdot G_{2D} \quad (1.8)$$

By a proper calibration of the optical setup, using a dye with a known diffusion coefficient, the dimensions ω_0 and ω_z of the detection volume are obtained, which are used to acquire the diffusion coefficient and concentration of labeled molecules from the number of particles N and the effective volume V_{eff} in solution or the effective area A_{eff} in the membrane.

$$D = \frac{\omega_0^2}{4\tau_D} \quad (1.9)$$

$$G(0) = \frac{1}{N} \quad (1.10)$$

$$V_{eff} = \pi^{\frac{3}{2}} \omega_0^2 \omega_z \quad (1.11)$$

$$A_{eff} = \pi \omega_0^2 \quad (1.12)$$

$$c = \frac{N}{V_{eff}} \quad (1.13)$$

$$c = \frac{N}{A_{eff}} \quad (1.14)$$

A further important parameter in FCS is the effective molecular brightness η_{eff} which is measured in counts per particle per second (cpps) and obtained through the average fluorescence intensity $\langle F(t) \rangle$ and the number of particles N .

$$\eta_{eff} = \frac{\langle F(t) \rangle}{N} \quad (1.15)$$

1.6.3 Fluorescence Cross-Correlation Spectroscopy (FCCS)

Fluorescence Cross-Correlation spectroscopy (FCCS) is an important technique to study interactions of molecules, which are labeled with spectrally separated dyes. The fluorescence is detected in two separate channels, here called red (r) and green (g). Both fluorescence intensity traces $F_g(\tau)$ and $F_r(\tau)$ are auto- and cross-correlated (**Fig. 1.5**).

$$G_{gr}(\tau) = \frac{\langle \delta F_g(t) \rangle \cdot \langle \delta F_r(t + \tau) \rangle}{\langle F_g(t) \rangle \cdot \langle F_r(t) \rangle} \quad (1.16)$$

The relative cross-correlation amplitude is the most interesting parameter and can be obtained from the amplitudes of the correlation curves. With an increasing number of interacting molecules, the amplitude of the cross-correlation curve increases.

$$G_{AC,g}(0) = \frac{1}{(c_g + c_{gr})V_{eff}} \quad , \quad G_{AC,r}(0) = \frac{1}{(c_r + c_{gr})V_{eff}} \quad (1.17)$$

$$G_{CC}(0) = \frac{c_{gr}}{(c_g + c_{gr})(c_r + c_{gr})V_{eff}}$$

$$\%CC = \frac{G_{CC}(0)}{G_g(0)} = \frac{c_{gr}}{c_r + c_{gr}} = \frac{N_{gr}}{N_r + N_{gr}} \quad (1.18)$$

$$\%CC = \frac{G_{CC}(0)}{G_r(0)} = \frac{c_{gr}}{c_g + c_{gr}} = \frac{N_{gr}}{N_g + N_{gr}}$$

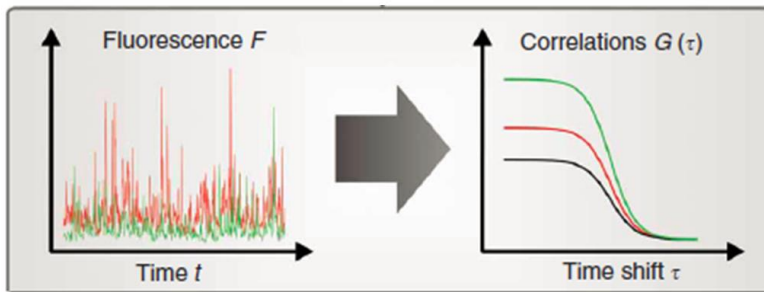


Figure 1.5: Dual-color FCCS

Spectrally separated fluorophores diffuse through the detection volume and give rise to two fluctuation intensity traces from which the auto-correlation curves (green and red) and the cross-correlation curve (black) can be calculated. Image adapted from (91).

1.6.4 Fluorescence Lifetime Imaging/ Förster Resonance Energy Transfer (FLIM/FRET)

The fluorescence lifetime is the time that the molecule, after absorbing a photon, remains in the excited state before returning to the ground state level by emitting a lower energy photon, as depicted in the Jablonski diagram (**Figure 1.4**). This process occurs in the nanosecond range. The lifetime is influenced by a second fluorescent molecule in close proximity with appropriate spectral properties to allow the absorption of the energy from the first molecule through fluorescence resonance energy transfer (FRET). Thus, the lifetime of the first fluorophore (donor) is decreased by a second fluorophore (acceptor), which can be measured in a FLIM-FRET experiment. The energy transfer from the donor to the acceptor can only occur when the two molecules are close enough to each other ($\sim 1-10$ nm). Therefore, FLIM-FRET provides an ideal tool to measure protein-protein interactions. The decrease of the donor fluorescence intensity depends on the distance between donor and acceptor and the fraction of interacting molecules. In a FRET situation (**Figure 1.6**), the bi-exponential decay curve delivers the slow lifetime τ_0 and the fraction b of the non-interacting donor molecules and the fast lifetime τ_{FRET} and the fraction a of the interacting donor molecules. From these parameters the FRET efficiency can be calculated from the following equation (92): $E_{FRET} = 1 - \left(\frac{\tau_{FRET}}{\tau}\right)$ (1.19)

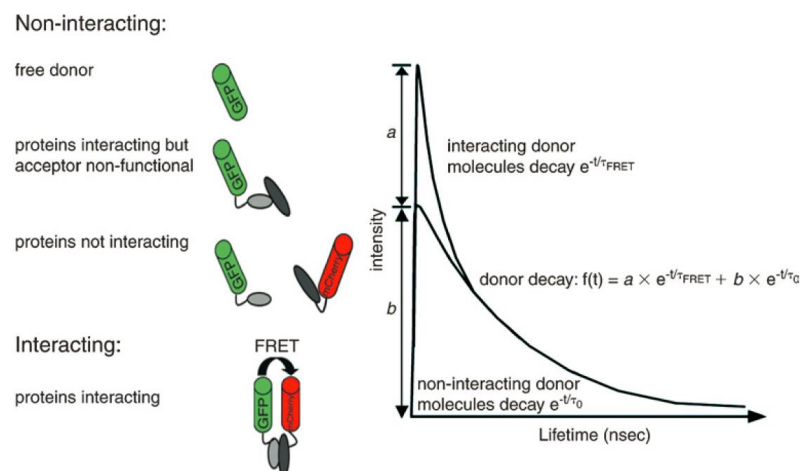


Figure 1.6: FLIM-FRET

Fluorescence decay curve, when FRET occurs. Image adapted from (92).

2 Aim of the work

Since its discovery one decade ago, Spir research has mainly focused on its actin nucleation mechanism and its cooperation with formins in actin organization. Besides Spir function in oogenesis, little is known today about the cell biological functions of Spir proteins in other tissues and its regulation. This project was aimed to gain more knowledge about the targeting and regulatory mechanisms of Spir proteins and their structural requirements. We wanted to determine the protein and lipid interactions necessary to form a functional membrane-associated actin nucleation complex. This would allow us to learn how Spir proteins are targeted towards membranes and how the targeting is regulated. Several cytoskeletal organizers like formins are regulated by intramolecular interactions. Thus, we further investigated whether Spir proteins are capable of forming such an intramolecular complex for auto-regulation as well. Spir proteins encode a modified version of the FYVE zinc finger motif which is a well-known phospholipid binding domain. Here we wanted to characterize the membrane binding properties of Spir-FYVE domain compared to canonical FYVE domains. Moreover, we wanted to figure out if the Spir FYVE domain possesses an extended function as a protein-protein interaction module. Vesicle processes are highly complex and their regulation requires key interactions. In mouse oocytes Spir-proteins were shown to work in concert with Fmn-2, Rab11 and Myosin Vb to drive vesicle transport processes by assembling and regulating a dynamic actin network in order to ensure proper spindle positioning. Within the scope of this work we wanted to gain more insights of the trans-regulatory interactions of Spir-2 to identify and characterize the key regulators of Spir-2

3 Material and Methods

3.1 Reagents

All general reagents and chemicals were purchased from Carl Roth (Karlsruhe, Germany) and Sigma-Aldrich (Hamburg, Germany), if not stated otherwise. Standard buffers and bacterial growth medium were supplied by the media kitchen of the BIOTEC, TU Dresden.

3.2 DNA constructs

The expression vector pEGFP-C1 was supplied from Takara Bio Europe/Clontech (Saint-Germain-en-Laye, France). All constructs used in this study are listed in the appendix. The cloning procedures were carried out by Annette Samol (Universität Regensburg).

3.3 Protein Expression and Purification

3.3.1 Expression and purification of Spir-2 variants

For prokaryotic expression of His₆-tagged proteins AcGFP-Spir-2-CT, AcGFP-Spir-2-LAFA, AcGFP-Spir-2-C1,2,78S, Spir-2-KIND and ΔH-Arf1 as well as the glutathione S-transferase (GST)-tagged Spir, Arf1 and formin proteins were expressed in *Escherichia coli* Rosetta(DE3) pLysS / BL21(DE3) pLysS. Bacteria were grown to an OD_{600nm} of 0.6-0.8, induced with 100 μM IPTG (Isopropyl-1-thio-β-D-galactopyranoside) and cultured at 20°C for 12-18-hours. Bacteria were harvested, lysed by ultrasonication and purified with Äkta purifier system (GE Healthcare) using nickel-nitrilotriacetic acid affinity chromatography with Ni-NTA FF columns (GE Healthcare) and GSH affinity with Sepharose HP columns (GE Healthcare) and subsequent size exclusion chromatography (Sephadex G200 16/60, GE Healthcare). Proteins were concentrated by ultracentrifugation using Amicon Ultra-4 ultracentrifugation devices (Millipore) and the purity of the proteins was analyzed by SDS-PAGE

(Figure 3.1). The expression and purification of these proteins were performed by Susanne Dietrich (Universität Regensburg).

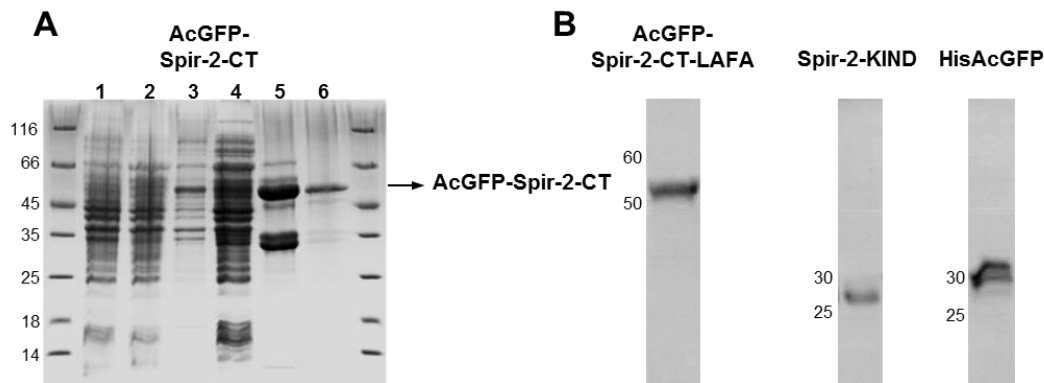


Figure 3.1: Expression and purification of His-tagged AcGFP-Spir-2-CT and their variants

(A) SDS-PAGE gel, visualized by Coomassie staining, shows following lanes (1) non-induced *E. coli* BL21(DE3) pLysS (2) IPTG-induced BL21(DE3) pLysS (3) insoluble fraction, (4) soluble fraction, (5) eluate pool after Ni-NTA chromatography, (6) eluate pool after Sephadex G200 16/60 size exclusion chromatography. Image courtesy of Susanne Dietrich (B) SDS-PAGE gel of purified AcGFP-Spir-2-CT-LAFA, Spir-2-KIND and HisAcGFP.

3.3.2 Expression and purification of myristoylated Arf1

Myristoylated Arf1 with an extra C-terminal cysteine was coexpressed in *E. coli* BL21 with N-myristoyltransferase in the presence of myristate/BSA. The Arf1/NMT duet plasmid encoding for Arf1 and human N-myristoyltransferase was kindly provided by Volker Haucke (FU Berlin) and Christoph Stange (TU Dresden). The purification was performed according to *Franco et al.* (1995) (93). The myristoylated Arf1 was expressed in *E. coli* BL21(DE3) pLysS. Bacteria were grown in 2xYT medium (+ kanamycin) at 27°C to an OD_{600nm} of 0.6. Preincubated 100x myristate/BSA solution (6 mM sodium myristate incubated with 3% (w/v) fatty acid free BSA in water) was added and protein expression was initiated by induction with 300 μM IPTG and cultured at 37°C. Cells were harvested by 15 min centrifugation at 3000 g and the cell pellet was resuspended in 80 ml extraction buffer (50 mM Tris/HCl pH 8.0, 1 mM MgCl₂, 1 mM DTT, 200 μM GDP, containing protease inhibitor (Roche)).

Cells were lysed with the homogenizer EmulsiFlex-C5 (Avestin, Canada). Cell debris was removed by 45 min centrifugation at 100,000 g. The protein was purified by ammonium sulfate precipitation followed by an anion exchange chromatography with HiPrep DEAE FF 16/10 column (GE Healthcare) under reducing conditions. After loading the protein solution and washing with three column volumes of loading buffer (10 mM Tris/HCl pH 8.0, 1 mM MgCl₂, 1 mM DTT) the protein was eluted with a linear gradient from 0 to 100% (v/v) elution buffer (1 M KCl, 10 mM Tris/HCl pH 8.0, 1 mM MgCl₂, 1 mM DTT). The purity of the protein was analyzed by SDS-PAGE (**Figure 3.2**). Proteins were concentrated by ultracentrifugation using Amicon Ultra-15 Centrifugal Filter Units with molecular mass cut offs of 10 kDa (Millipore). According to the shift in gel migration and mass spectrometry about 80% of the purified Arf1 was myristoylated.

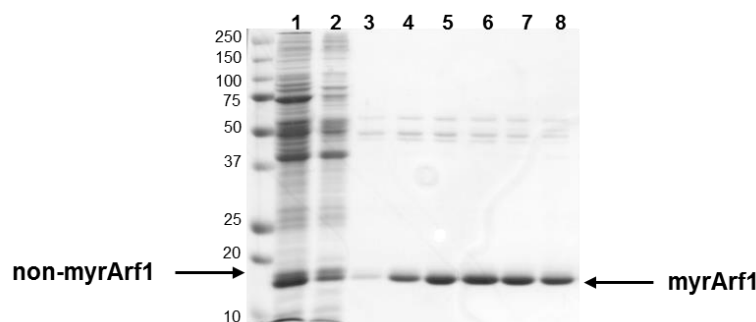


Figure 3.2: Purification of myristoylated Arf1

SDS-PAGE gel, visualized by Coomassie staining, shows the lanes (1) fraction after (NH₄)₂SO₄ precipitation and subsequent desalting (2) flow through and (3)-(8) elution fractions of the anion exchange chromatography. The shift in gel migration displays the myristoylation.

3.4 Labeling of the proteins

Spir-2-KIND was labeled with Alexa⁶⁴⁷ (Invitrogen) according to the manufacturer's protocol. Briefly, 7x excess of Alexa⁶⁴⁷-maleimide dye was added to 100 μM Spir-2-KIND in 1x PBS buffer and incubated for 2 h at room temperature and afterwards overnight at 4°C. Afterwards the labeled protein was separated from the non-reactive dye by extensive dialysis in 1x PBS buffer at 4°C. The protein concentration and degree of

labeling was estimated by UV-VIS spectroscopy. A labeling of 100% was obtained for Spir-2-KIND. The labeling of Spir-2-KIND was performed by Susanne Dietrich. By FCS measurements a fraction of 30% free dye was determined, which could not be removed by a subsequent gelfiltration (Nap 10 column, GE Healthcare) and Native-Page.

Myristoylated Arf1 was labeled at the extra cysteine at the C-terminus with Cy5-maleimide dye (GE Healthcare). MyrArf1 was dialyzed against HEPES buffer (20 mM HEPES pH 7.2, 100 mM KCl, 1 mM MgCl₂) and 100x excess TCEP was added and incubated for 30 min on ice. 10x excess of Cy5, solved in dimethylformamide, was added and incubated for 2 hours on ice. The free dye was removed by gelfiltration using a PD10 column (GE Healthcare) at 4°C, equilibrated with HEPES buffer. 100% labeling efficiency was obtained.

Arf1ΔH was labeled at the inserted C-terminal KCK motif with the maleimide dye Atto⁶⁵⁵. 2x excess of Atto⁶⁵⁵ dye was added to 200 μM Arf1ΔH and incubated at 4°C overnight. Unbound dye was removed by gelfiltration using a PD10 column (GE Healthcare) at 4°C, equilibrated with 1x TBS buffer (50 mM Tris-Cl, 150 mM NaCl, pH 7.6), containing 1 mM DTT. 50% labeling efficiency was obtained.

3.5 Gel electrophoresis and Western Blot

For the separation of proteins 12% SDS polyacrylamide gels from Bio-Rad Laboratories GmbH (München, Germany) were used. Before loading on the gel, the samples were boiled in 5x SDS sample buffer (300 mM Tris-HCl pH 6.8, 50% (v/v) glycerin, 15% (w/v) SDS, 25% (v/v) β-mercaptoethanol, 0.025% (w/v) Bromophenolblue) for 5 min at 95°C. The gels were run in 1x SDS running buffer (0.01 (w/v) SDS, 25 mM Tris, 19 mM Glycine) for 120 V and 300 mA for 20 min and afterwards the voltage was increased to 160 V.

For immunodetection of the separated proteins, the proteins were transferred onto nitrocellulose membrane (Protran, 0.45 μm pore size) in the presence of 20% (v/v) methanol and 0.01% (w/v) SDS using wet blot

system (Bio-Rad). Afterwards the membrane was blocked with 3% BSA in PBS for 1h at room temperature. The incubation with the primary antibody was carried out over night at 4°C. The membrane was washed 3x times with PBS and the incubation with the secondary HRP-conjugated antibody followed at room temperature for 1h. Then the membrane was washed again for 4x10min with PBS. The blots were developed using the ECL Western Blotting Analysis System (GE Healthcare) and detected by the LAS-3000 CCD-Imaging System (Fujifilm, Tokyo, Japan). For immuno-detection of HisAcGFP-Spir-2-CT and HisAcGFP the primary antibody Living Colors® Full-Length GFP Polyclonal Antibody (1:1000, species rabbit, Clontech) and the secondary antibody ECL™ Anti-Rabbit HRP IgG (1:5000, species donkey, GE Healthcare) were used.

3.6 GST-Pulldown assay

A pulldown is a technique for analyzing protein-protein-interactions. The “bait” protein was fused to a GST-tag, whereas the putative binding partner, the “prey” protein, was fused to an eGFP-tag. Hek293-cells were transfected with the expression vectors encoding eGFP-tagged constructs by Lipofectamin (Invitrogen). 24h post transfection cells were lysed in lysis-buffer (25 mM Tris pH 7.4 , 150 mM NaCl, 5 mM MgCl₂, 10% (v/v) Glycerol, 0.1% (v/v) Nonidet P-40), centrifuged at 20.000 x g and 4°C for 30 minutes to remove insoluble debris. The cell lysate was incubated with 20-50 µg GST-fusionprotein coupled to 20 µl GSH-sepharose 4B beads (GE Healthcare) for 2 hours at 8°C on a rotating wheel. The beads were subsequently washed 3 times (25 mM Tris pH 7.4, 300 mM NaCl, 5 mM MgCl₂, 10% (v/v) Glycerol and 0.1% (v/v) Nonidet P-40). Bound proteins were eluted by boiling the beads in 2x SDS sample buffer for 5 minutes. Proteins were separated by SDS-PAGE and analyzed by Western Blotting. The GST-pulldown assays were performed by Annette Samol (Universität Regensburg).

3.7 Preparation of model membranes

3.7.1 Lipids used in this study

The lipids, which were used in this work, were purchased from Avanti Polar Lipids (Alabaster, AL) and Sirius Fine Chemicals SiChem (Bremen, Germany) and are listed below.

Lipids purchased from Avanti Polar Lipids:

- 1,2-dioleoyl-*sn*-glycero-3-phosphocholine (DOPC)
- 1-palmitoyl-2-oleoyl-*sn*-glycero-3-phosphocholine (POPC)
- 1,2-dioleoyl-*sn*-glycero-3-phosphoethanolamine (DOPE)
- 1,2-dioleoyl-*sn*-glycero-3-phosphate (DOPA)
- 1-palmitoyl-2-oleoyl-*sn*-glycero-3-phosphate (POPA)
- 1,2-dioleoyl-*sn*-glycero-3-phospho-L-serine (DOPS)
- 1-palmitoyl-2-oleoyl-*sn*-glycero-3-phospho-L-serine (POPS)
- 1,2-dioleoyl-*sn*-glycero-3-phosphoinositol-3-phosphate (PI(3)P)
- 1,2-dioleoyl-*sn*-glycero-3-phosphoinositol-4-phosphate (PI(4)P)
- 1,2-dioleoyl-*sn*-glycero-3-phosphoinositol-5-phosphate (PI(5)P)
- 1,2-dioleoyl-*sn*-glycero-3-phosphoinositol-3,4-bisphosphate (PI(3,4)P₂)
- 1,2-dioleoyl-*sn*-glycero-3-phosphoinositol-3,5-bisphosphate (PI(3,5)P₂)
- 1,2-dioleoyl-*sn*-glycero-3-phosphoinositol-4,5-bisphosphate (PI(4,5)P₂)
- 1,2-dioleoyl-*sn*-glycero-3-phosphoinositol-3,4,5-trisphosphate (PI(3,4,5)P₃)

Lipids purchased from Sirius Fine Chemicals SiChem.

- 1,2-dipalmitoyl-*sn*-glycero-3-phosphoinositol-3-phosphate (PI(3)P)
- 1,2-dipalmitoyl-*sn*-glycero-3-phosphoinositol-4-phosphate (PI(4)P)
- 1,2-dipalmitoyl-*sn*-glycero-3-phosphoinositol-4,5-bisphosphate (PI(4,5)P₂)

Lipids were solved in chloroform, but phosphoinositides were solved in CHCl₃:MeOH:H₂O 1:2:0.8. Lipids were stored at -20°C.

3.7.2 Giant Unilamellar Vesicles (GUVs)

We prepared GUVs by the electroformation method (94). All lipids were from Avanti Polar Lipids and dissolved in chloroform. 5 μ l lipid mixture (1mg/ml) was spread onto two platinum wire electrodes. After drying the lipid film, the electrodes with the lipid films were placed into a chamber containing 300 mM sucrose solution. The Platinum wires were connected to a power generator. By applying an electric field with an alternating current of 10 Hertz and 2.3 V for 1 hour at room temperature (and for PIPs at 50°C) unilamellar vesicles were formed by swelling of the lipid bilayers in an aqueous environment. The GUVs were released from the electrodes by changing the frequency to 2 Hz for 30 minutes. For imaging, GUVs were mixed with TBS buffer and transferred into BSA coated 8-well LabTek chambers (Nunc, Thermo scientific).

3.7.3 Large Unilamellar vesicles (LUVs)

Lipids were purchased from Avanti Polar Lipids and the phosphoinositides from Sirius Fine Chemicals SiChem. The solvent of the lipid mixture (1-2 mg/ml) was removed under a stream of nitrogen and subsequently under vacuum for at least 1h. The lipids were resuspended in 1x TBS buffer (50 mM Tris, 150 mM NaCl pH 7.6) and vortexed, which induces the formation of multilamellar vesicles. For the preparation of large unilamellar vesicles, the lipid suspension was subjected to eight freeze-thaw cycles and extruded 19 times at 40°C through a 100-nm-diameter polycarbonate filter (Avanti Polar Lipids) using a mini-extruder (Avanti Polar Lipids).

3.8 LUV Flootation assay

For the characterization of the membrane binding of a protein, ultracentrifugation techniques are suitable to separate the liposome-bound fraction of protein from the unbound fraction. There are two techniques, either the liposome and bound protein can be a pellet or liposome and bound protein are floated on a sucrose density gradient. In the case of proteins which tend to aggregate and pellet independently of

the liposome binding, the floatation technique is more appropriate and was employed in this work according to Höfer *et al.* (95). Sucrose solutions of 25% and 75% were prepared in 1x TBS buffer. The protein was mixed with 80 μ l LUVs in a total volume of 150 μ l in 1.5-ml Polyallomer Microfuge tubes (Beckman Instruments Inc., Palo Alto, CA) and incubated for 10 minutes. The solution was mixed with 100 μ l of 75% sucrose, giving a final sucrose solution of 30%. This bottom fraction was overlaid with 200 μ l 25% sucrose and subsequently 100 μ l 1x TBS buffer. The tubes are centrifuged for 2 h at 50,000 rpm and 4°C using an ultracentrifuge (OptimaTMMax, Beckman Instruments Inc., Palo Alto, CA) and rotor TLA-55 (Beckman Instruments Inc., Palo Alto, CA). After centrifugation the fractions were gently collected and analyzed by SDS-PAGE and subsequent Western-Blotting.

3.9 Electrochemiluminescence immunoassay (EIA)

The electrochemiluminescence immunoassay (EIA) is a new technique to study protein-protein interactions and protein-lipid-interactions (96-98). It is based on a sandwich immunoassay which uses electrochemiluminescence to measure protein concentrations. One protein interaction partner (2 μ l 25 ng/ μ l Spir-2-KIND) or liposomes (2 μ l 1 mg/ml LUVs of different compositions) were passively adsorbed on the electrode surface of 384-well high bind plates (MSD, Meso Scale Discovery, Rockville, USA) for 1h at 23°C. The rest of the surface was blocked with 0.5% porcine gelatin in 1x TBS buffer for 1h at 23°C. The surface was then washed 3x times with 1x TBS buffer and subsequently the defined concentrations of protein (HisAcGFP-Spir-2-CT) were added to each well. The binding was carried out for 2h at 23°C. Afterwards, the wells were again washed and the primary antibody Living Colors® Full-Length GFP Polyclonal Antibody (species rabbit, Clontech) was applied for 1h at 23°C. The wells were again washed and the secondary antibody (goat anti-rabbit-STAG from Meso Scale Discovery, Rockville, USA) was added (1.25 μ g/ml, 23°C, 1h). The cells were washed and MSD surfactant free reading buffer (Meso Scale Discovery, Rockville, USA) was added. As a

background both primary and secondary antibody binding to gelatin was determined and subtracted. Data were acquired on the SECTOR imager 6000 (Meso Scale Discovery, Rockville, USA). The data were analyzed in Sigma Plot 12.5 software (Systat Software Inc.) using the following one site binding algorithm:

$$y = \frac{a \cdot x}{b + x} \quad 3.1$$

with a representing the maximum amplitude (B_{max}), and b representing the equilibrium dissociation constant (K_D). The electrochemiluminescence assay was performed by Aleksander Czogalla (TU Dresden).

3.10 Cell Culture

HeLa cells were cultured as adherent culture in DMEM medium (Invitrogen/Gibco) supplemented with 10% FCS (Fetal calf serum; Invitrogen/Gibco). The cells were cultured with 5% CO₂ at 37°C and were regularly passaged at subconfluency by trypsination. Cells were washed with 1x PBS and incubated with trypsin for 2 min at 37°C. By adding DMEM medium and subsequent centrifugation at 1000 rpm for 2 min trypsin is removed. Then cells were resuspended in DMEM medium and seeded at 6·10⁴ cells/ml in a 75 cm² flask (Nunc, Thermo Scientific).

3.11 Cell seeding and transfection

Cells were seeded 24 h before transfection. 8 well LabTek chambers (Nunc, Thermo scientific) were coated with Fibronectin (Roche Diagnostics, 10 µg/ml in PBS, including CaCl₂ and MgCl₂) and 300 µl 3·10⁴ cells were seeded. The cells were transfected with Turbofect (Life technologies) with a DNA:Turbofect ratio of 100 ng:0.3 µl. On the next day prior to imaging, cells were washed 2x with air buffer (150 mM NaCl, 20 mM HEPES pH 7.4, 15 mM Glucose, 150 µg/ml BSA, 20 mM Trehalose, 5.4 mM KCl, 0.85 mM MgSO₄, 0.6 mM CaCl₂).

3.12 Confocal Laser scanning microscopy

Confocal imaging was performed on a confocal Zeiss LSM780 microscope equipped with a 40x 1.2 numerical aperture water immersion objective. The 488 nm laser line was used to excite GFP, the 561 nm laser line was used to excite mStrawberry and the 633 nm laser was used to excite Alexa647, Atto655 and Cy5. The MBS 488/633 and MBS 488/561/633 were used to separate the green signal from the orange and red signals, respectively. Further, the detection range of 490-560 nm and 586-691 nm for green and orange emission and the detection range of 490-604 nm and 638-758 nm for green and red emission were employed.

3.13 FCS and FCCS Data Acquisition

FCS and FCCS were carried out on Zeiss LSM780 microscope with an attached Confocor 3 and equipped with a 40x 1.2 numerical aperture water immersion objective. The 488 nm Ar-laser-line was used to excite eGFP and AcGFP, the 561 nm line was used to excite mStrawberry and the 633 nm laser was used to excite Alexa647 and Cy5. The laser lines were attenuated by an acousto-optical tunable filter to an intensity of 2.2 μ W (AcGFP; FCCS in vitro), 1.7 μ W (FCCS with eGFP in cells), 1.0-2.5 μ W (FCS and FCCS with Cy5 and Alexa647 in vitro) or 2.2 μ W (FCCS with mStrawberry in cells). For eGFP and mStrawberry the excitation laser lines were directed by a 488/561 dichroic mirror (MBS). The fluorescence light was collected using 40x 1.2 numerical aperture water immersion objective (Zeiss, Oberkochen, Germany) and separated from the excitation light by the MBS, passing a confocal pinhole (35 μ m in diameter) and split by a second dichroic mirror NFT LP565 and the residual laser light was removed by a 495-555 nm bandpass and 580 nm longpass filter. For AcGFP and Alexa647/Cy5 the MBS 488/633, the NFT 635, the band pass 505-610 nm and long pass filter 655 nm were used. The fluorescence light was recorded by avalanche photodiode detectors (APDs). Before each experiment the setup was adjusted by using a dye mixture of Alexa488 and CF568 or Alexa488 and Alexa647 to determine the structural parameters of the green, orange and red channel in

solution, which was fixed during data fitting. Using double labelled DNA (488/633 in vitro FCCS standard probe from IBA, Goettingen, Germany) a yield of $68 \pm 3\%$ cross-correlation amplitude was achieved, due to imperfect overlap of the detection volume and imperfect labelling of the DNA sample. Consequently, FCCS measurements of a perfect interaction are not able to reach 100% cross-correlation amplitudes.

FCS and FCCS measurements in vitro were performed 100 μm above the cover slip. For each measurement 12-24 runs each 10 seconds long were done.

For intracellular measurements a confocal image was acquired and the FCCS focus was positioned into a cytoplasmic, homogenous region approximately 3 μm above the cover slip. For each measurement 24 runs each 10 seconds long were done.

3.14 FCS and FCCS Data Analysis

The fluorescence signal of each run was correlated by the Zeiss Zen Software according Eq. 1.16 and Eq. 1.17. Runs showing significant fluorescence intensity changes and diffusion of remaining cellular components or aggregates were discarded from data evaluation. For FCS and FCCS the auto- and cross-correlation data were analyzed by nonlinear least squares fit using the equations 1.7, 1.8, 1.16, 1.17.

3.14.1 *In vitro* FCS and FCCS

FCS was evaluated by applying a 3D+T model. FCS measurements on GUVs were evaluated by applying a 3D+2D+T model according to equation 1.7 and 1.8.

The amplitudes of the auto- and the cross-correlation curves $G_{AC,g}(0)$, $G_{AC,r}(0)$ and $G_{CC}(0)$ were corrected for background using the following algorithm, where F is the measured count rate and B the background count rate.

$$\tilde{G}_{AC,g}(0) = G_{AC,g}(0) \cdot \left(\frac{F_g}{F_g - B_g} \right)^2, \quad \tilde{G}_{AC,r}(0) = G_{AC,r}(0) \cdot \left(\frac{F_r}{F_r - B_r} \right)^2 \quad 3.2$$

$$\tilde{G}_{CC}(0) = G_{CC}(0) \cdot \frac{F_g}{F_g - B_g} \cdot \frac{F_r}{F_r - B_r} \quad 3.3$$

Further, the calculation of the average counts per particle (CPP) for brightness analysis were background corrected and calculated according to $CPP = \frac{F-B}{\tilde{N}}$ with $\tilde{N} = \left(1 + \frac{B}{F-B}\right)^{-2} \cdot G(\tau)^{-1}$ 3.4

For *in vitro* FCCS measurements with the Dyes AcGFP and Alexa647/Cy5 a cross-talk below 1% was measured and was neglected for data evaluation.

The background corrected amplitudes were used to calculate the number of particles and the concentration according to the equations 1.8-1.13. The amount of cross-correlation was calculated according to equation 1.14.

3.14.2 *In vivo* FCS and FCCS

In *in vivo* FCS and FCCS experiments, the background count rate was measured in HeLa cells transfected with water instead of a vector and the background correction was performed accordingly to 3.2-3.4. In addition to the background correction, the amplitudes were corrected for spectral crosstalk from the green into the red channel ($\beta = 8.7\%$). Since the green amplitude is not affected by crosstalk, only the red and cross-correlation amplitude were corrected for spectral crosstalk accordingly to the following algorithm:

$$\hat{G}_g(0) = G_g(0) \quad 3.5$$

$$\hat{G}_r(0) = \frac{F_r^2 G_r(0) + \beta^2 F_g^2 G_g(0) - 2\beta F_r F_g G_{CC}(0)}{(F_r - \beta F_g)^2} \quad 3.6$$

$$\hat{G}_{CC}(0) = \frac{F_g F_r G_{CC} - \beta F_g^2 G_g(0)}{F_g F_r - \beta F_g^2} \quad 3.7$$

The background and crosstalk-corrected amplitudes were used to calculate the number of particles and the concentration according to the equations the 1.10-1.14 and 1.15 (91,99). The amount of cross-correlation was calculated according to equation 1.18.

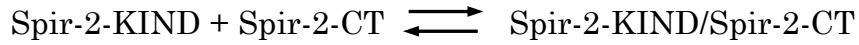
To take into account slow instabilities inside the cellular environment a 2-component 3D+3D+T fit model with a small fraction of an additional slow diffusion time (milliseconds) was applied (100).

3.14.3 Titration of HisAcGFP-Spir-2-CT and Spir-2-KIND*Alexa⁶⁴⁷

In the HisAcGFP-Spir-2-CT/Spir-2-KIND*Alexa⁶⁴⁷ titration experiment, 25 nM HisAcGFP-Spir-2-CT was kept constant while Spir-2-KIND*Alexa⁶⁴⁷ was added in the concentration range of 0-1000 nM. FCS measurements of AcGFP-Spir-2-CT were evaluated by applying a 3D+T model to the correlation curves. Due to imperfect removal of the free Alexa⁶⁴⁷ dye, the auto-correlation data of KIND*Alexa⁶⁴⁷ were fitted by a 3D+3D+T model, in which the diffusion time of the fast component was fixed to 30 μ s. This way, the fraction of free Alexa⁶⁴⁷ dye was determined (\sim 30%) and subtracted from N_r and N_{gr} . The cross-correlation was calculated by dividing the number of double labeled particles by all particles carrying a red label.

$$\%CC = \frac{G_{gr}(0)}{G_g(0)} = \frac{N_{gr}}{N_r + N_{gr}} \quad 3.8$$

To characterize the Spir-2-KIND/Spir-2-CT interaction we assume a simple 1:1 interaction to define an effective K_D



$$K_D = \frac{[\text{Spir-2-KIND}] \cdot [\text{Spir-2-CT}]}{[\text{Spir-2-KIND/Spir-2-CT}]} \quad 3.9$$

$$[\text{Spir-2-KIND}] = [\text{Spir-2-KIND}]_{\text{total}} - [\text{Spir-2-KIND/Spir-2-CT}]$$

$$[\text{Spir-2-CT}] = [\text{Spir-2-CT}]_{\text{total}} - [\text{Spir-2-KIND/Spir-2-CT}]$$

where the concentration of $[\text{Spir-2-KIND}]_{\text{total}}$ is the free and bound concentration of Spir-2-KIND*Alexa⁶⁴⁷ and $[\text{Spir-2-CT}]_{\text{total}}$ is the free and bound concentration of HisAcGFP-Spir-2-CT and $[\text{Spir-2-KIND/Spir-2-CT}]$ is the concentration of the Spir-2-KIND*Alexa⁶⁴⁷/HisAcGFP-Spir-2-CT complex.

The corresponding fraction of bound ligand and dissociation constant can be calculated as:

$$\frac{L_b}{R_0} = k \cdot (A - \sqrt{A^2 - 4 \cdot L_0 \cdot R_{max}}) \quad 3.10$$

$$A = L_0 + R_{max} + K_D$$

where L_b denotes the concentration of bound ligand Spir-2-KIND*Alexa⁶⁴⁷, L_0 the total concentration of ligand KIND*Alexa⁶⁴⁷ and R_0 the total concentration of HisAcGFP-Spir-2-CT. The factor k accounts for an unknown fraction of inactive GFP-tagged SPIR-2-CT as well as aberrations of the cross-correlation detection volume.

3.15 FLIM-FRET

FLIM measurements were performed on an inverted confocal laser scanning microscope (Zeiss LSM780) equipped with a 40x 1.2 numerical aperture water immersion objective (Zeiss). The eGFP donor was excited with a 473 nm pulsed diode laser (0.45 μ W, 50 MHz). Photons from the donor fluorophores were collected and counted using TCSPC software from Becker & Hickl (Germany). The lifetimes of all the pixels in the field of view (256×256) were calculated by the SPC image analysis software (Becker & Hickl Germany) to generate exponential decay curves. Pixel binning was set to 1 and the fit range was restricted to 1.7 -11.7 ns. To give a lifetime image of a cell the lifetime of every pixel in the image was calculated by employing a mono-exponential decay fit model. To calculate the mean lifetime, the lifetime of 5 vesicles of each cell was analyzed and averaged and the average lifetime of 10-23 cells per sample were then averaged. By using a bi-exponential decay model information about the lifetimes and the fractions of the interacting and non-interacting molecules were derived. From these parameters, the FRET efficiency was calculated by using the equation 1.19.

3.16 Statistical analysis

Statistical analysis was performed using the SigmaPlot software 12.5 (Systat Software Inc.). For single comparisons, Student's t-tests were performed if data passed normality assumptions. If data did not pass normality assumptions, the Mann-Whitney-U-test was performed. Significance levels are marked accordingly: * $p < 0.05$, ** $p < 0.01$, *** $p < 0.001$, n.s. not significant $p > 0.05$.

4 Results

4.1 Characterization of membrane binding of Spir-2

4.1.1 Preface

More than 10 years ago, it was shown that Spir proteins are vesicle associated. All Spir proteins encode a FYVE zinc-finger motif at the C-terminus. This domain is characterized by 8 cysteines which coordinate 2 zinc-ions (55) But the Spir-FYVE domain differs from canonical FYVE domains such as from EEA1, SARA, Vsp27, shown in **Figure 4.1.A**. This shows that, Spir-FYVE domain has an insertion loop between cysteine 6 and 7. FYVE domains are membrane-binding modules, which specifically recognize phosphatidylinositol 3-phosphate (PI(3)P) and recruit FYVE-domain containing proteins to endosomal vesicles, which are highly enriched in PI(3)P. Three sequence motifs of the FYVE domain coordinate the PI(3)P molecule: The N-terminal WxxD, the central R(R/K)HHCR, and the C-terminal RVC motifs, whereas the recognition of the phosphate group of the lipid is mediated by the Arg and His residues in the basic central R(R/K)HHCR motif between cysteins 2 and 3 (101,102). Vertebrate genomes encode two Spir genes, *Spir-1* and *Spir-2* (47). Both Spir-proteins of different origins are lacking the basic central R(R/K)HHCR sequence as well as the the WxxD-motif (**Figure 4.1A**, green). The basic amino acid arginine of the RVC-motif (**Figure 4.1A**, green) is replaced by the acidic amino acid glutamate in *Spir-1* and aspartate in *Spir-2* (**Figure 4.1A**, yellow). Several proteins, like rabphilin-3A and protrudin, have FYVE-related domains that lack some conserved residues of canonical FYVE domains. Another conserved feature among FYVE domains is the hydrophobic ‘turret loop’ that penetrates the lipid bilayer (**Figure 4.1A,B**, red box in A). This hydrophobic patch is relatively small, suggesting that the hydrophobic interactions are not the only and major force for membrane binding (56)

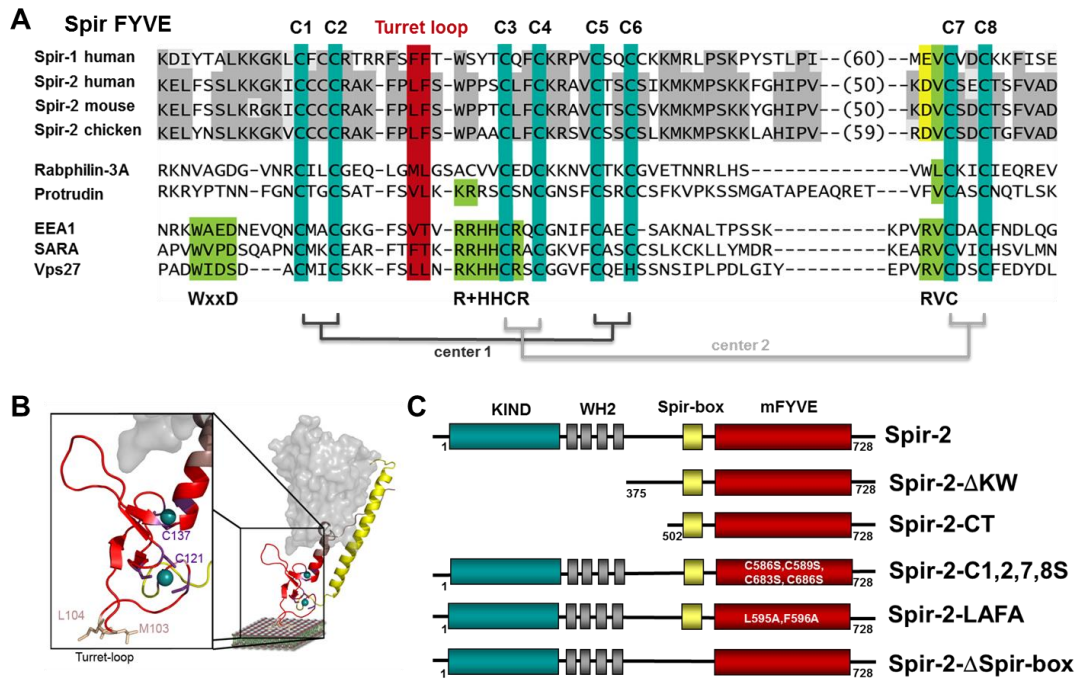


Figure 4.1: Characterization of membrane binding of Spir-2

(A) Multiple sequence alignment of Spir FYVE of different species in comparison to canonical FYVE domains of EEA1, SARA and VSP27 and FYVE-related domains of rabphilin 3b and protrudin, aligned by ClustalW. Conserved residues are highlighted in grey and conserved cysteines coordinating two Zinc²⁺-ions are displayed in blue. The red box marks the hydrophobic turret loop. The PI(3)P binding motifs of FYVE domains are highlighted in green. (B) Crystal structure of Rab-3a·Raphilin-3a complex in cartoon (Rab-3a, grey) and surface presentation (rabphilin-3a, color). FYVE zinc finger is highlighted in red with conserved zinc ions (deepteal cyan, as spheres) coordinating cysteines (purple). Cysteins C121 and C137 of rabphilin-3a correspond to cysteines 613 (6th) and 693(7th) in Spir-2-FYVE. Turret loop, formed by the residues M103 and L104 (wheat, sticks), is assumed to insert into the lipid bilayer. Image by the courtesy of Eugen Kerkhoff (C) Domain structures of Spir-2 and its variants used in this study.

The hydrophobic protrusion of rabphilin-3a is formed by the amino acids M103 and L104 which insert into the lipid bilayer (37,56) (Figure 4.1B). By sequence alignment we found that these amino acids correspond to the amino acids L595 and F596 in Spir-2. In this work we have focused on the Spir-2 protein. For expression in HeLa cells, full-length Spir-2 and its variants were labeled with eGFP at the N-terminus (Figure 4.1C). For *in vitro* studies the N-terminal truncated variant Spir-2-CT was expressed in *E.coli* and purified to homogeneity as attempts to produce

full-length recombinant Spir-2 was not successful due to low stability and aggregation of the protein. The production and purification of Spir-2-CT was established and carried out by Susanne Dietrich. Spir-2-CT was labeled with HisAcGFP at the N-terminus and respective variants based on that truncated variant.

4.1.2 Characterization of the membrane binding domains of Spir-2

We investigated Spir-2 in HeLa carcinoma cells, transiently expressing eGFP-Spir-2 and their variants (**Figure 4.2**). These studies confirmed previous observations (57), that Spir proteins are localized in the perinuclear compartment, mainly at vesicles in the central part of the cells and rarely at the cellular cortex. The Spir vesicles show partially tubulized structures. The variant Spir-2-CT and Spir-2- Δ KW, containing the Spir-box and FYVE domain, showed binding to vesicles, seen in HeLa cells (**Figure 4.2a,b**) and on artificial membranes such as Giant unilamellar vesicles (GUVs) (**Figure 4.2c**), Large unilamellar vesicles (LUVs) (**Figure 4.4**) and supported lipid bilayers (SLBs, data not shown), indicating that the C-terminal part mediates the membrane binding. The membrane binding requires an intact FYVE domain, as disrupting the integrity of the FYVE zinc finger domain by mutating two of the four cysteines in each of the two zinc ions coordinating centers, resulted in a loss of the membrane binding properties in HeLa cells (**Figure 4.2d**) and on GUVs (**Figure 4.2e**). Furthermore, the removal of the zinc ions by addition of EDTA resulted in a decreased binding to GUVs (**Figure 4.2f**). However, the FYVE domain is not solely responsible for membrane binding, as deletion of the adjacent Spir-box led to a loss of membrane binding (**Figure 4.2g**). To narrow down the structural requirements in the C-terminus we mutated the hydrophobic amino acids leucine and phenylalanine to alanine in the putative turret loop of Spir-2 (variant Spir-2-LAFA) (**Figure 4.1B**). This mutation led to a cytoplasmic distribution in HeLa cells (**Figure 4.2h**) indicating the contribution of the hydrophobic tip, penetrating into the lipid bilayer, in a similar

manner as shown for rabphilin-3a. These findings confirm previous studies (103). Interestingly, the variant Spir-2-LAFA was still able to bind to GUVs (DOPC:DOPA 8:2) (**Figure 4.2i**), where strong electrostatic interactions presumably counterbalance the lack of the hydrophobic interactions.

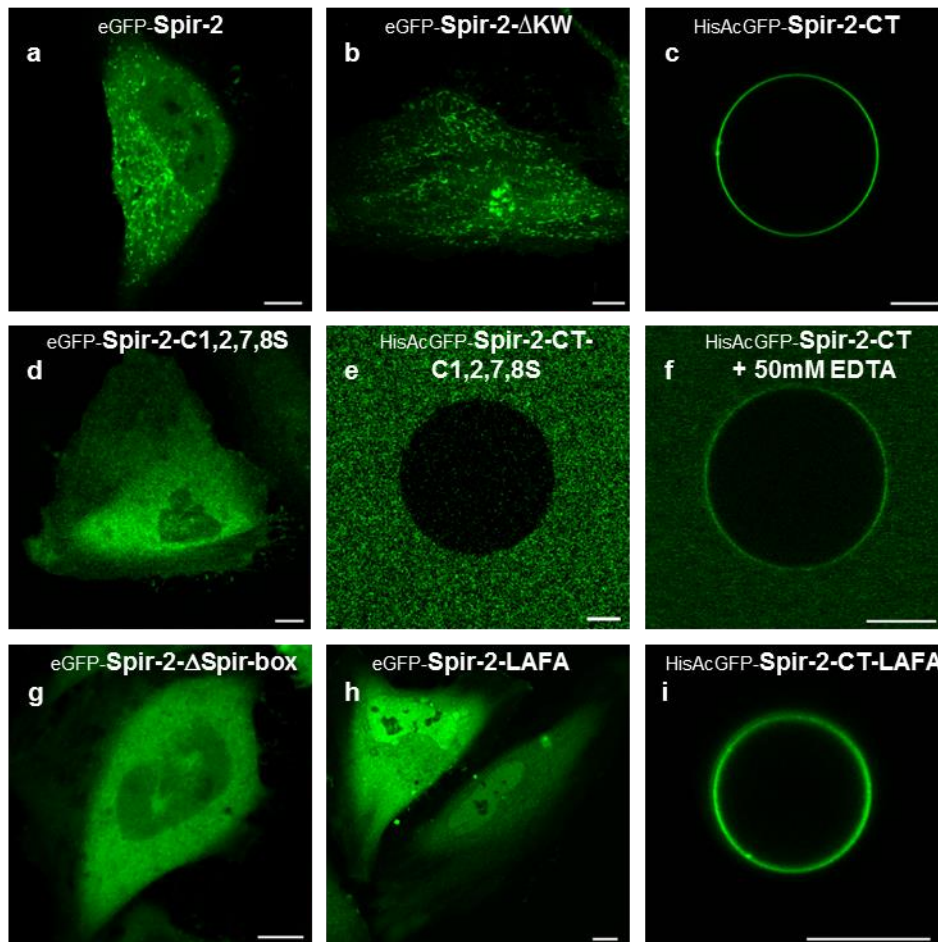


Figure 4.2: Characterization of membrane binding of Spir-2 in HeLa cells and on Giant Unilamellar Vesicles

Live cell imaging of HeLa cells transiently transfected with pEGFP-C1-Spir-2 and their variants. Recombinant produced HisAcGFP-Spir-2-CT and their variants were tested for membrane binding on GUVs (DOPC:DOPA 8:2). The C-terminal part is sufficient (**a-c**), but requires an intact FYVE domain (**d-f**), Spir-box (**g**) and hydrophobic LF tip (**h**) for membrane binding. On GUVs (DOPC:DOPA 8:2) strong electrostatic interactions counterbalance the lack of the hydrophobic tip (**i**). Scale bar: 10 μ m

4.1.3 Characterization of the phospholipid interactions of Spir-2

FYVE domains are well-known phospholipid interaction modules, which recognizes phosphatidylinositol 3-phosphate (PI(3)P), a phospholipid which is enriched in membranes of early endosomes and other endocytic vesicles. As a first step, phospholipid studies with membrane lipid strips were already performed and displayed no significant specificity. Spir-1-CT and Spir-2-CT exhibit a binding to PI(3)P, PI(4)P, PI(5)P, PA and weakly to PI(3,4)P₂, PI(3,5)P₂, PI(4,5)P₂ and PI(3,4,5)P₃ (104). However, strips with immobilized lipids are often not very precise and not quantitative and need to be combined with other techniques (105).

To probe the lipid specificity of Spir-2, HisAcGFP-tagged Spir-2-CT was expressed and purified and tested for membrane binding on GUVs of different phospholipid compositions (**Figure 4.3A**). In a control experiment purified HisAcGFP exhibits no significant binding to negatively charged GUVs, so that an influence of the HisAcGFP-tag on the membrane binding properties can be excluded (**Figure 4.3B**).

Spir-2-CT binds to all tested negatively charged phospholipids without any apparent specificity. It does not bind to neutrally charged phospholipids such as phosphatidylcholin (PC) and phosphatidylethanolamin (PE). The importance of electrostatic interactions for membrane binding could be shown by increasing the percentage of the negatively charged phosphatidic acid (PA) in GUVs (**Figure 4.3C**). Spir-2-CT could only bind to GUVs which contain at least 4% PA. In the previous chapter we reported that the variant Spir-2-LAFA lacks membrane binding in cells but is still able to bind to artificial membranes with 20% DOPA possibly due to counterbalanced electrostatic interactions. Further analysis revealed that the mutation of the hydrophobic loop requires a higher percentage of negative charges for membrane binding, at least 6% of PA, compared to the wild type with 4% (**Figure 4.3D**). Thus, the hydrophobic interactions of the turret loop

which are essential for membrane binding in cells also make a contribution to the binding to artificial membranes.

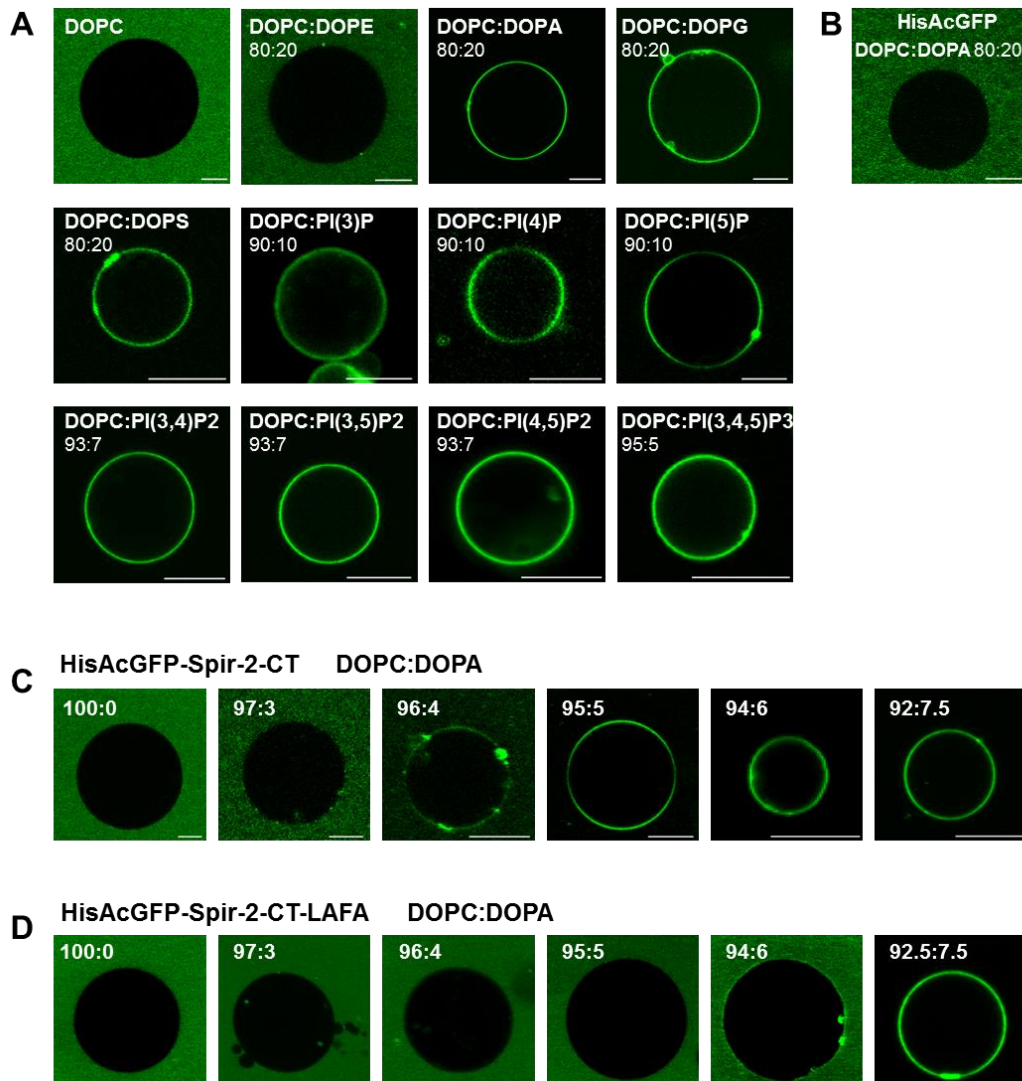


Figure 4.3: Phospholipid interactions of Spir-2 probed on GUVs

(A) HisAcGFP-Spir-2-CT binds to negatively charged phospholipids without any apparent lipid specificity. The net negative charge of the lipids was adjusted to 20% to facilitate comparability between the distinct lipid compositions. **(B)** In a control experiment HisAcGFP does not bind to negatively charged GUVs (DOPC:DOPA 80:20) **(C)** HisAcGFP-Spir-2-CT binding was monitored on GUVs with increasing DOPA concentrations. It requires at least 4% DOPA for binding. **(D)** The variant HisAcGFP-Spir-2-CT-LAFA requires at least 6% DOPA for membrane binding. Scale bar: 10 μ m

Unfortunately, we observed heterogeneity in membrane binding on GUVs as has been also reported recently (80), which made a quantitative analysis based on intensity complicated. Therefore, we decided to use an established assay to quantitatively probe the PI(3)P specificity of the Spir FYVE domain. The electrochemiluminescence immunoassay (EIA) allows quantification of protein-protein and protein-liposome interactions (96,97). We assumed that all lipids used for liposome preparation are homogeneously incorporated (106). As shown in **Figure 4.4A,B**, Spir-2-CT binds with an affinity between 20-50 nM to LUVs and does not bind PI(3)P specifically. It binds PI(4)P and PI(4,5)P₂ in a similarly strong manner (**Figure 4.4A,B**). In addition, an established liposome floatation assay was performed, which has been reported to identify the high PI(3)P specificity for EEA1 FYVE and *S. cerevisiae* PROPPIN Hsv2 (106,107). It confirmed a similar strong interaction of Spir-2-CT to PI(3)P, PI(4)P and PI(4,5)P₂ and even stronger interactions to PA (**Figure 4.4C,D**). In consistence with the binding studies on GUVs, Spir-2-CT does not bind to the neutrally charged PC and the HisAcGFP-tag does not influence the binding.

In conclusion, the Spir FYVE domain does not bind specifically to PI(3)P as can be expected from the lack of the conserved PI(3)P interaction motifs. It binds to negatively charged phospholipids but not to neutrally charged phospholipids. Therefore, the binding is most likely mediated by non-specific electrostatic interactions and hydrophobic interactions of the turret-loop. Thus, Spir FYVE domain represents a FYVE-related domain as known for rabphilin-3a and protrudin. These findings indicate that ancillary protein factors might play a crucial role for specific targeting of Spir proteins.

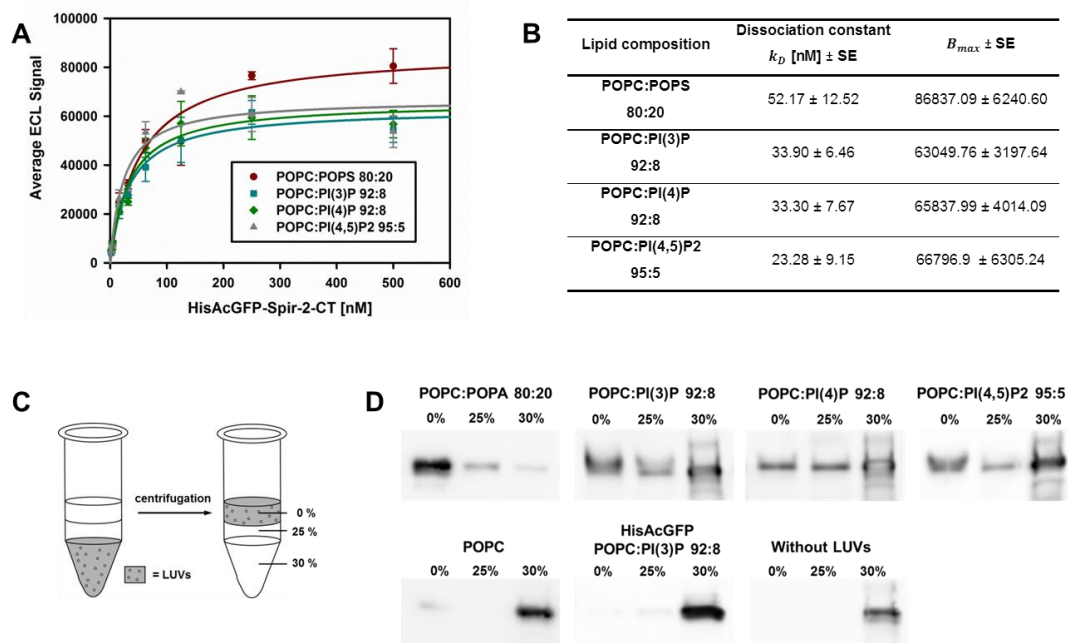


Figure 4.4: Phospholipid interactions of Spir-2 probed on Large Unilamellar vesicles (LUVs)

(A) Membrane binding of HisAcGFP-Spir-2-CT was probed on LUVs of different lipid compositions by an electrochemiluminescence immunoassay (EIA). The binding curve was analyzed by hyperbolic curve-fitting. (B) Dissociation constants and B_{max} values of the interaction of HisAcGFP-Spir-2-CT with LUVs obtained from EIA assay from (A) (C) In the LUV floatation assay, the protein is incubated with LUVs and mixed with 30% sucrose. A sucrose gradient of 25% and 0% sucrose is created. By centrifugation LUVs and bound protein float to the top fraction of 0% sucrose. Fractions are collected separately and analyzed by SDS-Page and Western-Blot. (D) The binding of HisAcGFP-Spir-2-CT to LUVs, investigated by the LUV floatation assay, revealed binding to all tested negatively charged phospholipids (PA, PI(3)P, PI(4)P, PI(4,5)P2) without any specificity for PI(3)P, but no binding to the neutrally charged POPC. HisAcGFP does not bind to negatively charged liposomes in a control experiment. No protein could be detected in the top fraction in absence of LUVs, validating the assay.

4.1.4 Spir-2 is a monomer in the cytosol

Another feature of FYVE domain which influences their ability to bind to endosomes is their ability to form dimers. Dimerization is mediated through interaction with regions within the FYVE domain or outside the FYVE domain, which vary from protein to protein (108). The FYVE-domain containing proteins EEA, SARA and Hrs have been shown to exist as dimers in intact cells (108). Endosomal targeting of EEA1 is based on a multivalent mechanism in which domain organization and dimerization amplify weak affinity and specificity for the head group of PI(3)P (109).

In order to probe a potential oligomerization of Spir proteins we performed FCS experiments of eGFP-tagged-Spir-2 and their variants in HeLa cells and analyzed the molecular brightness of the green fluorescent protein (**Figure 4.5A,B**). The brightness was normalized to 1x eGFP. As a reference for oligomerization, tandem constructs of 1x eGFP, 2x eGFPs and 3x eGFPs were measured. Accordingly, they showed increasing molecular brightness. Spir-2 and Spir-2-CT exhibit no increasing average brightness compared to 1x eGFP. Hence, Spir-2 occurs as a monomer in the cytosol. In agreement all cytoplasmic variants of Spir-2 (Spir-2-LAFA, Spir-2- Δ Spir-box, Spir-2-C1,2,7,8S) are monomeric. In a further control experiment, the addition of the drug brefeldin A, which leads to a release of Spir proteins from vesicles (**Figure 4.5C**), confirmed the monomeric occurrence of Spir in the cytosol. In addition, HisAcGFP-Spir-2-CT eluted as a monomer from an analytical gel filtration column, indicating a monomeric state in solution (preliminary data of Susanne Dietrich).

While the isolated FYVE domain of Sara forms dimers, the isolated FYVE domain of EEA1 elutes as a monomer from a gel filtration column (108). Also the isolated FYVE domain of Hrs was cytoplasmic, but induced dimerization resulted in vesicle targeting which was depend on PI(3)P binding. This indicates that dimerization is a necessary step for vesicle targeting. The strength of dimerization differs within several

FYVE domains. Moreover, regions outside the FYVE domains can support dimerization for some FYVE domains (108). In contrast Spir-2 does not dimerize in the cytosol and is able to target to vesicles. A dimerization on the vesicles cannot be excluded and needs to be investigated. However, the movement of the small Spir-vesicles impedes brightness analysis of vesicle-bound Spir proteins by FCS. The vesicles are too small and mobile to position the FCS laser focus stably on them. Therefore, other techniques such as FLIM-FRET are more appropriate to probe dimerization on vesicles in the future.

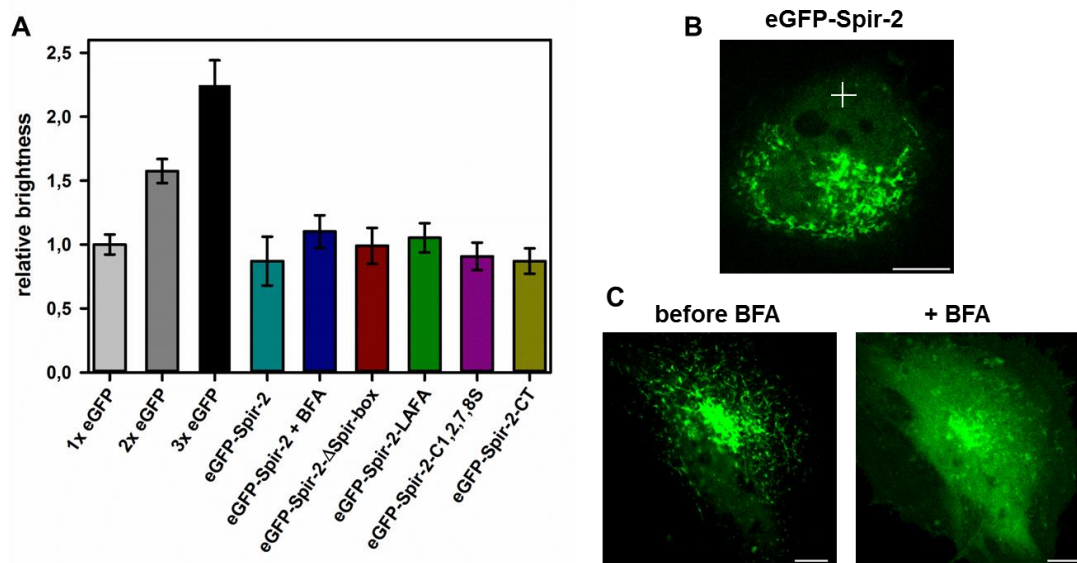


Figure 4.5: Spir-2 occurs monomeric in the cytosol

(A) Brightness analysis of the green fluorescence signal measured by FCS in HeLa cells transiently transfected with pEGFP-C1-Spir-2 and their variants. The mean relative brightness is shown, which is normalized to the brightness of a single GFP molecule, of 5-15 cells \pm SD. The FCS spot was positioned in the cytosol. 1x eGFP, 2x eGFP and 3x eGFP as tandem constructs were transfected and analyzed as reference for dimerization and trimerization. Spir-2-CT, Spir-2 and their variants, which are cytoplasmically distributed, occur monomeric in the cytosol. **(B)** Respective image of the position of the laser focus for FCCS in HeLa cells, marked by a cross. **(C)** By addition of 5 μ g/ μ l BFA, Spir-2 is released from vesicles. Scale bar: 10 μ m

4.2 Cis-regulatory interactions of Spir-2

4.2.1 Preface

Spir proteins were shown to interact with formin subgroup proteins across several species (44,110). In the past years the molecular basis of this interaction was studied in detail. Thus, the structural requirements for the interaction could be narrowed down to the KIND domain of Spir and a short sequence at the C-terminus of the formin subgroup proteins Fmn and Cappuccino called FSI sequence (**f**ormin **s**pire **i**nteraction) (36). Recently, the crystal structure of that complex was solved (45,46), displaying that the interaction is mediated by acidic residues of the Spir KIND domain and basic residues of the FSI sequence (**Figure 4.6B**). The basic residues of the FSI sequence are highly conserved within formin subgroup proteins of different species (**Figure 4.6A**). Interestingly, we found highly conserved basic residues within the Spir-FYVE domain which are homologous to the basic residues of the formin FSI sequence. That brings us to the question if these basic residues of Spir-FYVE can also interact with the acidic residues of Spir-KIND to form an intramolecular complex. Intramolecular interaction as an auto-regulatory element has been identified and well-characterized for formin proteins (22,111). This raises the question if also Spir proteins are regulated by an intramolecular complex.

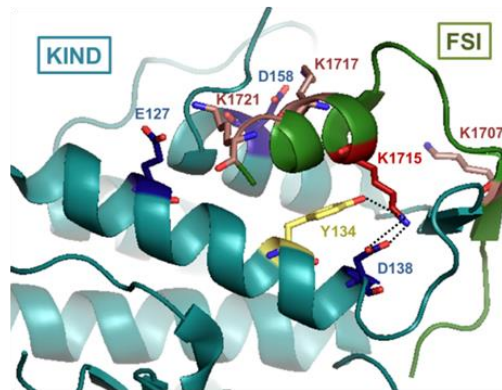
A Spir FYVE

	C1	C2	C3	C4	C5	C6	C7	C8
<i>Spir-1_human</i>	KLQFC	RTRRFSFFT	.WSYT	QQFC	RPVCS	QQCKKMR	LPSK	YSTLP
<i>Spir-1_mouse</i>	KLQFC	RTRRFSFFT	.WSYT	QQFC	RPVCS	QQCKKMR	LPSK	YSTLP
<i>Spir-1_chicken</i>	KLQFC	RTRRFSFFT	.WSYT	QQFC	RPVCS	QQCKKMR	LPSK	YSTLP
<i>Spir-1_zebrafish</i>	KLQFS	RSKKFSLFT	.WSYT	QQFC	RPVCS	QQCKKMR	LPSK	HASLP
<i>Spir-2_human</i>	KIQCC	RAKFP	LS	WPPT	CLFC	RAVCT	SSSI	KMKM
<i>Spir-2_mouse</i>	KIQCC	RAKFP	LS	WPPT	CLFC	RAVCT	SSSV	KMKM
<i>Spir-2_chicken</i>	KVQCC	RAKFP	LS	WPAAC	LF	RSVCS	SSSL	KMKM
<i>Spir-2_zebrafish</i>	KIQCC	RAKFP	LS	WPST	LCLC	RSVCS	SSSA	KMKI
<i>Spir-A</i>	RVCF	LRLTR	FSF	GPWG	IQQ	KL	CTV	CAKCYT

Fmn FSI

<i>Fmn-1_human</i>	SVSKLTSE	KVET	.KK	INPTAS	KER	RQK	EASVTTN
<i>Fmn-1_mouse</i>	SVSKLTSE	KVET	.KK	INPTAS	KER	RQK	EASVATN
<i>Fmn-1_chicken</i>	SVSKLTAE	KVET	.KK	INPTAS	KER	RQK	EANVNAN
<i>Fmn-1_zebrafish</i>	SVRNMTAE	KVET	.RR	AHANG	L	KER	LCM
<i>Fmn-2_human</i>	EVCRQKKG	KS	LYK	.I	PRHDSG	KAK	ISMKT
<i>Fmn-2_mouse</i>	EVCRQKKG	KS	LYK	.V	PRHDSG	KAK	ISMKT
<i>Fmn-2_chicken*</i>	EVCRQKKG	KS	LYN	.I	PKHDSG	KAK	ISMK
<i>Fmn-2_zebrafish</i>	ECFRQVKE	KAT	YS	.V	KPHASG	KAK	IGMK
<i>Capu</i>	KQAQ	IESR	ENV	STKVE	KSGR	ISL	KER

B



C

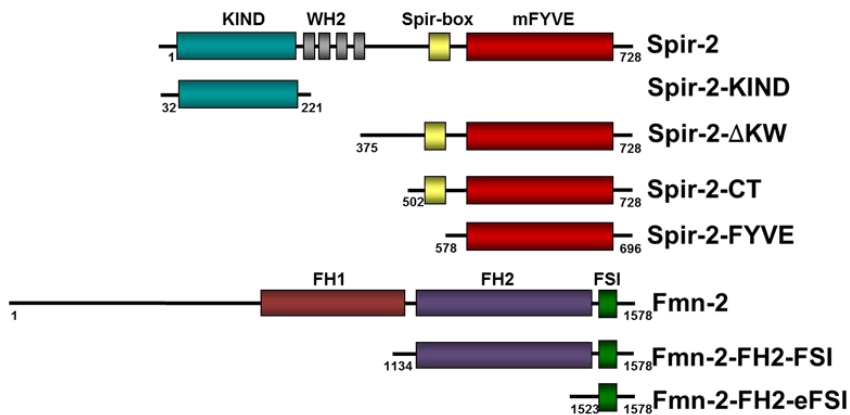


Figure 4.6: Spir-KIND interacts with conserved basic residues of Fmn, also findable in Spir-FYVE

(A) Multiple sequence alignment of Spir-FYVE domain and FSI sequence of formin subgroup proteins of different species. Conserved basic residues (red) in Spir FYVE are homologous to conserved basic residues (red) in FSI, which have been identified to mediate the interaction with Spir-KIND. Conserved hydrophobic residues are highlighted in green. Alignment by the courtesy of Susanne Dietrich (B) Crystal structure of the interaction surface of Spir-1-KIND (cyan) and Fmn2-FSI (green) displaying acidic residues (blue, yellow) of Spir-KIND mediates the interaction with basic residues (red, pink) of Fmn2-FSI. The tertiary structure was taken from Protein data bank PDB ID 2YLE and edit with Pymol. (C) Domain structures of Spir-2 and Fmn-2 and their variants used in the following studies.

4.2.2 Identification of an intramolecular Spir-2-interaction

Fluorescence cross-correlation spectroscopy (FCCS) is an ideal tool to address specific interactions. With single-color FCS the concentration and diffusion times of single-labeled molecules can be determined. In its dual-color extension (FCCS), using two differently labeled interaction partners, both detection channels are simultaneously recorded to obtain auto-correlation curves in each color channel (**Figure 4.7A**, red and green) and additionally the signal between the two spectral channels is cross-correlated (**Figure 4.7A**, blue). The cross-correlation amplitude is proportional to the fraction of codiffusing particles, indicating molecular interactions. By using FCCS with the two potential interactions partners Alexa⁶⁴⁷-labeled Spir-2-KIND and HisAcGFP-Spir-2-CT we discovered a hitherto unknown interaction of Spir-2-KIND with the C-terminus of Spir-2 showing cross-correlation of $18.46 \pm 5.1\%$ (\pm SD) (**Figure 4.7A,B**). In a control experiment the interaction of HisAcGFP with KIND*Alexa647 and HisAcGFP with Alexa⁶⁴⁷ were measured and showed cross-correlation below 2%, indicating that the contribution of unspecific interaction between the protein domains and the dyes were very low (**Figure 4.7B**, grey). The measured cross-talk from the green channel into the red channel was below 1%, so that a cross-talk correction is not necessary for further FCCS studies with these chosen dyes (99,112). Furthermore, in a GST-pulldown assay the interactions of Spir-2-KIND and the C-terminus of Spir could also be confirmed (**Figure 4.7C**, right).

The Y134K mutant of human Spir-1-KIND (**Figure 4.6B**, yellow stick) has been reported to result in a drastically reduced interaction to the formin construct, Fmn2-FH2-FSI (46). The Y134K mutant of Spir-1-KIND corresponds to the Y120K mutant of Spir-2-KIND. Congruently, the Y120K mutant of Spir-2-KIND did not bind to Fmn2-FH2-FSI (**Figure 4.7C**, left), probed by a GST-pulldown assay. Interestingly, beyond that the Y120K mutant of Spir-2-KIND bound

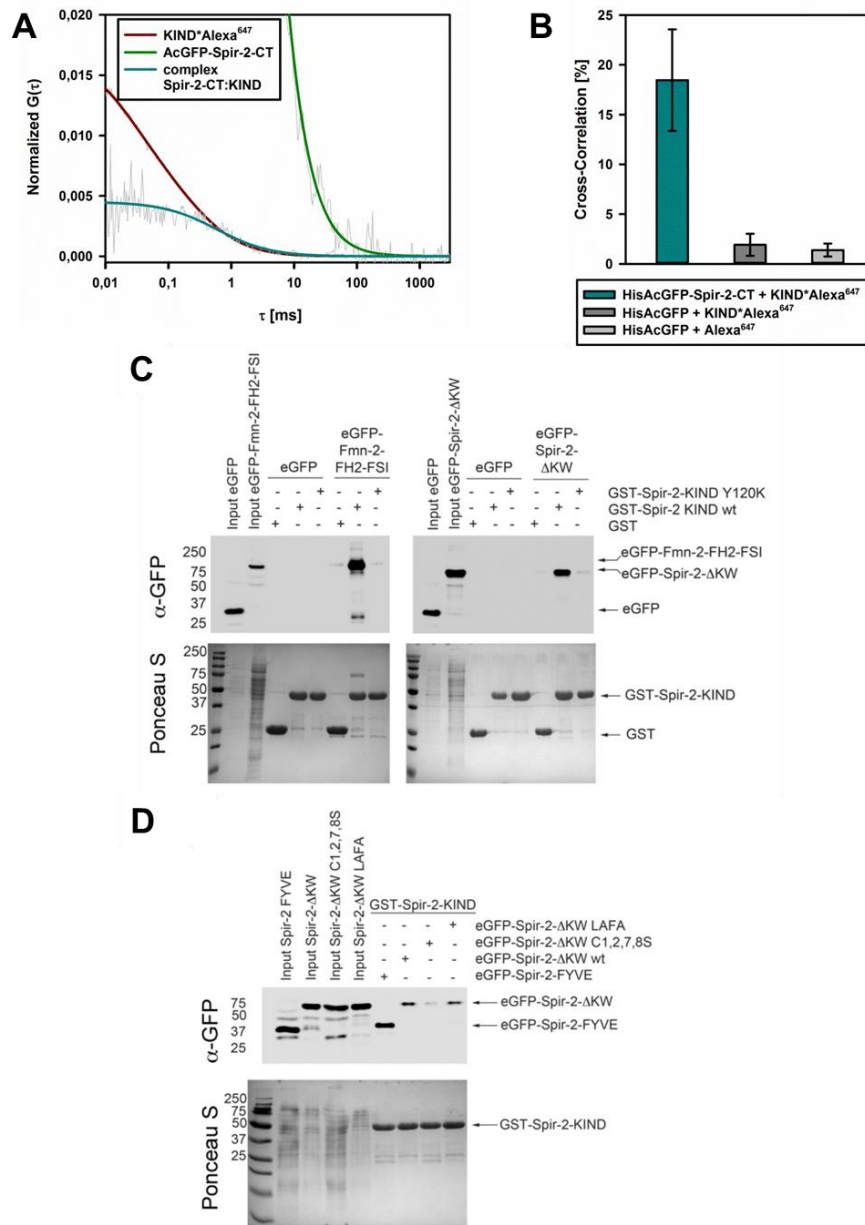


Figure 4.7: Spir-2-KIND interacts with the C-terminus of Spir-2

Interaction studies by FCCS (A-B) and GST-pulldown assay (B-D) (A) Measurement of Spir-2-KIND and Spir-2-CT interaction by FCCS in solution. The fitted autocorrelation curves of HisAcGFP-Spir-2 (green) and KIND*Alexa⁶⁴⁷ (red) are shown. The amplitude of the fitted cross-correlation curve (blue) indicates formation of Spir-2-CT:KIND complex. (B) The control experiments (grey) indicates very low unspecific binding of the dyes and proteins compared to the Spir-2-CT:KIND complex formation (blue). Errors bars represent \pm SD (C) GST-pulldown assay displaying the interaction of Spir-2-KIND with eGFP-Fmn-2-FH2-FSI (left) and interaction of Spir-2-KIND with the C-terminus of Spir-2 (right). Both eGFP-tagged Fmn-2-FH2-FSI and Spir-2- Δ KW interact only with GST-Spir-2-KIND wt and not with the Spir-2 Y120K mutant. (D) Spir-2-KIND interacts with the FYVE domain of Spir-2. Disruption of the integrity of the FYVE zinc-finger by mutation of the coordinating cysteines markedly reduces the binding of Spir-2- Δ KW to the KIND-domain. GST-pulldown data by the courtesy of Eugen Kerkhoff.

neither to the C-terminal part of Spir-2 (**Figure 4.7C**), indicating that the cis- and transregulatory interactions bind an overlapping region on the surface of the KIND domain.

To narrow down the structural elements in the C-terminus of Spir-2 that are required for binding to the KIND domain, GST-pull-downs were performed with the isolated FYVE domain, a Spir-2- Δ KW variant that has mutations in the turret loop (Spir-2- Δ KW LAFA) and a mutant in which the integrity of the FYVE zinc finger was disrupted by mutating two of the four cysteines in each of the two zinc coordinating centers (Spir-2- Δ KW-C1,2,7,8S). As shown in **Figure 4.7D**, GST-Spir-2-KIND binds to eGFP-tagged Spir-2-FYVE indicating the FYVE domain is necessary and sufficient for binding KIND. This finding is validated by the observation that the FYVE-disintegrated Spir-2- Δ KW C1,2,7,8S construct is unable to bind Spir-2-KIND. On the other hand mutations within the turret loop of FYVE (Spir-2- Δ KW LAFA) did not significantly affect the binding.

4.2.3 Quantification of the intramolecular Spir-2-interaction

In order to quantify the newly-discovered Spir-2-KIND/Spir-2-FYVE interaction we used two assays to determine dissociation constants. The electrochemiluminescence immunoassay (EIA) is an established assay to study and quantify protein-protein interactions (96,97). In this assay small electrodes of a multi-well plate are coated with Spir-KIND and incubated with different concentrations of HisAcGFP-Spir-2-CT until saturation values. Anti-GFP-antibodies were used for protein detection and anti-rabbit-STAG antibodies for the electrochemiluminescence reaction. (**Figure 4.8A**). HisAcGFP was utilized as a negative control and did not show unspecific binding (data not shown). By applying a 1:1 binding model we obtained an apparent K_d of 15.97 ± 6.38 nM (\pm SE). To confirm the strength of interaction we used a second approach, based on FCCS measurements of HisAcGFP-SpirCT and Spir-2-KIND*Alexa⁶⁴⁷ (**Figure 4.8B**). By titrating KIND*Alexa⁶⁴⁷ to

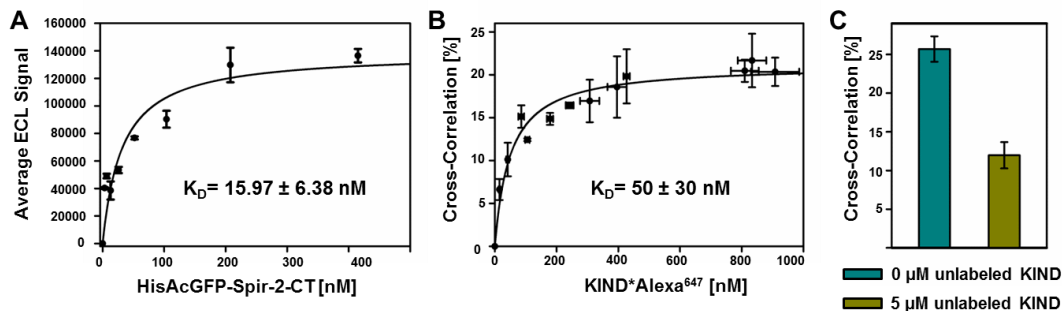


Figure 4.8: Quantification of Spir-2-KIND/Spir-2-CT interaction

(A) Binding of HisAcGFPSpir-2-CT to Spir-2-KIND measured by EIA. The binding was quantified by fitting a one-site binding model Eq. 3.1 (B) Binding of Spir-2-KIND*Alexa⁶⁴⁷ (0-1000 nM) to HisAcGFPSpir-2-CT (25±5nM) by FCCS. The binding curve was fitted by Eq.3.10 (C) The complex formation of HisAcGFP-Spir-2-CT and Spir-2-KIND*Alexa⁶⁴⁷ is a reversible process which could be partially dissolved in a competition experiment with 5 μM unlabeled KIND measured by FCCS. Error bars represent ± SD.

HisAcGFP-SpirCT we achieved single-phase hyperbolic binding curves from where we could calculate a K_d of 50±30 nM (±SE) accordingly to Equation 3.10. This dissociation constant is in the same order of magnitude as the dissociation constant obtained by EIA. The small discrepancy can be a result of the necessity of labeling of Spir-2-KIND in the FCCS experiment, which might interfere with the interaction surface and lower the binding affinity, whereas in the EIA experiment unlabeled Spir-2-KIND could be used. The Spir-2-CT:Spir-2-KIND complex could be partially dissolved in a competition experiment with unlabeled Spir-2-KIND, confirming the validity of the newly discovered interaction (Figure 4.8C).

The dissociation constant of the Spir-2-KIND/Spir-2-CT interaction is in the range of the published dissociation constant of the Spir-2-KIND/Fmn-2-eFSI interaction ($k_d = 60$ nM), probed by fluorescence anisotropy (36), indicating competing cis- and trans-regulatory interactions.

4.2.4 Membrane binding regulates the intramolecular Spir-2 interaction

In the previous chapter we discovered, that N-terminal Spir-2-KIND interacts with the C-terminal part of Spir-2. Surprisingly, this intramolecular interaction is drastically reduced, when measuring on the membrane of GUVs (**Figure 4.9A**, red) compared to measurements in solution (**Figure 4.9A**, blue). The cross-correlation value on the membrane is almost on the level of the negative controls (**Figure 4.9A**, grey). As shown in **Figure 4.9B** in the presence of GUVs HisAcGFP-Spir-2-CT is still able to bind to the membrane (**a**) whereas Alexa⁶⁴⁷labeled-KIND remains in solution and is not targeted to the membrane (**b**).

The Laser focus is positioned on the pole of GUVs and by applying a 2D3D-fit model to the FCS measurements the concentration of the membrane-bound fraction of Spir-2-CT can be determined. Thus, we monitored no significant changes in the concentration of bound Spir-2-CT molecules on negatively charged GUVs in the presence and absence of Spir-2-KIND (**Figure 4.9C**). In contrast, the concentration of Spir-2-CT molecules bound to neutrally charged GUVs was very low, validating the approach to measure differences in membrane binding properties.

In living cells Spir-2-CT binds to vesicles, whereas Spir-2-KIND shows a cytoplasmic distribution and is not able to target to vesicles (**Figure 4.9D**). These results are in good agreement with the binding studies on GUVs and denote that the membrane binding properties of Spir-2 are not affected by the intramolecular interactions.

From these findings, it can be hypothesized that the membrane could function as a regulatory element to open the intramolecular complex.

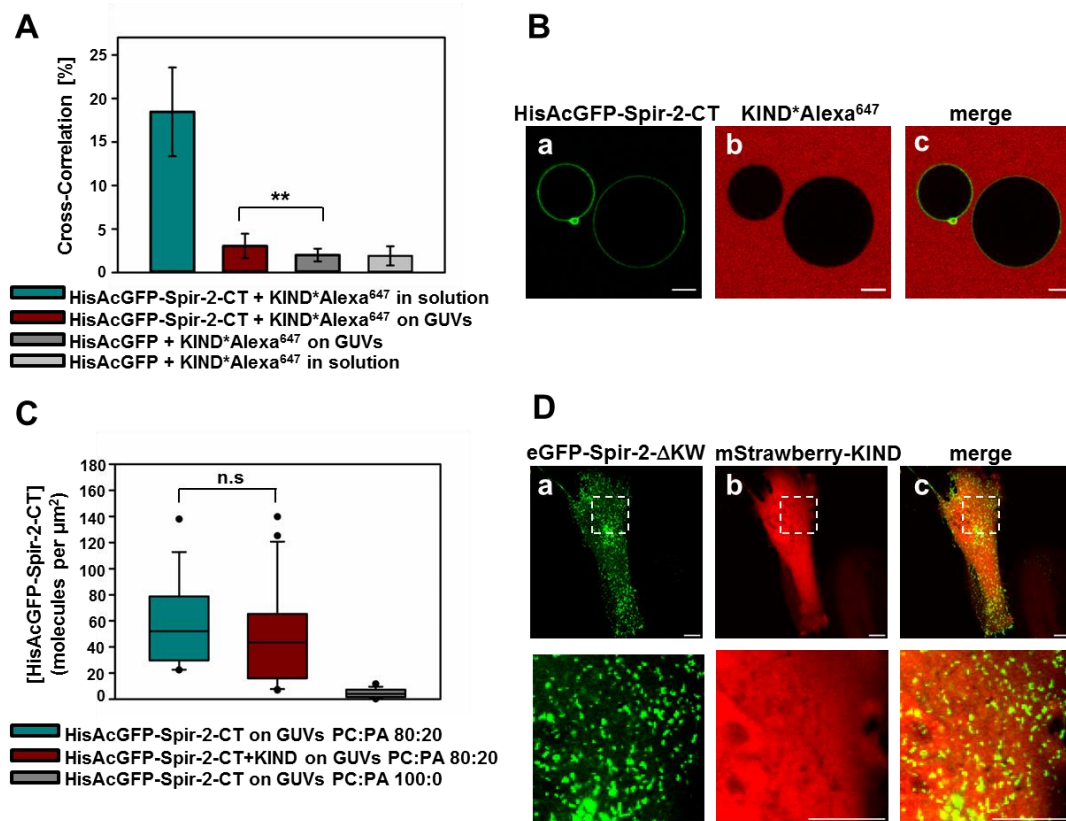


Figure 4.9: Membrane binding regulates the intramolecular Spir-2-KIND/Spir-2-CT interaction

(A) The cross-correlation of formed Spir-2-KIND/Spir-2-CT complex in solution (blue) is drastically reduced when measuring on the pol of GUVs (red) by FCCS. Negative controls with HisAcGFP were performed in solution and on GUVs (grey). Errors bars represent \pm SD ($n=10-24$), $**p<0.01$. **(B)** Confocal images show HisAcGFP-Spir-2-CT bound to GUVs **(a)** and KIND*Alexa⁶⁴⁷ remaining unbound in solution **(b)**. **(C)** Spir-2-CT molecules bound to GUVs in the membrane focal area of GUVs (DOPC:DOPA 8:2) measured by FCS in absence (blue) and presence of Spir-2-KIND*Alexa⁶⁴⁷ (red) does not significantly change. In contrast a very low concentration of Spir-2-CT is bound to neutrally charged GUVs (grey). n.s = not significant ($n=15-25$) **(D)** Confocal images of eGFP-Spir-2-ΔKW **(a)** and mStrawberry-KIND **(b)** in HeLa cells reveal Spir-2-CT bound to vesicles whereas Spir-2-KIND shows cytoplasmic localization. Scale bar: 10 μm.

4.2.5 Fmn-2-eFSI regulates the intramolecular Spir-2 interaction

The discovery of the hitherto unknown interaction of the C-terminal FYVE domain with the N-terminal KIND domain of Spir-2 and the high homology of the conserved basic residues of the Spir-FYVE domain and Fmn-2-FSI leads us to the questions if Spir-FYVE and Fmn-2-FSI compete for the interaction with Spir-KIND. Also the involvement of the amino acid Y134 in both interactions, as shown in chapter 4.2.2, backs up the assumption of overlapping interfaces and competing interactions. To probe this assumption, we performed FCCS and GST-pulldown measurements in the absence and presence of Fmn-2-eFSI, which is a variant containing the last 55 amino acids of the C-terminus of Fmn-2. In the FCCS experiment, the Spir-2-KIND/Spir-2-CT interaction is markedly decreased in the presence of μM concentrations of Fmn-2-eFSI (**Figure 4.10A**) and is even abolished in the GST-pulldown assay (**Figure 4.10C**). The effect is specific for Fmn-2-eFSI, so BSA cannot reduce the Spir-2-KIND/Spir-2-CT interaction (**Figure 4.10B**). Moreover, the Fmn-2-FH2-FSI construct, which is an enlarged sequence of Fmn-2-eFSI and additionally encodes the FH2 domain and shows a lower affinity to KIND (36), was tested. This construct is also able to reduce the Spir-2-KIND/Spir-2-CT interaction (**Figure 4.10D**). These results indicate that the Spir-2-KIND domain can either interact with the Spir-FYVE domain or with the Fmn-2-FSI motif, but not with both at the same time.

Furthermore, the addition of EDTA, which removes the zinc ions, and the disruption of the FYVE motif each resulted in reduced Spir-FYVE/Spir-KIND interaction, confirming the importance of the integrity of the FYVE domain for the interaction, which is maintained by addition of ZnCl_2 (**Figure 4.10D**).

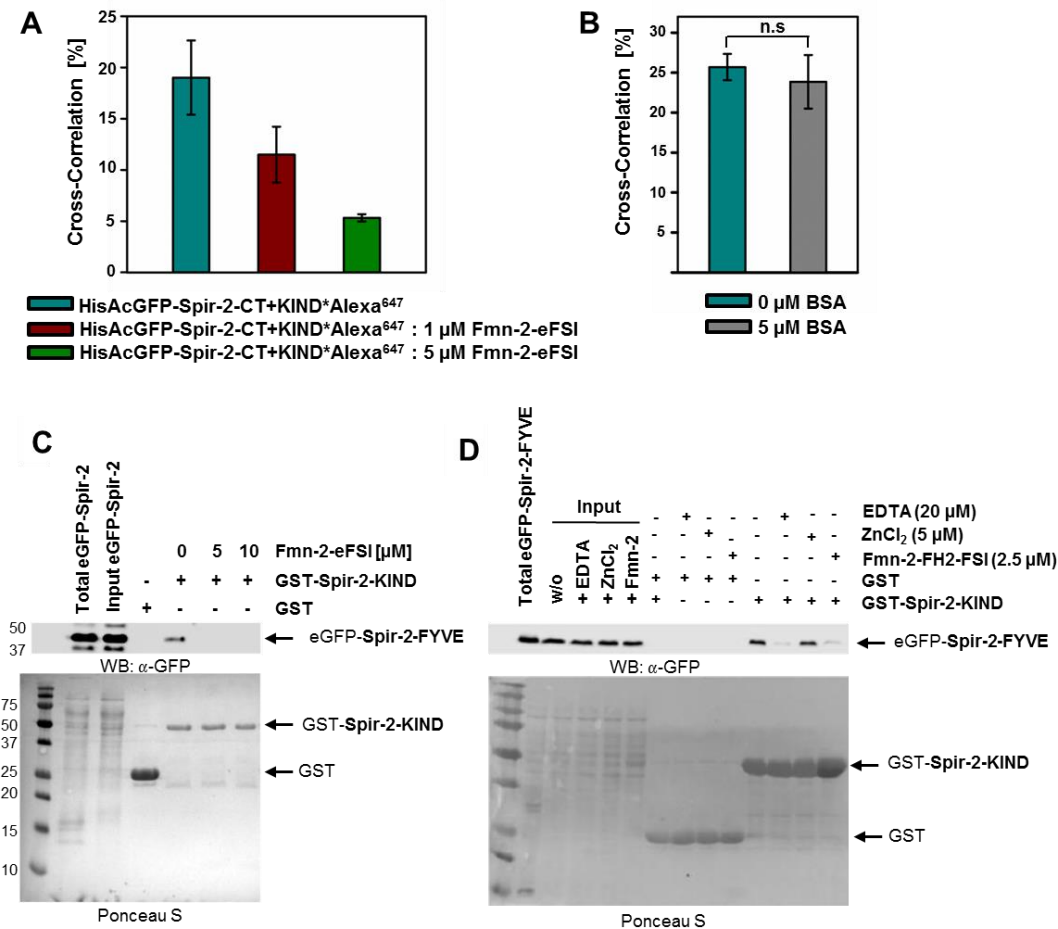


Figure 4.10: Fmn-2-eFSI regulates the intramolecular Spir-2-KIND/Spir-2-CT interaction

(A) Competitive interactions were tested by FCCS. Cross-correlation of Spir-2-CT/Spir-2-KIND was decreased by increasing concentrations of eFSI. (B) In a control experiment, BSA did not reduce the cross-correlation of Spir-2-CT/Spir-2-KIND. Error bars represent \pm SD, n.s.=not significant. (C) A pull-down assay of GST-Spir-2-KIND and eGFP-Spir-2-FYVE in absence and presence of Fmn-2-eFSI revealed abolished Spir-2-KIND/Spir-2-FYVE interaction in the presence of Fmn-2-eFSI. (D) GST-pulldown assay displayed reduced Spir-2-KIND/Spir-2-FYVE interaction in the presence of EDTA and Fmn-2-FH2-FSI. Untreated condition and ZnCl₂-addition allows Spir-2-KIND:Spir-2-FYVE interaction. GST-pulldown data by the courtesy of Eugen Kerkhoff.

4.3 Trans-regulatory interactions of Spir-2

4.3.1 Spir interacts with Arf1 protein

The ADP-ribosylation factors (Arfs) of the Ras superfamily play a crucial role in membrane trafficking within the exo- and endocytic pathways (70). Arf family small G proteins are considered to be molecular switches which regulate binding and the release of coat proteins that polymerize on membrane to form transport vesicles (70,113,114). During the first attempts to identify regulatory elements of vesicle-associated Spir proteins, the lab of Eugen Kerkhoff discovered that the drug brefeldin A caused a rapid (within minutes) and reversible release of Spir proteins from the vesicle membranes, as also shown in chapter 4.1.4. **Figure 4.5C**. Brefeldin A (BFA) is a fungal toxin which affects the activity of a subset of Arf proteins by blocking the GDP/GTP exchange by binding to the Arf-GDP-Sec7 domain complex (115). Treating cells with BFA results in a rapid release of Arf1 and Golgi-associated coat proteins from the Golgi (116,117). Taken together, the release of Spir-2 proteins from vesicular membranes by BFA and colocalization of Spir-2 and Arf1 in HeLa cells suggested that Spir-2 could be an Arf1 effector (unpublished data of Eugen Kerkhoff).

In order to confirm this assumption we probed a potential interaction of Spir proteins with Arf1 in solution (**Figure 4.11A**) and on membranes (**Figure 4.11B**) by two different techniques. Arf1 Δ Helix is a variant which lacks the N-terminal amphipathic helix (17 residues) as well as the myristoyl group. It possesses an improved solubility and enables an efficient guanine nucleotide exchange in the absence of a GEF without the requirements of detergents or phospholipids (118). Arf1 Δ Helix was exchanged with non-hydrolyzable GTP and GDP analogues GTP γ S and GDP β S and the success was confirmed by a C18 reversed phase chromatography. A GST-pulldown assay employing the GTP γ S- and GDP β S-loaded form of Arf1 Δ Helix and GST-Spir-2- Δ KW

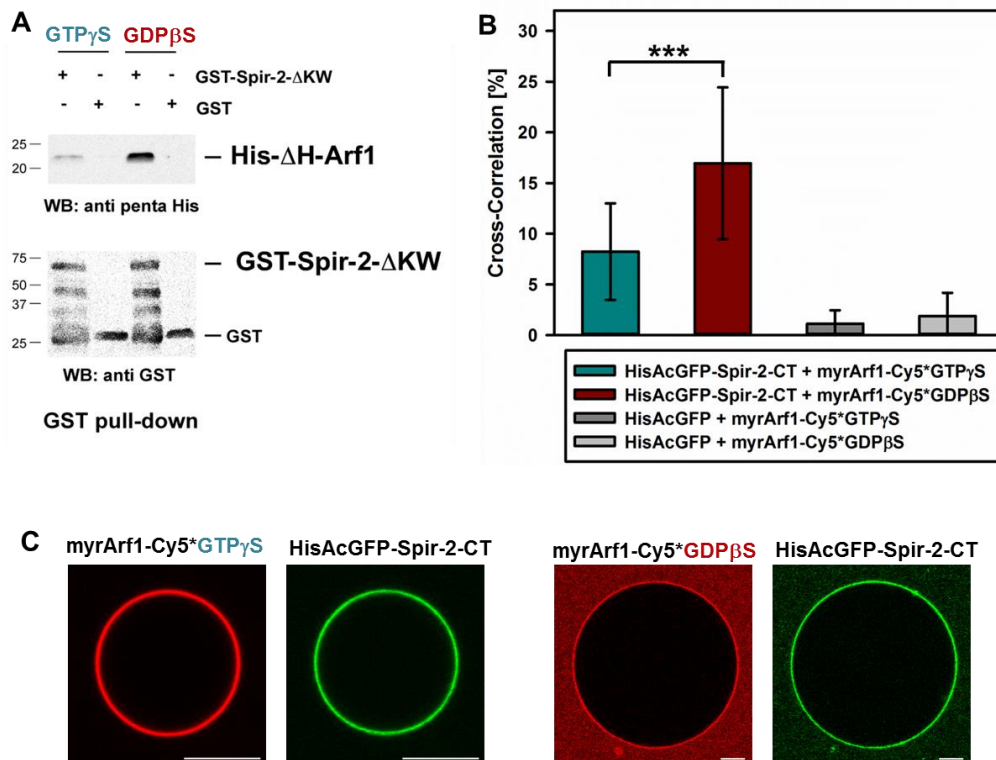


Figure 4.11: Spir-2 binds to Arf1, preferentially to the GDP-bound form

(A) GST-pulldown shows interaction of C-terminal Spir-2 variant (Spir-2- Δ KW) and the variant His Δ H-Arf1, lacking the helix and myristoylation responsible for membrane binding. GST-pulldown image by courtesy of Annette Samol. (B) The cross-correlation of Spir-2-CT/myrArf1 complex formation with myrArf1 bound to GUVs (DOPC:DOPA) in the GTP γ S bound form (blue) and GDP β S bound form (red). Negative controls with HisAcGFP attached on GUVs by DOGS-(Ni)NTA were performed accordingly (grey). Error bars represent \pm SD (n=10-30), ***p<0.001. (C) Confocal images of myrArf1-Cy5 loaded with GTP γ S and GDP β S and HisAcGFP-Spir-2-CT bound to GUVs (DOPC:DOPA 8:2). Scale bar: 10 μ m

revealed an interaction of Spir-2-CT with Arf1. Surprisingly, we found that GDP β S-loaded Arf1 interacts much stronger with Spir-2-CT than the GTP γ S-loaded form (Figure 4.11A). To gain further support for this unconventional interaction with the GDP-loaded small G protein, we probed the interaction of GTP- and GDP-bound form of Arf1 at membranes in a biomimetic membrane system. Membrane binding of Arf1 proteins requires the N-terminal myristoylation, as well as the N-terminal amphipathic helix (93,119). Therefore, Arf1 was coexpressed in bacteria with N-myristoyltransferase NMT1 to generate myristoylated

Arf1. The success of myristoylation was confirmed by mass spectroscopy. In order to investigate Spir/Arf1 interaction on GUVs by FCCS we inserted an extra C-terminal cysteine for labelling with the dye Cy5. This C-terminal labelling has been reported not to influence the function of the protein (85,120). As shown in **Figure 4.11B**, FCCS measurements of HisAcGFP-Spir-2-CT and the GTP γ S- and GDP β S-loaded form of myrArf1-Cy5 revealed an interaction of Spir-2-CT and myrArf1 on the membrane of GUVs. In agreement with the GST-pulldown assay, the GDP β S form of Arf1 showed a significant stronger interaction with Spir-2-CT than the GTP γ S-loaded form. In a negative control experiment HisAcGFP was attached to GUVs containing DOGS-(Ni)NTA for binding via His-tag and the cross-correlation by unspecific interactions was very low. In addition to these findings, the lab of Eugen Kerkhoff performed colocalization studies in HeLa cells and found a higher colocalization to the constitutively GDP-bound Arf1-mutant T31N than to the GTP-bound Arf1-mutant Q71L (unpublished data, not shown), supporting our interaction studies. Taken together, these data show that Spir-2 interacts preferentially with the GDP-bound form of Arf1.

4.3.2 Spir-Arf1 interaction does not influence their binding properties

The discovery of an interaction between Spir-2 and Arf1, preferentially in the GDP-bound form led us to the question of the function of that interaction. Arf1 is known to recruit coat proteins to budding vesicles and modulates actin structures (121-123). We wanted to probe if Arf1 can also recruit Spir proteins to vesicles as it does for coat proteins. Since the interaction is stronger in the GDP-bound form, which represents the inactive, cytosolic form (115), the effect could be also vice versa. Thus, we probed if cytosolic Arf1 proteins are stabilized on the membrane by Spir-2. As already seen in the previous section (**Figure 4.11C**) myrArf1 and Spir-2-CT bind both to negatively charged GUVs. By applying the Atto⁶⁵⁵-labelled variant Arf1 Δ H, lacking the

amphipathic helix and myristoyl group, on negatively charged GUVs we found that Arf1 Δ H does not bind to the membrane, while Spir-2-CT is membrane-bound, independent on the GTP- or GDP-bound form of Arf1 Δ H (**Figure 4.12A,B**). Consequently, the interaction is neither in solution nor on membrane strong enough to target or stabilize the membrane-binding deficient variant of Arf1 on membranes. Interestingly, the interaction of Arf1 and Spir-2-CT, seen in the pulldown assay in solution, could not be detected in solution by FCCS (data not shown). FCCS is a technique which is able to measure only strong interactions with binding affinities in the nM range (91,99,100), whereas pulldown-assay can detect interactions in μ M range (124), indicating that the Spir-2-CT/Arf1 interaction probably is of low nature in solution.

To probe the case if Arf1 proteins can recruit Spir proteins to membranes as it does for several effector proteins, we used neutrally charged GUVs, where Atto⁶⁵⁵-labeled-myrArf1 can bind only in the GTP γ S-loaded form (**Figure 4.12C**) but not in the GDP β S-bound form (**Figure 4.12D**). These phenomena have already been described for Arf1 binding to LUVs (125). This helps probe the targeting interactions of Spir proteins to GUVs by Arf1 proteins, since we found out (as shown in chapter 4.1.3) that Spir proteins do not interact with neutrally charged phospholipids. However, Spir proteins remain non-membrane-bound even in the presence of membrane-bound Arf1 proteins (**Figure 4.12C**). The shown stronger interaction of Spir to the GDP β S-form of Arf1 raises the question if the GDP β S-bound Arf1 can recruit Spir to the membrane. In chapter 4.1.3 we showed that Spir is not able to bind to GUVs containing only 3% PA. By incorporating 3% PA into GUVs we found that Arf1-GDP β S bound to GUVs, but Spir remained in solution (**Figure 4.12E**). Furthermore, by coexpressing mStrawberry-Arf1 and the variant eGFP-Spir-2-LAFA, which, as we found in chapter 4.1.2, loses the membrane binding property, we revealed that mStrawberry-Arf1 is bound to the Golgi, whereas eGFP-Spir-2-LAFA remains cytoplasmic in HeLa cells (**Figure 4.12F**). This result confirms the previous observation

on GUVs that Spir is not recruited to vesicle membranes by Arf1. Altogether, these findings indicate that the interaction between Spir and Arf1 proteins does not influence each other's targeting and membrane binding properties. Presumably, the binding affinity for Spir and Arf1 is very low in solution and most likely increased when both proteins are membrane-bound.

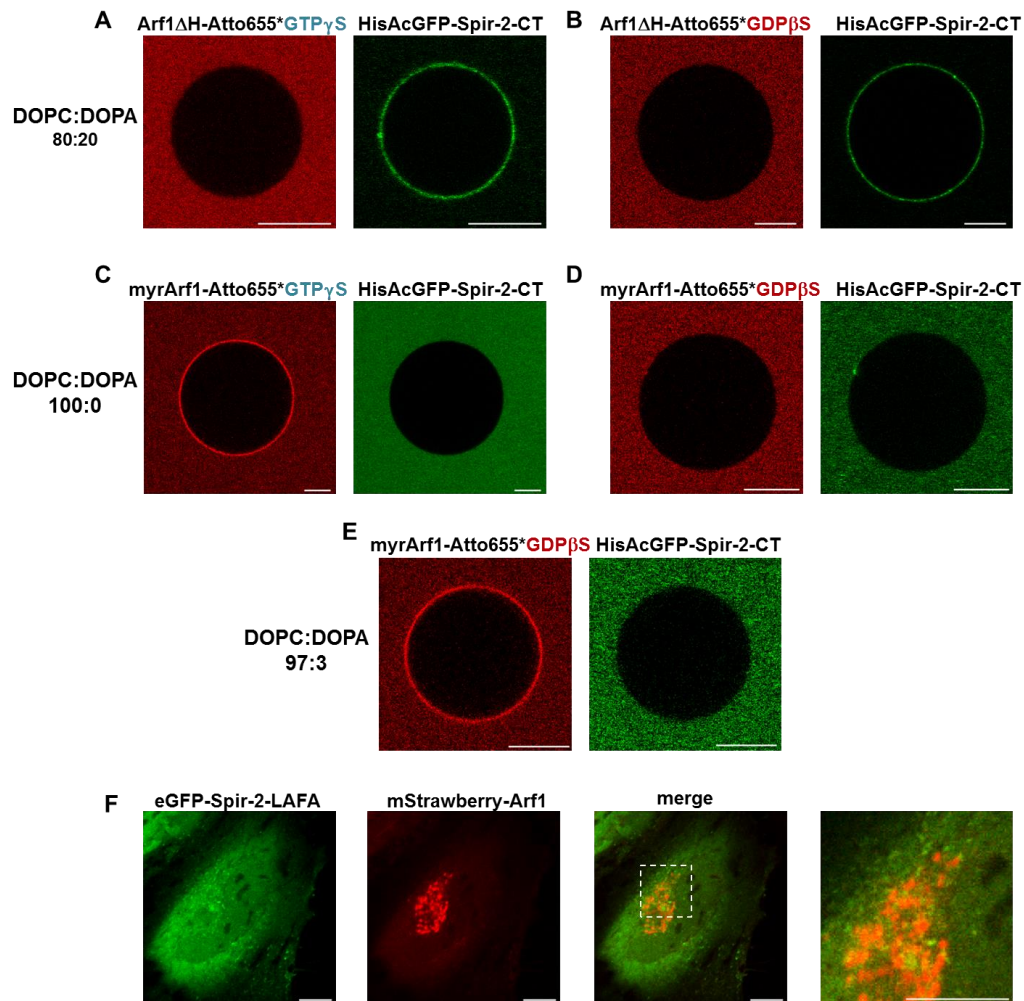


Figure 4.12: Spir-2 and Arf1 do not influence each others membrane binding properties

(A-B) Confocal images of Atto⁶⁵⁵-labeled Arf1 Δ H (His-Arf1 Δ H-KCK, KCK inserted for labeling) in the (A) GTP γ S and (B) GDP β S loaded form and HisAcGFP-Spir-2-CT solely bound to negatively charged GUVs (DOPC:DOPA 8:2) (C-D) Atto⁶⁵⁵-labeled myrArf1 can bind to neutrally charged GUVs (DOPC) only in the (C) GTP γ S form but not in the (D) GDP β S form, where no HisAcGFP-Spir-2-CT is able to bind either. (E) GDP β S loaded myrArf1 can bind to GUVs, when 3% PA is incorporated, but no HisAcGFP-Spir-2-CT is targeted to the membrane. (F) Coexpressing the membrane-binding deficient variant eGFP-Spir 2-LAFA and mStrawberry-Arf1 in HeLa cells shows, that Spir remains cytoplasmic and is not recruited to the vesicles where Arf1 is bound. Scale bar: 10 μ m

4.3.3 Spir-2 interacts with myosin Vb

Along with the Arf subfamily, the Rab subfamily also belongs to the Ras superfamily and both subfamilies are found to regulate several different intracellular transport processes. Spir/formin-2 dependent vesicular protrusion outgrowth from Rab11a vesicles has been shown to mediate long-range vesicle transport in mammalian oocytes (49). The transport along the actin tracks was found to be dependent on the motor protein myosin Vb. Interestingly, Rab11a has been reported to interact with the globular myosin Vb tail domain (74). After the first description of the functional relationships of Spir-2 with these potential interaction partners, we wanted to go into detail and find the evidence for these interactions. We coexpressed eGFP-tagged Spir-2 and mStrawberry-tagged truncated myosin Vb which contains the C-terminal coiled coil structure and the tail domain known to be sufficient for interaction with Rab11a and membrane binding. As seen in **Figure 4.13A**, we found a high colocalization of Spir-2 and myosin Vb-cc-tail as well as of Spir-2 and Arf1 and partial colocalization of Spir-2 with Rab11a, confirming previous observations by the group of Eugen Kerkhoff (104). As described in the previous section the drug brefeldin A caused a release of Spir proteins as well as of Arf1 proteins from vesicles (**Figure 4.13B**). When Rab11a is coexpressed, its localization is not affected by the drug, but Spir-2 is released into the cytosol. Surprisingly, upon coexpressing myosin Vb-cc-tail, Spir-2 is retained on the vesicles, even in the presence of brefeldin A and a complete colocalization of Spir-2 and myosin Vb is observed, indicating interactions of Spir-2 and myosin Vb.

In order to probe the potential interactions, we performed FCCS measurements in the cytosol of HeLa cells transiently expressing eGFP-Spir-2 and coexpressing mStrawberry-Arf1, mStrawberry-Rab11a or mStrawberry-myosinVb-cc-tail in the presence of brefeldin A (**Figure 4.14A**). We were able to detect an interaction of Spir-2 and myosin Vb with 14% cross-correlation in the cytosol. This interaction was validated by performing a negative control experiment of coexpressing eGFP and mStrawberry-myosinVb as well as eGFP-Spir-2 and

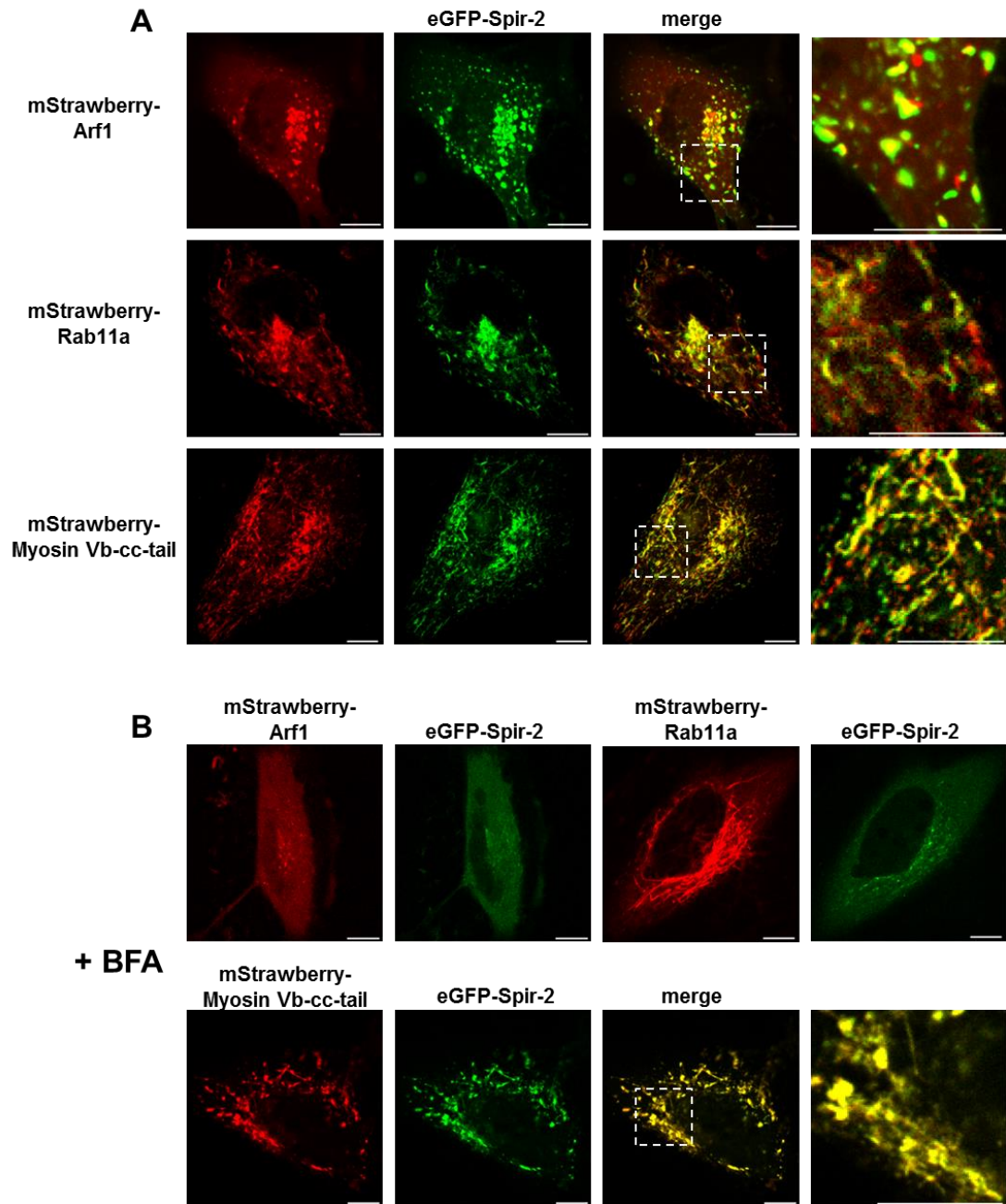


Figure 4.13: Spir-2 forms a stable complex with myosin Vb-cc-tail

(A) Confocal images of HeLa cells transiently expressing eGFP-Spir-2 and coexpressing mStrawberry-Arf1, mStrawberry-Rab11a or mStrawberry-myosin Vb-cc-tail. Spir-2 colocalizes with Arf1 and myosin Vb-cc-tail and partially with Rab11a (B) Addition of 5 μ g/ml brefeldin A (BFA) caused a cytoplasmatic distribution of Spir-2 when coexpressing Arf1 or Rab11a, but Spir-2 remained bound on vesicles when coexpressing myosin Vb-cc-tail. Scale bar: 10 μ m

mStrawberry, which show cross-correlation significantly below the cross-correlation of Spir-2 and myosin Vb. The positive control of a double labeled eGFP-linker-mStrawberry construct revealed a maximal cross-correlation of 50%. In contrast Spir-2 does not interact with Arf1 and Rab11 in the cytosol of the cell, proven by cross-correlation values in the range of the negative control.

Cells are highly compartmentalized and these endogenous membranes are associated with the Golgi complex or endoplasmatic reticulum and normally located on one side of the nucleus. Cytoplasmic regions which are more stable and homogenous are located at the opposite side and were used to position the laser spot for FCS measurements (**Figure 4.14B**) (100). To take into account slow instabilities inside the cellular environment a 2-component fit model with a small fraction of an additional slow diffusion time (milliseconds) was applied (100). For *in vivo* FCCS we chose the fluorophores eGFP and mStrawberry, which have the disadvantage of eGFP showing cross-talk into the ‘wrong’ red channel, which we corrected according to an established mathematical formalism for dual-color FCCS (91,99).

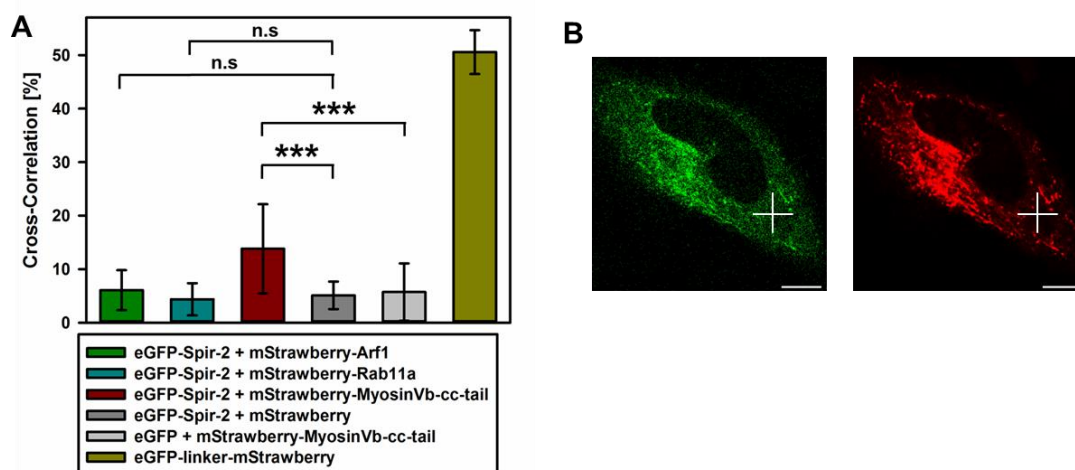


Figure 4.14: Spir-2 interacts with myosin Vb-cc-tail in the cytosol

(A) FCCS in HeLa cells of eGFP-Spir-2 and coexpressing mStrawberry-Arf1, mStrawberry-Rab11a, mStrawberry-myosin Vb-cc-tail or mStrawberry (negative control) in the presence of 5 μg/μl brefeldin A. Errors bars represent ± SD (n=10-30),***p<0.001, n.s.=not significant **(B)** Respective image of the position of the laser focus for FCCS in the green and red channel in HeLa cells. Scale bar: 10 μm

Rab11a, Arf1, myosin Vb and Spir localize to vesicles which leads us to the question if these proteins interact with each other on vesicles, even if we did not detect any interaction in the cytosol. However, FCCS analysis of proteins bound to intracellular vesicles is rather difficult. It requires either rapidly transported vesicles with homogeneous bound protein concentrations or relatively static large endosomal structures where the FCS spot can be stably positioned (91). Spir-2 vesicles are too small and mobile, but not rapid enough to perform proper FCCS experiments on vesicles in living cells. Therefore, other techniques such as FLIM-FRET are more appropriate to probe interactions on vesicles. FLIM-FRET has the advantage of detecting and spatially resolving protein-protein interactions. We performed fluorescence lifetime imaging with HeLa cells, transiently expressing eGFP- and mStrawberry-labeled constructs. To extract the mean fluorescence lifetime, the decay curves were fitted with a mono-exponential function. 5 vesicles of each cell were analyzed and averaged and 10-23 cells per sample were measured. As shown in **Figure 4.15A,B**, eGFP-myosin Vb-tail (donor only sample) has an average lifetime of 2.53 ± 0.07 ns (\pm SD) **(a)**, which is markedly reduced to 2.17 ± 0.12 ns when mStrawberry-Spir-2- Δ KW is coexpressed (donor + acceptor sample) **(b)**, indicating an interaction of myosin Vb-tail and Spir-2- Δ KW, lacking the KIND and WH2 domains. In a negative control experiment, eGFP-myosin Vb-tail and mStrawberry were coexpressed **(c)** and showed no reduction in the average lifetime (2.57 ± 0.01 ns), validating the experiment. In a positive control experiment, eGFP was linked to mStrawberry by a linker of 5 flexible amino acids (ASGAG) and showed an average lifetime of 2.06 ± 0.1 ns **(d)**. Applying a mono-exponential decay model is appropriate as a first step to detect a reduction of fluorescence lifetime, and thereby interaction (92). But the decay curves of the FLIM-FRET samples **(b,d)** showed a better fit with χ^2 (chi-squared goodness-of-fit test) closer to 1, by employing a bi-exponential fluorescence decay model, which provides information about the lifetimes and the fraction of two populations of molecules, the interacting

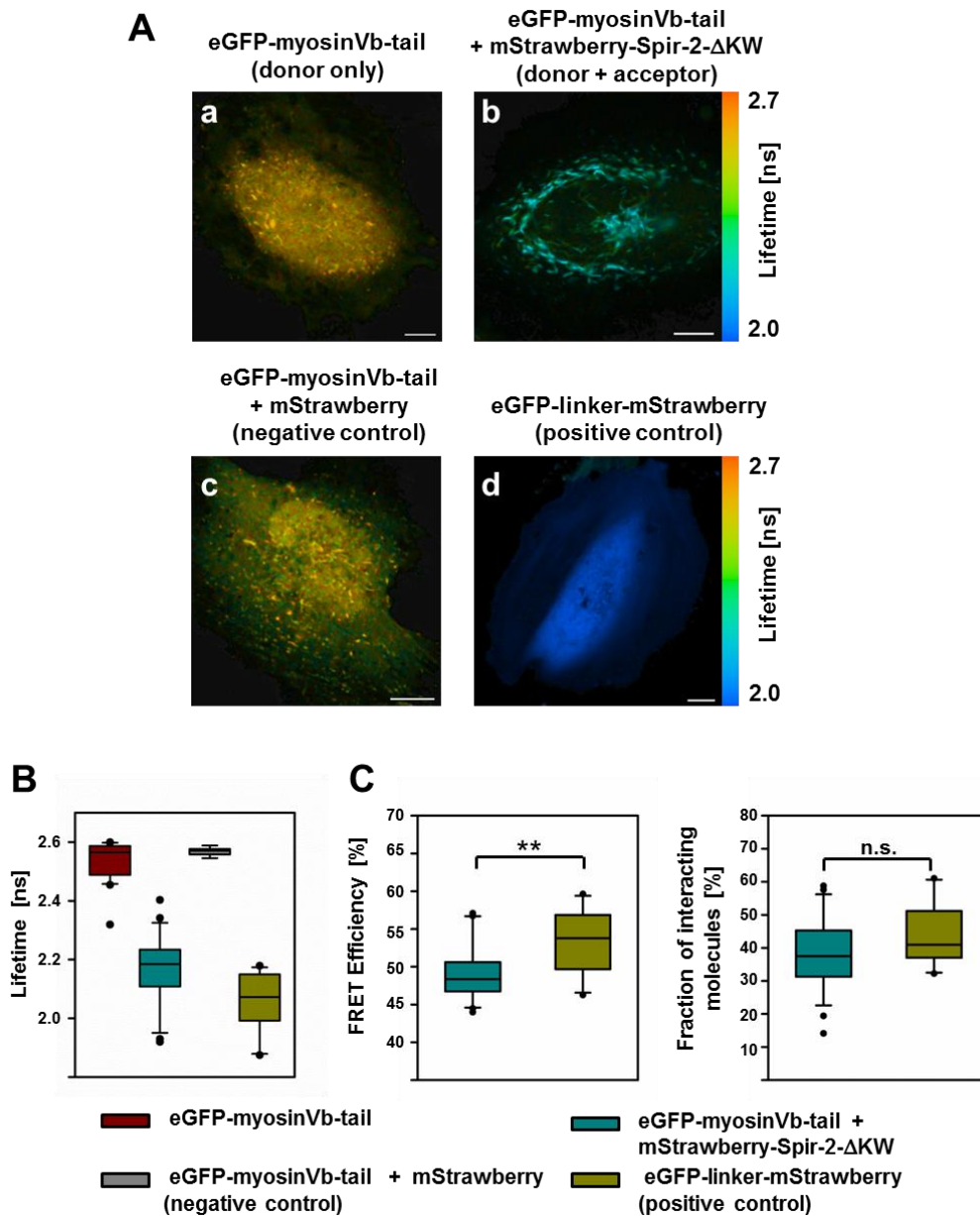


Figure 4.15: Spir-2-ΔKW interacts with myosin Vb-tail on vesicles

(A) Fluorescence lifetime images of eGFP-myosin Vb-tail (a) and coexpressing mStrawberry-Spir-2-ΔKW (b) and coexpressing mStrawberry (c) as a negative control and eGFP-linker-mStrawberry (d) as positive control, expressed in HeLa cells. (A,B) The lifetime of eGFP-myosin Vb-tail (a, red) decreases markedly in the presence of mStrawberry-Spir-2-ΔKW (b, blue), but does not change in the presence of mStrawberry (c, grey). The eGFP-linker-mStrawberry variant reveals a much lower lifetime than donor only (d, yellow). (C) The FRET efficiency and the fraction of interacting molecules of eGFP-myosin Vb-tail and mStrawberry-Spir-2-ΔKW in comparison to the positive control eGFP-linker-mStrawberry showing high values almost in the range of the positive control, indicating a strong interaction. ** $p < 0.01$, n.s. not significant. Scale bar: 10 μm

molecules (with the lifetime τ_{FRET} and fraction a) and non-interacting molecules (with the lifetime of the donor τ_0 and fraction b). The lifetime τ_0 of the non-interacting population was set to 2.53 ns, which was determined by the donor only sample. The average lifetime τ_{FRET} of eGFP-myosin Vb + mStrawberry-Spir-2- Δ KW (1.28 \pm 0.1 ns) and eGFP-linker-mStrawberry (1.16 \pm 0.1 ns) are in the same range. From these parameters, the FRET efficiency was calculated according to the equation $E_{FRET} = 1 - \tau_{FRET}/\tau$. As depicted in **Figure 4.15C**, eGFP-myosin Vb-tail and mStrawberry-Spir-2- Δ KW showed a FRET efficiency of 49.47 \pm 4.1 %, which was slightly, but still significantly lower than eGFP-linker-mStrawberry with 53.45 \pm 4.11 %. The fraction a of interacting molecules of eGFP-myosin Vb + mStrawberry-Spir-2- Δ KW with 38.21 \pm 11.02 % is in the same range as eGFP-linker-mStrawberry with 43.84 \pm 9.38 %. Our positive control construct eGFP-linker-mStrawberry showed a FRET efficiency and a fraction of interacting molecules a in the same range as a published construct where eGFP was fused to mStrawberry by the peptide linker SGLRSRGDPPVAT, which showed a FRET efficiency of 58 \pm 2 % and interacting fraction a of 37 \pm 7 % (126). By Western Blot analysis, a proteolytic degradation of the linker construct could be excluded. Thus, the interacting fraction of maximal 37 \pm 7% was found to be a consequence of the spectroscopic heterogeneity and maturation process of the acceptor fluorophore mStrawberry (126). Apparently, a FLIM-FRET sample in which all molecules are in a complex cannot reach an interacting fraction value a above ~40%. For eGFP-myosin Vb-tail and mStrawberry-Spir-2- Δ KW, we determined an interacting fraction value a of 38.21%, which indicates that almost all molecules occur in a complex, disregarding endogenous level of protein. These findings account for the very strong interaction of myosin Vb-tail and Spir-2- Δ KW on vesicles. We also performed FLIM-FRET experiments with eGFP-Spir-2- Δ KW and mStrawberry-labeled Rab11 and Arf1, but no FLIM-FRET has been detected yet. Since the FRET energy transfer is highly dependent on the distance, FRET detection has the requirement

that the fluorophores need to be in close proximity (~1-10 nm). Thus, if the fluorophores are positioned too far away from each other within the complex, no FLIM-FRET can be detected despite the interaction. This means, that no FLIM-FRET detection is not necessarily a proof of non-interaction. Different labeling at C- and N-terminus and shortening the putative interacting region might bring the fluorophores close enough for FRET detection.

4.3.4 Spir-2 linker region mediates the interaction with myosin Vb-tail

In order to specify the interacting region of Spir-2 responsible for myosin Vb binding, we expressed eGFP-Spir-2- Δ KW (aa 375-729), lacking the KIND and WH2 domains (**Figure 4.16A**), alone and together with mStrawberry-myosin Vb-cc-tail. As seen in **Figure 4.16B**, by adding BFA Spir-2- Δ KW showed a cytoplasmic distribution, but it remained bound to the vesicles when mStrawberry-myosin Vb-cc-tail was coexpressed, indicating that the C-terminal part of Spir is sufficient to form a stable complex with myosin Vb. The variant Spir-2-LAFA, where the hydrophobic amino acids of the turret loop are mutated to alanine, has been found to lack the membrane binding properties, but is targeted to vesicle membranes when mStrawberry-myosin Vb-cc-tail is coexpressed (**Figure 4.16C**), which accounts for a strong Spir/myosin Vb interaction. To find out if the Spir-box mediates the Spir/myosin Vb interaction, the variant eGFP-Spir-2- Δ Spir-box, where the Spir-box is deleted, was expressed in HeLa cells. This mutation resulted in a cytoplasmic distribution, but the variant is targeted to vesicles in the presence of myosin Vb (**Figure 4.16D**), showing that the Spir-box is not responsible for the Spir/myosin Vb interaction. To probe if the FYVE domain, whose role as a protein-protein interaction module was discovered in this work, mediates the interaction with myosin Vb, the variant Spir-2-C1,2,7,8S, where the integrity of the FYVE zinc finger is destroyed, was expressed and showed a loss of membrane binding when expressed alone (**Figure 4.16E**, left). However, by coexpressing

mStrawberry-myosin Vb-cc-tail the variant Spir-2-C1,2,7,8S was targeted to the membrane (**Figure 4.16E**, right), indicating that the FYVE domain is not important for the interaction with myosin Vb. Taking the results together, the C-terminal part of Spir-2, but not the FYVE domain nor the Spir-box, mediates the Spir-2/myosin Vb interaction, indicating that the linker region between the WH2 domains and Spir-box might be the interacting region. This hypothesis has been further reinforced by recent GST-pulldown studies in the lab of Eugen Kerkhoff which showed that the linker region mediates the interaction with myosin Vb-tail (preliminary data of Eugen Kerkhoff). Additionally, mutagenesis studies are ongoing to map the Spir/myosin Vb interaction sequence in the Spir-2-linker region. Further *in vitro* interaction studies with recombinant proteins will be performed.

In conclusion, we revealed for the first time a direct and strong interaction of Spir-2 and myosin Vb, mediated by the linker region of Spir-2 and the tail region of myosin Vb. This interaction is able to recruit membrane-binding deficient Spir-2 variants to vesicle membranes.

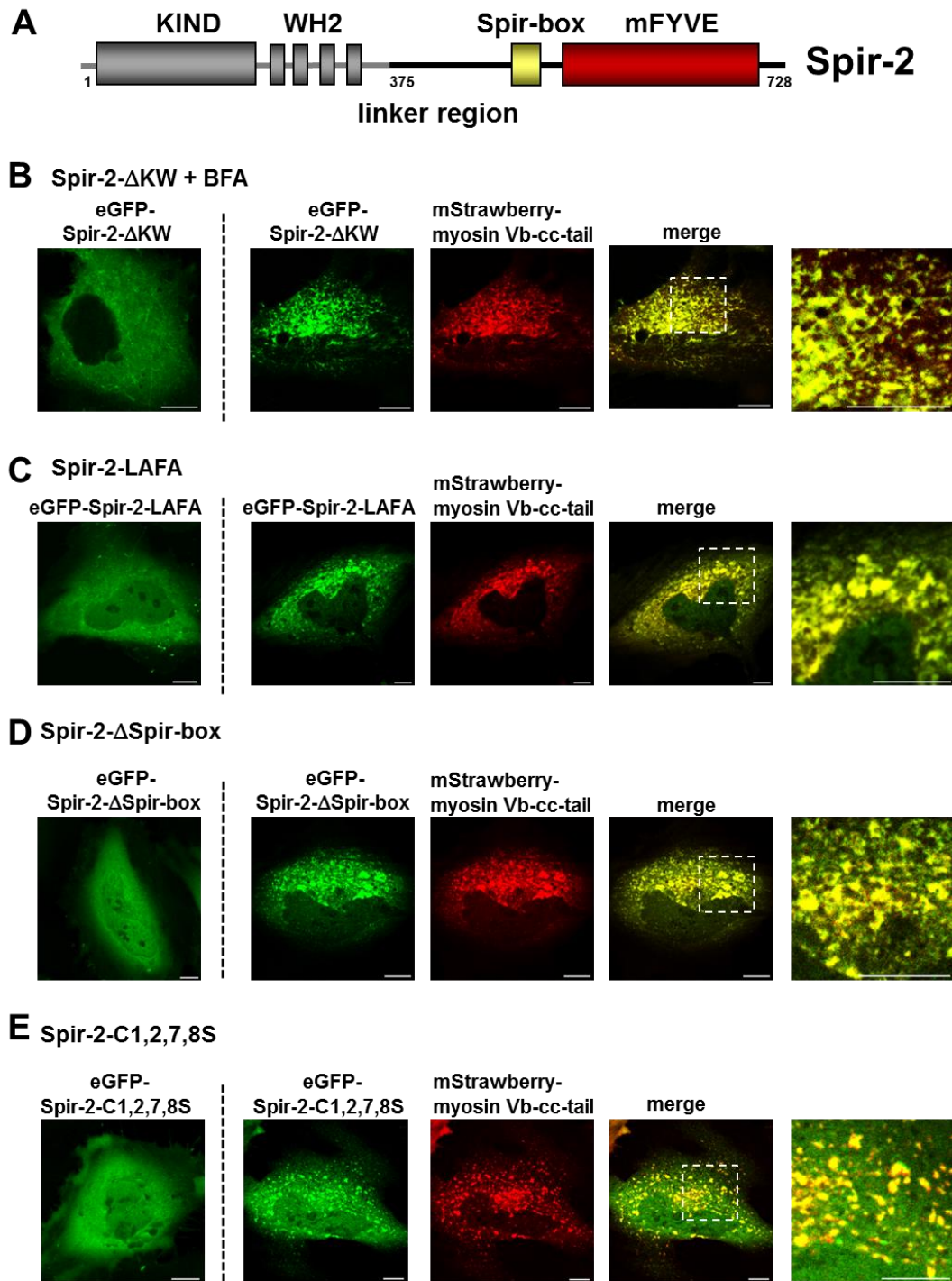


Figure 4.16: Spir-2-linker region forms a stable complex with myosin Vb-cc-tail
(A) Domain structure of Spir-2 **(B-D)** Confocal images of HeLa cells transiently expressing variants of eGFP-Spir-2 alone (**left**) and coexpressing mStrawberry-myosin Vb-cc-tail and the respective variants of eGFP-Spir-2 (**right**). **(B)** eGFP-Spir-2- Δ KW, lacking the KIND and WH2 domains, is released from vesicles by adding 5 μ g/ μ L BFA, but is retained on vesicles when coexpressing mStrawberry-myosin Vb-cc-tail. The Spir-2 variants **(C)** eGFP-Spir-2-LAFA **(D)** eGFP-Spir-2- Δ Spir-box, lacking the Spir-box and **(E)** Spir-2-C1,2,7,8S with a destroyed FYVE domain are cytoplasmic, but are targeted to vesicles when coexpressing mStrawberry-myosin Vb-cc-tail

5 Discussion

5.1 Spir-2 possesses a FYVE-related domain

Spir proteins were found to localize to vesicular structures. After the discovery of Spir in *Drosophila* (p150-Spir), sequence studies disclosed a modified FYVE domain at the C-terminus. A distinct feature of the Spir-FYVE domain is a big insertion loop between the cysteine 5 and 6 and the lack of the pocket of basic amino acids shown to mediate the specific binding of PI(3)P in canonical FYVE domains (103). Phospholipid-binding motifs contribute to the distribution of many membrane-binding proteins by specific recognition of phospholipids which differ among the membrane compartments. Whereas PIP(4,5)P₂ is found in the plasma membrane, endosomal vesicles are enriched in PI(3)P (127). Spir proteins localize to the perinuclear compartment, mostly at the trans-Golgi network and endosomes in the central part of the cell and rarely at vesicles at the cellular cortex.

To find out how Spir proteins are targeted to specific subcellular compartments, we first studied the phospholipid specificity of Spir-2 on established model membrane systems such as GUVs and LUVs to quantitatively describe the protein-lipid-interactions. The C-terminal part of Spir-2, consisting of the FYVE domain and Spir-Box, bound to negatively charged GUVs without any apparent specificity. Additionally, we used two quantifying assays based on LUVs (Electrochemiluminescence immunoassay and LUV floating assay) which revealed that the Spir-FYVE domain unspecifically binds to negatively charged phospholipids with nanomolar affinity. Thus, the Spir-FYVE does not exhibit PI(3)P specificity, as can be expected from the lack of the conserved PI(3)P interaction motifs. Mammalian endosomes are enriched in acidic phospholipids other than PI(3)P, in particular in PS and PA which contribute to the interaction of FYVE domains with endosomal

membranes (127,128). It has been shown that membrane recruitment of FYVE domains of several proteins such as EEA1, Hrs and Vps27p is facilitated by non-specific electrostatic interactions of the basic residues of the FYVE motif and the negatively charged phospholipids (128). In addition, the turret loop plays an important role for the endosomal localization of FYVE domains. Mutagenesis studies of the FYVE domains of EEA1 and SARA revealed the importance of the hydrophobic residues within the turret loop of the FYVE domain (108). Consistent with that, our studies showed that the mutation of the hydrophobic tip (turret loop) in the FYVE domain of Spir (variant Spir-2-LAFA) resulted in a cytoplasmic distribution in HeLa cells. Likewise, our *in vitro* studies on GUVs revealed the contribution of the hydrophobic tip of the Spir FYVE domain in membrane binding. The turret loop of Spir is even more hydrophobic than the turret loop of EEA1 and might have a higher impact on binding than in EEA1.

The FYVE domain of EEA1 is essential, but also not sufficient for endosome targeting. It requires an additional region N-terminal to the FYVE domain, which functions as the Rab5 binding region, indicating that targeting in EEA1 depends on both- interactions with Rab5 and PI(3)P (107,109). Accordingly, localization of Spir proteins to vesicles requires both the FYVE domain and the adjacent Spir-box, which is assumed to be a GTPase binding domain. The Spir-box shares a sequence similarity to the α -helical structure of rabphilin-3a, which mediates the interaction with the small GTPase Rab3a, suggesting that the Spir-box might function as a GTPase binding domain as well (57). Consequently, non-specific lipid interactions and the interaction with suitable ancillary proteins factors might mediate the targeting of Spir to vesicles.

Endosomal targeting of EEA1 is based on a multivalent mechanism in which domain organization and dimerization amplify weak affinity and specificity for the head group of PI(3)P (109). The isolated FYVE domain of Hrs was cytoplasmic, but induced dimerization led to vesicle targeting which was dependent on PI(3)P binding (101).

Homodimerization can provide the avidity to PI(3)P necessary to target to early endosomes. However, we found that Spir proteins are monomeric proteins in the cytosol, which could contribute to the lack of specificity to PI(3)P. Altogether, the following three determinants of canonical FYVE domains synergistically mediate the endosome targeting: 1) PI(3)P recognition, mediated by highly conserved sequences 2) the turret loop, which ranges from weak (EEA1) to strong (SARA, frabin), and 3) dimerization, which also varies from weak (EEA1) to strong (SARA) (108). In Spir-2-FYVE we identified only one determinant of the canonical FYVE domain, the strong turret loop. Spir-2 does not exhibit PI(3)P specificity and does not dimerize in the cytosol. We have to take into account that the dimerization was only probed in the cytosol and cannot be excluded for vesicle-bound Spir, which needs to be investigated with proper techniques. Consequently, we conclude that Spir-2 possesses a FYVE-related domain, as do rabphilin-3A and protrudin. The lack of phospholipid specificity could account for the fact that Spir protein localization encompasses not only early endosomes, but also the trans-Golgi network (TGN) and vesicles of the exocytic pathway (57,59), which show differences in lipid and protein compositions (127).

In conclusion, Spir proteins bind to membranes via non-specific electrostatic and hydrophobic interactions. As both interactions are rather unspecific, the interaction with membrane-bound ancillary protein factors might mediate the targeting of Spir proteins towards the specific subcellular compartments.

5.2 Spir-2-FYVE domain is a protein-protein interaction module

The FYVE-related domain mediates the interaction of Spir-2 to vesicular structures. Thus, the FYVE-related domain acts as a typical phospholipid-binding module for which it is known. Intriguingly, we discovered that the Spir-FYVE domain also acts as a protein-protein interaction module. Here, we found that the Spir-FYVE domain binds to the Spir-KIND domain. However, the FYVE domain acting as a

protein-protein interaction module in Spir is not a unique finding. The FYVE domain of Hrs (Hepatocyte growth factor-regulated tyrosin kinase substrate) has been found to interact with Citron kinase. This interaction inhibits the Citron kinase-induced HIV-budding (129). The interacting region in Citron kinase has not been identified yet. In this regard it is interesting to note, that the KIND domain of Spir evolved from a functional kinase and possesses the entire C-lobe of the kinase, but without the essential catalytic residues. Thus, if the Hrs-FYVE domain interacts with the C-lobe of the Citron kinase, similar to the interaction of Spir-2-FYVE to Spir-2-KIND remains an open question.

5.3 Spir-2 is regulated by an intramolecular complex

The distinct actin nucleation factors Spir and formin have been shown to interact with each other and cooperate in actin nucleation (36,44). This Spir/formin cooperation has been discovered to direct two crucial steps in mammalian oocyte maturation, the asymmetric spindle positioning and polar body extrusion during meiosis (48,49).

Many formins are regulated by the formation of an auto-inhibited complex in the cytosol and must be activated by specific ligands. The best studied mechanism of regulation is the autoinhibitory interactions of the N-terminal DID domain and C-terminal DAD domain in Diaphanous-related formins, which inhibit the actin polymerization. The autoinhibited complex is released by binding of a Rho GTPase. Mutational studies have identified a basic region in the DAD domain, which is involved in the interaction, indicating that electrostatic interactions between the basic amino acids of DAD and acidic amino acids of DID play an important role for the intramolecular interaction (27). Whereas the regulation of formins has been studied intensively, little is known about the regulation of Spir proteins. By homology studies we found basic residues in the Spir-FYVE domain homologous to basic residues to the FSI motif of formins, known to mediate the trans-regulatory interaction with acidic residues of the Spir-KIND domain (36). These findings raised the question of an intramolecular interaction of

Spir proteins similar to formin proteins, which we proved for the first time by performing FCCS and pulldown experiments. We found that the KIND domain at the N-terminus and the FYVE domain at the C-terminus mediate the intramolecular interaction. Due to instability of the full-length Spir protein, we used truncated variants and separately expressed domains of Spir to investigate the cis-regulatory interactions. This approach raises the problem that the KIND/FYVE interaction could also be a result of an intermolecular head-to-tail interaction of two Spir molecules. Taking into account that we discovered Spir proteins as monomers in the cytosol by using FCCS, an intermolecular interaction can be excluded.

In formin proteins, the intramolecular interaction has been shown to impede the actin polymerization activity by masking the FH1 and FH2 domains (130). In a similar manner the intramolecular complex formation of Spir proteins might inhibit the actin polymerization by masking the WH2 domains and keep the Spir proteins in an inactive state, which remains to be investigated. Moreover, it has been reported that formin binding is essential for Spir nucleation activity (36). We found overlapping interfaces and competing interaction of Spir-2-KIND domain with the formin Fmn2-FSI motif and Spir-2-FYVE domain, where we determined similar affinity of the Spir-2-KIND domain to the Spir-2-FYVE domain and to Fmn-2-FSI (36). Thus, the KIND/FYVE interaction might mask the interaction surface necessary for Fmn-2 binding. Thus, we assume that the intramolecular complex formation might prevent the enhancement of Spir activity due to the hindrance of formin binding. Interestingly, we found an almost abolished KIND/FYVE interaction on membranes, suggesting the membrane binding of Spir proteins as a mechanism to open the inactive intramolecular complex and to activate Spir proteins to initiate the actin polymerization. Consequently, we propose a model (**Figure 5.1**) in which Spir forms an intramolecular complex in the cytosol, which inhibits Spir nucleation activity. Upon binding of the FYVE domain to the membrane, the intramolecular

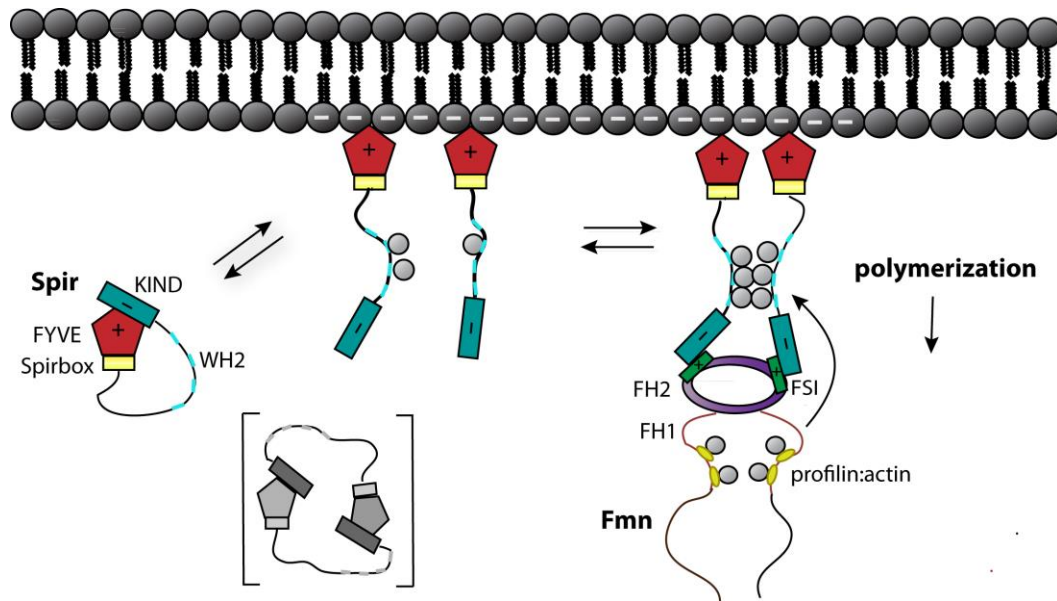


Figure 5.1: Proposed model of the Spir-2 autoregulation

In the cytoplasm Spir-2 exists in a closed conformation which is achieved by binding of the N-terminal KIND domain (blue) to the C-terminal FYVE domain (red). Upon binding of the positively charged FYVE domain to negatively charged phospholipids of the membrane the intramolecular KIND/FYVE interaction is released and the KIND domain is accessible for the interaction with the positively charged FSI motif (green) of Fmn-2 and the actin polymerization is initiated on the vesicles. A putative intermolecular interaction between two Spir molecules (grey brackets) could be excluded by showing the monomeric state of Spir-2 in the cytosol.

complex is released and the Fmn protein binds to the KIND domain via its FSI motif. Then the Spir/formin interaction enhances the Spir activity and the actin polymerization on vesicles is initiated.

So far, the auto-regulation for the class of Diaphanous-related Formins has been intensively studied. The Fmn subfamily of formins does not contain a DAD and DID domain for auto-regulation. Nevertheless an auto-regulation for the FMN subfamily protein Cappuccino from *Drosophila* and mammalian Fmn-1 has been described (131). But the potential auto-regulation for mammalian Fmn-2 remains an open question. In *Drosophila*, the N-terminal part of Cappuccino has similar affinity for the C-terminal part of Cappuccino and Spir-KIND, suggesting that external factors, such as small GTPases and post-translational modifications, play a role in regulating both interactions - the

auto-inhibition of Cappuccino and the Spir-Cappuccino interaction (132). In this work we also found that the N-terminal Spir-2-KIND domain has similar affinity to the C-terminal Spir-2-FYVE domain and to Fmn-2-FH2-eFSI (published K_d of the Spir-2-KIND/Fmn-2-FH2-eFSI interaction from (36)), and in addition, the Spir-FYVE domain has also similar affinity to the membrane (all dissociation constants between 10-60 nM). For the regulation of this network of competing interactions, external factors such as small GTPases and post-translational modifications might be important, as well. A possible post-translational modification of Spir proteins as a regulatory element was studied in the lab of Eugen Kerkhoff (unpublished data). Previous studies disclosed the *Drosophila* p150-Spir as a downstream target of c-Jun N-terminal kinase (JNK). Thus, the p150-Spir protein was phosphorylated by the constitutively active Jun N-terminal kinase form JNK-MKK7 (103). Three phosphorylation sites in Spir-2 have been found, one in the KIND domain, one in the central region and one in the FYVE domain. The phosphorylation of the KIND domain does not influence the trans-regulatory Spir-KIND/Fmn-FSI interaction, but increases the cis-regulatory KIND/FYVE interaction of Spir (preliminary data, (133)). Consequently, a phosphorylation might keep the Spir proteins in an autoinhibited complex in the cytosol. The formin nucleation activity is blocked by the Spir-KIND/Fmn-FSI interaction, in which the KIND domain possibly sterically prevents the binding of actin monomers to Fmn-FH2 domain (134). Thus, Spir-2 represents an inhibitor for formin proteins. Therefore, the intramolecular Spir-KIND/FYVE interaction provides a mechanism that impairs the Spir/formin interaction and allows formin activation. Recent FCCS studies in HeLa cells showed that the cytoplasmic full-length Spir-2 protein interacts weaker with the C-terminal Fmn-2 protein compared to the strong interacting isolated Spir-2-KIND domains (unpublished data of Thomas Weidemann), suggesting that the full-length Spir-2 protein exist in an backfolded conformation in the cytoplasm, which prevents the assembly of an cytoplasmic Spir/formin complex.

The Spir-KIND domain (Kinase non-catalytic C-lobe domain) evolved from a functional kinase and turned into a protein-protein-interaction module. A common concept of regulation of kinases is the intramolecular backfolding mechanism to convert the active kinase into an autoinhibited state. Thus, the PAK-1 kinase contains an inhibitory segment, which binds to the C-lobe of the kinase domain and blocks thereby its kinase activity (135). (**Figure 5.2A**). The Spir KIND/FYVE interaction shows some similarity to the autoregulation of PAK-1 kinase (**Figure 5.2C**). Spir-KIND possesses the entire C-lobe of the protein kinase, but without the catalytic residues and thus the catalytic activity. However, the KIND/FYVE interaction blocks presumably the Spir nucleation activity directly by masking the binding of actin to the adjacent WH2-domains or indirectly by occupying the interaction surface for formin binding, which is necessary for enhancement of the Spir nucleation activity. The autoinhibited complex of the PAK-1 kinase is disrupted by binding of the GTPases Cdc42 or Rac (135). Similarly, besides the membrane as a regulatory element to open the autoinhibited complex, effector proteins such as small GTPases could regulate the cis-regulatory interactions of Spir. In this work, we were able to reveal interactions of Spir-2 with the GTPases Arf1, colocalization with Rab11 and a strong interaction with the motor protein myosin Vb, which is able to recruit membrane-binding deficient Spir-2 to vesicle membranes. These interactions might target Spir proteins to vesicles and thereby open the autoinhibited complex. Their impact in the regulation of the cis-regulatory interactions of Spir remains to be investigated.

In this regard it is also interesting to note that the cis- and trans-regulation of Spir activity shows some similarity to the regulation of Raf kinase/Rok- α kinase, which plays a role in tumorigenesis and cell motility (**Figure 5.2B**). The Raf kinase is regulated by the intramolecular interaction of a N-terminal domain to the catalytic active kinase domain. The autoinhibition is relieved upon binding to the GTPases Ras or Rho. The Raf N-terminal domain was additionally shown to inhibit the Rok- α kinase by binding to its catalytic domain (136). Similarly, Spir activity is

presumably inhibited by an intramolecular FYVE/KIND interaction. In addition, the Spir N-terminal KIND domain inhibits the formin activity by binding to a region close to its catalytic domain (**Figure 5.2C**).

In conclusion, Spir might follow a common concept of kinase regulation by a cis- and transregulatory interplay to regulate its activity and the activity of effector proteins.

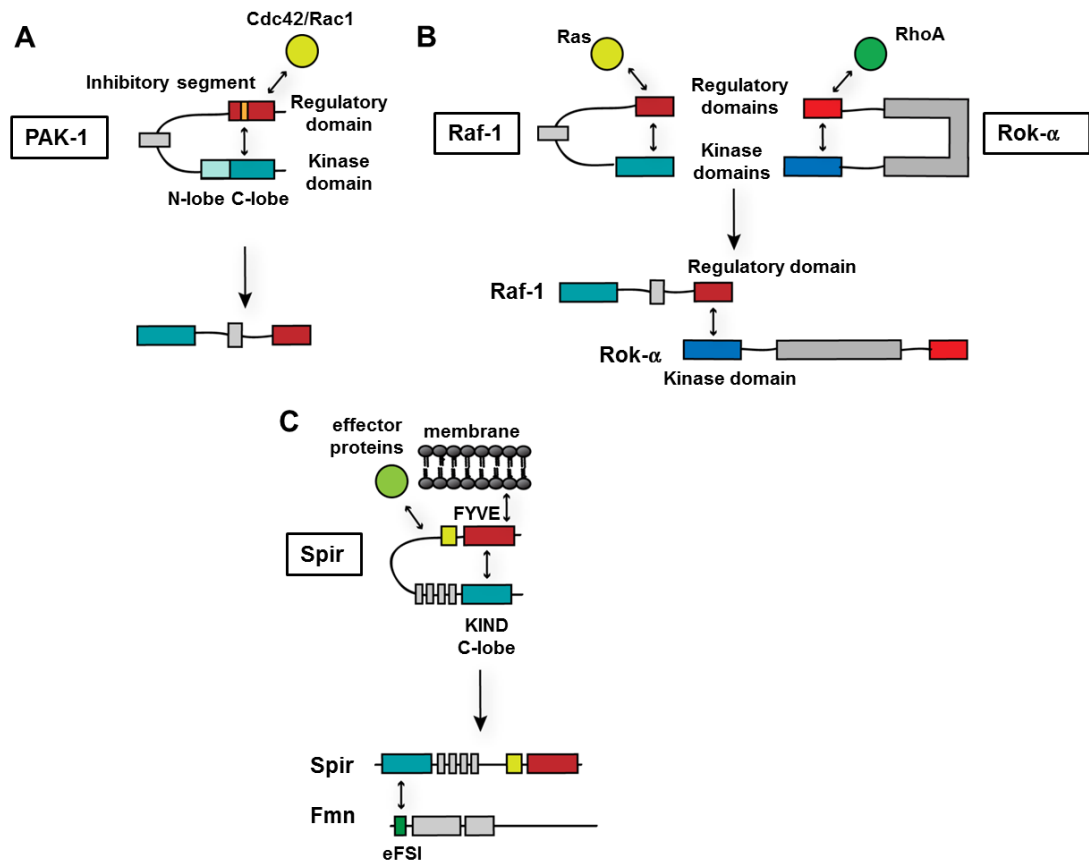


Figure 5.2: Concepts of the cis- and trans-regulation of kinases and Spir

(A) Cis-regulation of Pak-1. Pak-1 kinase activity is inhibited by binding of the N-terminal inhibitory segment to the C-lobe of the kinase domain to form an intramolecular complex, which is relieved upon binding of the GTPases Cdc42 or Rac1. **(B)** Trans-regulation of Raf-1 and Rok- α . Raf-1 and Rok- α kinases form an intramolecular complex by binding of the regulatory domain to the kinase domain which is released by binding of the small GTPases Ras and RhoA. Raf-1 mediates an inhibition of Rok- α in trans, where the regulatory domain of Raf-1 binds to the kinase domain of Rok- α . **(C)** Model of the autoregulation of Spir. Spir-2 forms an intramolecular complex by the interaction of the FYVE domain and the KIND domain, which possesses the entire C-lobe of a kinase. Upon membrane binding and/or binding of effector proteins the autoinhibited complex is released and Spir KIND interacts in trans with the FSI sequence of Fmn whereby its activity is enhanced and the Fmn activity is inhibited.

5.4 Spir-2 is an unconventional effector protein of Arf1

Like most GTPases Arf1 proteins cycle between a membrane-localized, GTP-bound, “active” state and a cytosolic GDP-bound “inactive” state. In the active GTP-bound conformation Arf1 interacts with multiple effector proteins, including coat proteins that sort membrane proteins into forming vesicles, and lipid modifying enzymes such as phospholipase D and phosphatidylinositol-4-phosphate kinase (114,137). Through these interactions Arf proteins mediate membrane trafficking in cells.

When overexpressed, Arf1 shows a prominent localization at the Golgi apparatus but also a substantial cytosolic “inactive” pool of molecules. Arf1 localization on peripheral endosomal structures also has been reported (113). When Arf1 and Spir-2 were coexpressed, we found a high colocalization on the Golgi complex, trans-Golgi network (TGN) and cytoplasmic vesicular structures, which has been already reported (104). We were able to reveal a Spir-2/Arf1 interaction by intensive protein-protein interactions studies, such as GST-pulldown assay and FCCS. Interestingly, in contrast to common Arf1 effectors Spir-2 binds preferentially to Arf1 in its “inactive” GDP-bound form. In addition preliminary NMR experiments were able to observe a binding of Arf1-GDP to the Spir-box of Spir-2, indicating that the Spir-box might function as a GTPase binding domain (138). There are two classes of proteins known to interact with Arf1-GDP, the nucleotide exchange factors (GEFs) and members of the p24 family of transmembrane proteins. P24 family members were also found in COPII vesicles and associated with the Golgi complex and ER (137). The association between Arf and p24 proteins was only revealed for Arf-GDP and not Arf-GTP and is related to the putative role of p24 as cargo receptor proteins in the early secretory pathway (139). Thus, it was proposed that Arf1-GDP is recruited to membranes by p23, a member of the p24 family (140). However, in our membrane binding studies on GUVs, Spir-2 does not

recruit Arf1 to membranes and likewise, Arf1 is not involved in Spir-2 membrane targeting. Congruently, their functional relationship cannot be sought in their targeting mechanism. Knock-down of endogenous Spir-1 and Spir-2 by RNAi resulted in a reduced motility of Arf1-positive vesicles (unpublished data of Eugen Kerkhoff). During vesicle budding from the Golgi-network, GTP-bound Arf1 organizes a rigid coat complex of coatamer COPI and clathrin adaptor protein complexes AP-1, AP-3 and AP-4 (141,142), which is released by switching Arf1-GTP to Arf1-GDP by GTP hydrolysis. We suggest that Spir-2/Arf1 interaction is now increased in the GDP-bound form and the resulting vesicles have a very dynamic actin/myosin coat, which provides the force for forming vesicular protrusions to contact the microtubule network and move along these microtubule tracks (**Figure 5.3**).

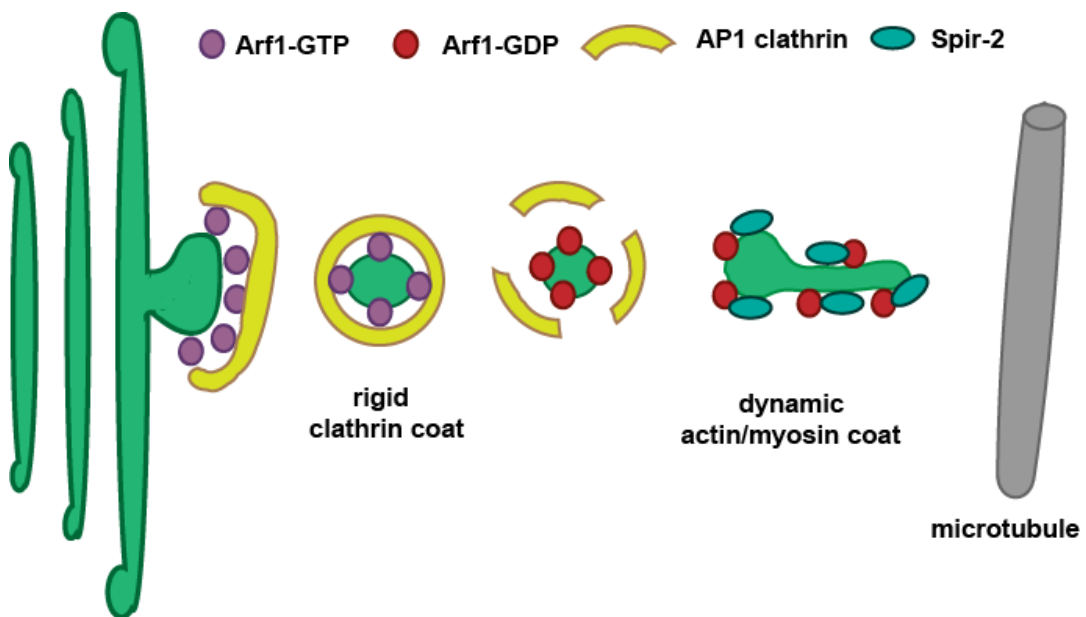


Figure 5.3: Proposed model of the functional switch of Arf1-GTP/GDP regulating morphological vesicle dynamics

Budding vesicles from the trans-Golgi network form an Arf1-GTP organized rigid AP-1/clathrin coat which dissociates by the hydrolysis of Arf1-GTP to Arf1-GDP and a dynamic Spir-2/actin/myosin complex associates with the vesicles. The actin/myosin forces mediate protrusions of the vesicles which can reach the microtubule network.

5.5 Spir-2/myosin Vb interaction regulates vesicle processes

In this work, we found that unspecific electrostatic and hydrophobic interactions of the FYVE-type zinc finger domain mediate the interaction of Spir to the membrane. Since these interactions are rather unspecific, further regulatory steps, which most likely involve membrane bound proteins, might target Spir proteins towards the specified subcellular compartments. Observations from colocalization studies hint towards the membrane-bound proteins Rab11a, Arf1 and myosin Vb as possible candidates.

The Rab and Arf1 subfamilies of Ras small G proteins regulate many different intracellular transport processes (70,143). The Rab11 small G proteins (Rab11a, b, Rab25) encompass a huge diversity of cellular functions. Rab11 is localized to the trans-Golgi network (TGN), post-Golgi vesicles and recycling endosomes and is involved in endocytic, exocytic and lysosomal pathways (64,68). Through their effector proteins, Rab GTPases regulate vesicle formation, actin- and tubulin-dependent vesicle movement and vesicle fusion (64), generally in the ‘active’ GTP-bound form. Myosins are motor proteins, which are responsible for actin-based mobility.

Through FCCS, we showed that Spir-2 interacts directly with the tail domain of myosin Vb in the cytosol. In addition, Spir-2 colocalizes strongly with myosin Vb. Spir-2 proteins are released from vesicle membranes upon BFA treatment, but they are retained on the vesicles when myosin Vb is coexpressed. These findings indicate a very stable Spir-2/Myosin Vb complex on vesicles, which we were able to reveal by FLIM-FRET. In the FLIM-FRET experiment, we found that the tail of myosin Vb, which is known to interact with effector proteins, also mediates the strong interaction with Spir-2. In further studies, we found that the linker region of Spir-2 mediates the interaction with myosin Vb, which is now being confirmed by GST-pulldown assays in the lab of Eugen Kerkhoff (preliminary data). Thus, besides the KIND domain, the

FYVE domain and presumably the Spir-box, Spir-2 contains a further protein-protein interaction module - the linker region. We found that membrane-binding deficient Spir variants are targeted to vesicle membranes by the Spir/myosin Vb interaction. Thus, myosin Vb might act as an effector protein for Spir and recruit Spir to vesicle membranes, thereby regulating the intramolecular interaction of Spir. Moreover, the Spir/myosin Vb interaction might also regulate the autoinhibited conformation of myosin Vb to activate its motor activity (144,145).

The tail domain of myosin Vb is known to directly interact with the GTP bound form of the Rab11 small G-protein (74). In addition, a high colocalization of myosin Vb and Rab11a in HeLa and MDCK cells was found (74,104). But we found that Spir-2 colocalises only partially with Rab11a-positive vesicles, and FCCS studies showed that Spir-2 does not interact with Rab11a in the cytosol of somatic cells. Previous attempts to probe a direct Spir/Rab11a interaction by a GST-pulldown assay could not show an interaction of Spir-2 with Rab11a and Rab25 (104). Interestingly, the lab of Eugen Kerkhoff performed a triple-stain experiment of Spir-2, Rab11a and myosin Vb-cc-tail and revealed that Spir-2 and Rab11a show a complete colocalisation in the presence of myosin Vb-cc-tail (104). Taken together, these findings suggest that myosin Vb might mediate the formation of a bigger regulatory complex.

It has been shown in mouse oocytes that the localization of Spire-2 on vesicles requires Rab11a (50). The work of Melina Schuh uncovered that cells can use vesicles as network nodes to establish a dynamic intracellular actin network whose density can be regulated. In particular, it has been reported that Rab11a-positive vesicles drive the network dynamics in a myosin Vb-dependent manner. Thorough studies with further Rab GTPases and related myosin proteins such as Rab5a, Rab27, myosinVa tail and myosin VI tail identified Rab11a and myosin Vb as key regulators of the actin network (50). Previous studies already identified Spire-1 and Spire-2 as key factors in asymmetric division of mouse oocytes (48). Together with Fmn-2 they assemble an actin network from the surface of the vesicles connecting the vesicles with each other and the

plasma membrane. In a myosin Vb-dependent manner the vesicles moves along their own tracks to converge and reach the plasma membrane. So this long-range vesicle transport is actin-dependent, but microtubule-independent (49). This vesicle-based mechanism of actin network modulation by clustering Spir and Formin drives the asymmetric spindle positioning of the meiotic spindle in mouse oocytes (48,49). Thus, the first physiological functions of Spir actin nucleators and the functional relationships to myosin Vb were uncovered. Here, for the first time, we could provide details of the interaction on a molecular basis.

Somatic cells differ from metaphase oocytes. Whereas metaphase oocytes lack microtubule tracks, which are usually involved in long-range transport processes, somatic cells possess an extended network of microtubule tracks. We studied the interactions in somatic cells and suggest a model (**Figure 5.4**) in which the actin nucleator Spir is targeted to vesicle membranes by myosin Vb and forms a complex with the actin nucleator formin. By this interaction, the nucleation activity of formin is blocked, but the Spir activity is enhanced. This enhancement of the Spir activity is essential to nucleate actin polymerization, where subsequently the Spir/formin complex dissociates and the formin nucleator gets activated and remains associated with the fast-growing barbed end of the actin filament. Whether Spir stays associated with the barbed (146-148) or pointed end (34) or even dissociates from the growing actin filament (149) is still being strongly debated, because experimental data has been obtained supporting all three hypotheses. Cooperative actin nucleation, subsequent complex dissociation and filament elongation have been shown for the formin cooperations of APC/mDia1 and yeast Bud6/Bni1, where the interaction partner APC and Bud6 stays at the pointed end and the formin mDi1 and Bni1 is bound to the barbed end, indicating a general mechanism for formin cooperations (150,151). It is still open if this mechanism is similar for the Spir/formin cooperation. Spir is recruited to vesicle membranes by myosin Vb. In addition, myosin Vb has been described to be anchored to the vesicle membrane by forming a ternary myosin Vb/FIP2/Rab11a complex. Myosin Vb interacts

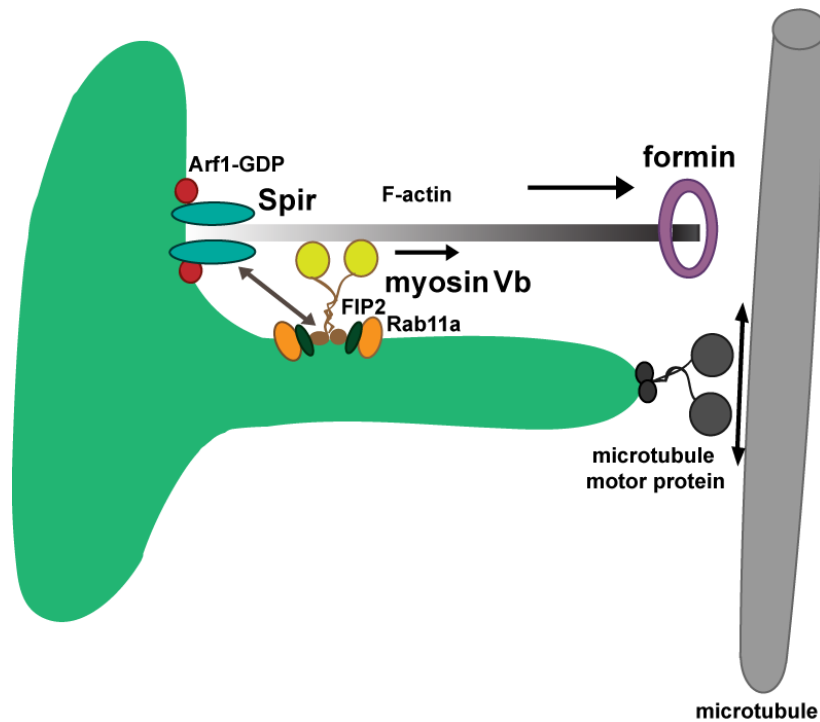


Figure 5.4 Proposed model of the Spir regulated vesicle dynamics

The Spir/formin complex is targeted to vesicle membranes to nucleate actin polymerization, where formin stays associated with the fast-growing barbed end of the actin filament. Spir interacts directly with the motor protein myosin Vb, which is membrane anchored in a ternary myosin Vb/FIP2/Rab11a complex. Myosin Vb moves along the actin filament and generates the forces to pull out membrane protrusions, which can reach and contact the microtubules. Postulated microtubule motor proteins then mediate fast movement of the vesicles on the microtubule filaments.

with both the Rab11a protein and the Rab11-interaction adaptor protein FIP2 (76). Thus, whether Spir functions as an adaptor protein in the ternary myosinVb/Spir/Rab11 complex or FIP2 is still involved as an adaptor protein remains to be investigated. Moreover, whether the Spir/myosinVb complex dissociates or remains associated during formin binding and subsequent Spir/formin initiated actin polymerization, remains open. By coexpressing Spir-2- Δ KW an increased vesicle length of myosin Vb-cc-tail-positive or Rab11a-positive vesicles was measured in the lab of Eugen Kerkhoff (104). Thus, by moving along the polymerized actin filament, the myosin Vb motor protein generates a force that pulls out membrane protrusions which can reach microtubules. We postulate

that microtubule motor proteins localize on the Spir/myosin Vb vesicles, which can contact microtubules and enables fast movement of the vesicles along the microtubule tracks. Fast movement of tubular Spir vesicles on microtubules in HeLa cells was observed in the lab of Eugen Kerkhoff (134).

In conclusion, the Spir/formin cooperation together with Rab11 and myosin Vb can drive several vesicle processes. We described a mechanism in somatic cells, where the Spir/formin complex mediates an actin-dependent tubulation of vesicles which can attach to microtubules for fast long-range transport. In mouse oocytes a concept of vesicles transport was reported, where the long-range vesicle transport was actin-dependent, but microtubule independent and mediated by the Spir/formin complex (49). Moreover, Spir was found to be expressed in a diversity of mammalian cells such as oocytes, spermatocytes, epithelial cells of the digestive tract and neuronal cells, indicating that Spir plays a role in numerous cellular processes (41). It was found that Spir-1 deficient mice exhibit a reduction of dendritic spines (51). Dendritic spines are membrane protrusions of neuronal dendrites, where the cytoskeleton is made by F-actin. Dendritic spine formation and spine growth is related to the AMPA receptor trafficking, which mediates excitatory neurotransmission in mammalian central nervous system. Recycling endosomes, containing the AMPA receptor, localizes to the base of the dendritic spines. These endosomes are rapidly mobilized upon long-term potentiation (LTP) stimulus and transported along actin filaments to the plasma membrane and the AMPA receptor is finally inserted. By altering the degree of AMPA receptor insertion and the rates of AMPA receptor exocytosis and endocytosis, the synaptic strength can be adjusted (152). Learning and memory processes involve changes in synaptic strength (153). Myosin Vb is enriched in the hippocampus (78) and the Rab11/FIP2/myosin Vb complex mediates the actin-dependent transport of AMPA receptor containing recycling endosomes (79). Recently, in neuronal dendrites Spir vesicles were found on the base and within dendritic spines (preliminary data of Eugen Kerkhoff, Seonil Kim and

Edward B. Ziff, NYU Langone Medical Center, New York), indicating that the membrane protrusions and transport of the recycling endosomes might be mediated by the ternary myosin Vb/FIP2/Rab11a complex together with Spir proteins nucleating the actin tracks. The forces to transport the vesicles are generated by myosin Vb. Behavioural studies of formin-2 deficient mice and Spir-1 mutant mice uncovered a phenotype in emotional fear learning, showing enhance fear expression, which might be a consequence of the deregulation of the AMPA receptor trafficking (51). In this work we found a direct interaction between Spir and myosin Vb. It would be interesting to resolve its function in neuronal signaling via its role in post-synaptic AMPA receptor trafficking in the future.

6 Future directions

In this study, we revealed an intramolecular interaction of Spir-2 proteins which is released upon membrane binding and allows formin to bind to Spir, which enhances Spir nucleation activity while formin activity is blocked. Whereas the formin is known to be associated with the fast-growing barbed end, the position of Spir on the pointed or barbed end of the actin filament still remains unclear. This question could be solved by a triple-color TIRF experiment. Also, for several auto-inhibited proteins involved in membrane trafficking, GTPases act as regulators which open the intramolecular complex. We revealed that Spir interacts with the GTPase Arf1 and partially colocalizes with the GTPase Rab11. However, their roles in the auto-regulation, following a common concept of regulation of intramolecular interactions, remain to be investigated. Moreover, the function of the Spir-box as a potential GTPase binding motif remains to be solved. We showed a direct and strong interaction of Spir-2 with the motor protein myosin Vb, which mediates the targeting of Spir to vesicle membranes. In this way myosin Vb might also regulate the intramolecular interaction of Spir, which remains to be tested. Spir vesicles show tubular structures, especially when myosin Vb and Rab11a are coexpressed. These tubular vesicles have been seen to rapidly move along microtubule tracks. We proposed a model with minimal requirements in which the Spir/formin complex polymerizes actin filaments on which the motor protein myosin Vb moves along to generate the forces that pull out membrane protrusions. This hypothetical model could possibly be supported experimentally by the reconstitution of the Spir/formin complex and myosin Vb on giant unilamellar vesicles in presence of G-actin which is then polymerized to F-actin. If these minimal constituents allow myosin Vb to generate tubes, or need to be augmented by further factors, remains to be seen.

7 Bibliography

1. The 2013 Nobel Prize in Physiology or Medicine - Advanced Information. Retrieved from *Nobelprize.org*. Nobel Media AB 2013. Web. 26 Apr 2014. http://www.nobelprize.org/nobel_prizes/medicine/laureates/2013/advanced.html
2. Directing Traffic: How Vesicles Transport Cargo., *Genetic Science Learning Center*. Retrieved April 26, 2014, from <http://learn.genetics.utah.edu/content/cells/vesicles/>
3. Alberts, B., A. Johnson, J. Lewis, M. Raff, K. Roberts, and P. Walter. (2007) *Molecular Biology of the Cell*. Edition 5. Garland Science
4. Chesarone, M. A., and Goode, B. L. (2009) Actin nucleation and elongation factors: mechanisms and interplay. *Current opinion in cell biology* **21**, 28-37
5. Pollard, T. D., and Cooper, J. A. (2009) Actin, a central player in cell shape and movement. *Science* **326**, 1208-1212
6. Dominguez, R., and Holmes, K. C. (2011) Actin structure and function. *Annual review of biophysics* **40**, 169-186
7. Pollard, T. D., and Borisy, G. G. (2003) Cellular motility driven by assembly and disassembly of actin filaments. *Cell* **112**, 453-465
8. Pollard, T. D. (2007) Regulation of actin filament assembly by Arp2/3 complex and formins. *Annual review of biophysics and biomolecular structure* **36**, 451-477
9. Chhabra, E. S., and Higgs, H. N. (2007) The many faces of actin: matching assembly factors with cellular structures. *Nature cell biology* **9**, 1110-1121
10. Kelly, A. E., Kranitz, H., Dotsch, V., and Mullins, R. D. (2006) Actin binding to the central domain of WASP/Scar proteins plays a critical role in the activation of the Arp2/3 complex. *J Biol Chem* **281**, 10589-10597
11. Pollard, T. D., and Beltzner, C. C. (2002) Structure and function of the Arp2/3 complex. *Current opinion in structural biology* **12**, 768-774

12. Otomo, T., Otomo, C., Tomchick, D. R., Machius, M., and Rosen, M. K. (2005) Structural basis of Rho GTPase-mediated activation of the formin mDia1. *Mol Cell* **18**, 273-281
13. Vavylonis, D., Kovar, D. R., O'Shaughnessy, B., and Pollard, T. D. (2006) Model of formin-associated actin filament elongation. *Mol Cell* **21**, 455-466
14. Kerkhoff, E. (2006) Cellular functions of the Spir actin-nucleation factors. *Trends in cell biology* **16**, 477-483
15. Mullins, R. D., Heuser, J. A., and Pollard, T. D. (1998) The interaction of Arp2/3 complex with actin: nucleation, high affinity pointed end capping, and formation of branching networks of filaments. *Proc Natl Acad Sci U S A* **95**, 6181-6186
16. Veltman, D. M., and Insall, R. H. (2010) WASP family proteins: their evolution and its physiological implications. *Mol Biol Cell* **21**, 2880-2893
17. Takenawa, T., and Suetsugu, S. (2007) The WASP-WAVE protein network: connecting the membrane to the cytoskeleton. *Nature reviews. Molecular cell biology* **8**, 37-48
18. Rottner, K., Hanisch, J., and Campellone, K. G. (2010) WASH, WHAMM and JMY: regulation of Arp2/3 complex and beyond. *Trends in cell biology* **20**, 650-661
19. Campellone, K. G., Webb, N. J., Znameroski, E. A., and Welch, M. D. (2008) WHAMM is an Arp2/3 complex activator that binds microtubules and functions in ER to Golgi transport. *Cell* **134**, 148-161
20. Firat-Karalar, E. N., Hsiue, P. P., and Welch, M. D. (2011) The actin nucleation factor JMY is a negative regulator of neuritogenesis. *Mol Biol Cell* **22**, 4563-4574
21. Zigmond, S. H. (2004) Formin-induced nucleation of actin filaments. *Current opinion in cell biology* **16**, 99-105
22. Goode, B. L., and Eck, M. J. (2007) Mechanism and function of formins in the control of actin assembly. *Annual review of biochemistry* **76**, 593-627
23. Higgs, H. N. (2005) Formin proteins: a domain-based approach. *Trends in biochemical sciences* **30**, 342-353
24. Higgs, H. N., and Peterson, K. J. (2005) Phylogenetic analysis of the formin homology 2 domain. *Mol Biol Cell* **16**, 1-13

25. Witke, W. (2004) The role of profilin complexes in cell motility and other cellular processes. *Trends in cell biology* **14**, 461-469
26. Schonichen, A., and Geyer, M. (2010) Fifteen formins for an actin filament: a molecular view on the regulation of human formins. *Biochimica et biophysica acta* **1803**, 152-163
27. Wallar, B. J., Stropich, B. N., Schoenherr, J. A., Holman, H. A., Kitchen, S. M., and Alberts, A. S. (2006) The basic region of the diaphanous-autoregulatory domain (DAD) is required for autoregulatory interactions with the diaphanous-related formin inhibitory domain. *J Biol Chem* **281**, 4300-4307
28. Rose, R., Weyand, M., Lammers, M., Ishizaki, T., Ahmadian, M. R., and Wittinghofer, A. (2005) Structural and mechanistic insights into the interaction between Rho and mammalian Dia. *Nature* **435**, 513-518
29. Li, F., and Higgs, H. N. (2005) Dissecting requirements for auto-inhibition of actin nucleation by the formin, mDia1. *J Biol Chem* **280**, 6986-6992
30. Qualmann, B., and Kessels, M. M. (2009) New players in actin polymerization--WH2-domain-containing actin nucleators. *Trends in cell biology* **19**, 276-285
31. Ahuja, R., Pinyol, R., Reichenbach, N., Custer, L., Klingensmith, J., Kessels, M. M., and Qualmann, B. (2007) Cordon-bleu is an actin nucleation factor and controls neuronal morphology. *Cell* **131**, 337-350
32. Chereau, D., Boczkowska, M., Skwarek-Maruszewska, A., Fujiwara, I., Hayes, D. B., Rebowski, G., Lappalainen, P., Pollard, T. D., and Dominguez, R. (2008) Leiomodin is an actin filament nucleator in muscle cells. *Science* **320**, 239-243
33. Wellington, A., Emmons, S., James, B., Calley, J., Grover, M., Tolia, P., and Manseau, L. (1999) Spire contains actin binding domains and is related to ascidian posterior end mark-5. *Development* **126**, 5267-5274
34. Quinlan, M. E., Heuser, J. E., Kerkhoff, E., and Mullins, R. D. (2005) Drosophila Spire is an actin nucleation factor. *Nature* **433**, 382-388
35. Ciccarelli, F. D., Bork, P., and Kerkhoff, E. (2003) The KIND module: a putative signalling domain evolved from the C lobe of the protein kinase fold. *Trends in biochemical sciences* **28**, 349-352

36. Pechlivanis, M., Samol, A., and Kerkhoff, E. (2009) Identification of a short Spir interaction sequence at the C-terminal end of formin subgroup proteins. *J Biol Chem* **284**, 25324-25333
37. Ostermeier, C., and Brunger, A. T. (1999) Structural basis of Rab effector specificity: crystal structure of the small G protein Rab3A complexed with the effector domain of rabphilin-3A. *Cell* **96**, 363-374
38. Stenmark, H., Aasland, R., and Driscoll, P. C. (2002) The phosphatidylinositol 3-phosphate-binding FYVE finger. *Febs Lett* **513**, 77-84
39. Lemmon, M. A. (2008) Membrane recognition by phospholipid-binding domains. *Nature reviews. Molecular cell biology* **9**, 99-111
40. Gaullier, J. M., Simonsen, A., D'Arrigo, A., Bremnes, B., Stenmark, H., and Aasland, R. (1998) FYVE fingers bind PtdIns(3)P. *Nature* **394**, 432-433
41. Pleiser, S., Rock, R., Wellmann, J., Gessler, M., and Kerkhoff, E. (2010) Expression patterns of the mouse Spir-2 actin nucleator. *Gene expression patterns : GEP* **10**, 345-350
42. Manseau, L. J., and Schupbach, T. (1989) cappuccino and spire: two unique maternal-effect loci required for both the anteroposterior and dorsoventral patterns of the Drosophila embryo. *Genes & development* **3**, 1437-1452
43. Dahlgaard, K., Raposo, A. A., Niccoli, T., and St Johnston, D. (2007) Capu and Spire assemble a cytoplasmic actin mesh that maintains microtubule organization in the Drosophila oocyte. *Developmental cell* **13**, 539-553
44. Quinlan, M. E., Hilgert, S., Bedrossian, A., Mullins, R. D., and Kerkhoff, E. (2007) Regulatory interactions between two actin nucleators, Spire and Cappuccino. *The Journal of cell biology* **179**, 117-128
45. Vizcarra, C. L., Kreutz, B., Rodal, A. A., Toms, A. V., Lu, J., Zheng, W., Quinlan, M. E., and Eck, M. J. (2011) Structure and function of the interacting domains of Spire and Fmn-family formins. *Proc Natl Acad Sci U S A* **108**, 11884-11889
46. Zeth, K., Pechlivanis, M., Samol, A., Pleiser, S., Vonrhein, C., and Kerkhoff, E. (2011) Molecular basis of actin nucleation factor cooperativity: crystal structure of the Spir-1 kinase non-catalytic C-lobe domain (KIND)*formin-2 formin SPIR interaction motif (FSI) complex. *J Biol Chem* **286**, 30732-30739

47. Schumacher, N., Borawski, J. M., Leberfinger, C. B., Gessler, M., and Kerkhoff, E. (2004) Overlapping expression pattern of the actin organizers Spir-1 and formin-2 in the developing mouse nervous system and the adult brain. *Gene expression patterns : GEP* **4**, 249-255
48. Pfender, S., Kuznetsov, V., Pleiser, S., Kerkhoff, E., and Schuh, M. (2011) Spire-type actin nucleators cooperate with Formin-2 to drive asymmetric oocyte division. *Curr Biol* **21**, 955-960
49. Schuh, M. (2011) An actin-dependent mechanism for long-range vesicle transport. *Nature cell biology* **13**, 1431-1436
50. Holubcova, Z., Howard, G., and Schuh, M. (2013) Vesicles modulate an actin network for asymmetric spindle positioning. *Nature cell biology* **15**, 937-947
51. Pleiser, S., Banhaabouchi, M. A., Samol-Wolf, A., Farley, D., Welz, T., Wellbourne-Wood, J., Gehring, I., Linkner, J., Faix, J., Riemenschneider, M. J., Dietrich, S., and Kerkhoff, E. (2013) Enhanced fear expression in Spir-1 actin organizer mutant mice. *European journal of cell biology*
52. Gates, M. A., Kannan, R., and Giniger, E. (2011) A genome-wide analysis reveals that the Drosophila transcription factor Lola promotes axon growth in part by suppressing expression of the actin nucleation factor Spire. *Neural development* **6**, 37
53. Ferreira, T., Ou, Y., Li, S., Giniger, E., and van Meyel, D. J. (2014) Dendrite architecture organized by transcriptional control of the F-actin nucleator Spire. *Development* **141**, 650-660
54. Sioud, M., and Hansen, M. H. (2001) Profiling the immune response in patients with breast cancer by phage-displayed cDNA libraries. *European journal of immunology* **31**, 716-725
55. Stenmark, H., Aasland, R., Toh, B. H., and D'Arrigo, A. (1996) Endosomal localization of the autoantigen EEA1 is mediated by a zinc-binding FYVE finger. *J Biol Chem* **271**, 24048-24054
56. Misra, S., and Hurley, J. H. (1999) Crystal structure of a phosphatidylinositol 3-phosphate-specific membrane-targeting motif, the FYVE domain of Vps27p. *Cell* **97**, 657-666
57. Kerkhoff, E., Simpson, J. C., Leberfinger, C. B., Otto, I. M., Doerks, T., Bork, P., Rapp, U. R., Raabe, T., and Pepperkok, R. (2001) The Spir actin organizers are involved in vesicle transport processes. *Curr Biol* **11**, 1963-1968

58. Sonnichsen, B., De Renzis, S., Nielsen, E., Rietdorf, J., and Zerial, M. (2000) Distinct membrane domains on endosomes in the recycling pathway visualized by multicolor imaging of Rab4, Rab5, and Rab11. *The Journal of cell biology* **149**, 901-914
59. Morel, E., Parton, R. G., and Gruenberg, J. (2009) Annexin A2-dependent polymerization of actin mediates endosome biogenesis. *Developmental cell* **16**, 445-457
60. Vetter, I. R., and Wittinghofer, A. (2001) The guanine nucleotide-binding switch in three dimensions. *Science* **294**, 1299-1304
61. Wennerberg, K., Rossman, K. L., and Der, C. J. (2005) The Ras superfamily at a glance. *Journal of cell science* **118**, 843-846
62. Bernards, A., and Settleman, J. (2004) GAP control: regulating the regulators of small GTPases. *Trends in cell biology* **14**, 377-385
63. Pereira-Leal, J. B., and Seabra, M. C. (2001) Evolution of the Rab family of small GTP-binding proteins. *Journal of molecular biology* **313**, 889-901
64. Stenmark, H., and Olkkonen, V. M. (2001) The Rab GTPase family. *Genome biology* **2**, REVIEWS3007
65. Zerial, M., and McBride, H. (2001) Rab proteins as membrane organizers. *Nature reviews. Molecular cell biology* **2**, 107-117
66. Goldenring, J. R., Shen, K. R., Vaughan, H. D., and Modlin, I. M. (1993) Identification of a small GTP-binding protein, Rab25, expressed in the gastrointestinal mucosa, kidney, and lung. *J Biol Chem* **268**, 18419-18422
67. Lai, F., Stubbs, L., and Artzt, K. (1994) Molecular analysis of mouse Rab11b: a new type of mammalian YPT/Rab protein. *Genomics* **22**, 610-616
68. Bock, J. B., Matern, H. T., Peden, A. A., and Scheller, R. H. (2001) A genomic perspective on membrane compartment organization. *Nature* **409**, 839-841
69. Kahn, R. A., Cherfils, J., Elias, M., Lovering, R. C., Munro, S., and Schurmann, A. (2006) Nomenclature for the human Arf family of GTP-binding proteins: ARF, ARL, and SAR proteins. *The Journal of cell biology* **172**, 645-650
70. D'Souza-Schorey, C., and Chavrier, P. (2006) ARF proteins: roles in membrane traffic and beyond. *Nature reviews. Molecular cell biology* **7**, 347-358

71. Hammer, J. A., 3rd, and Sellers, J. R. (2012) Walking to work: roles for class V myosins as cargo transporters. *Nature reviews. Molecular cell biology* **13**, 13-26
72. Watanabe, S., Mabuchi, K., Ikebe, R., and Ikebe, M. (2006) Mechanoenzymatic characterization of human myosin Vb. *Biochemistry-Us* **45**, 2729-2738
73. Akhmanova, A., and Hammer, J. A., 3rd. (2010) Linking molecular motors to membrane cargo. *Current opinion in cell biology* **22**, 479-487
74. Lapierre, L. A., Kumar, R., Hales, C. M., Navarre, J., Bhartur, S. G., Burnette, J. O., Provance, D. W., Jr., Mercer, J. A., Bahler, M., and Goldenring, J. R. (2001) Myosin vb is associated with plasma membrane recycling systems. *Mol Biol Cell* **12**, 1843-1857
75. Volpicelli, L. A., Lah, J. J., Fang, G., Goldenring, J. R., and Levey, A. I. (2002) Rab11a and myosin Vb regulate recycling of the M4 muscarinic acetylcholine receptor. *J Neurosci* **22**, 9776-9784
76. Hales, C. M., Vaerman, J. P., and Goldenring, J. R. (2002) Rab11 family interacting protein 2 associates with Myosin Vb and regulates plasma membrane recycling. *J Biol Chem* **277**, 50415-50421
77. Chen, Y., Tian, L., Zhang, F., Liu, C., Lu, T., Ruan, Y., Wang, L., Yan, H., Yan, J., Liu, Q., Zhang, H., Ma, W., Yang, J., Li, K., Lv, L., Zhang, D., and Yue, W. (2013) Myosin Vb gene is associated with schizophrenia in Chinese Han population. *Psychiatry research* **207**, 13-18
78. Zhao, L. P., Koslovsky, J. S., Reinhard, J., Bahler, M., Witt, A. E., Provance, D. W., Jr., and Mercer, J. A. (1996) Cloning and characterization of myr 6, an unconventional myosin of the dilute/myosin-V family. *Proc Natl Acad Sci U S A* **93**, 10826-10831
79. Wang, Z., Edwards, J. G., Riley, N., Provance, D. W., Jr., Karcher, R., Li, X. D., Davison, I. G., Ikebe, M., Mercer, J. A., Kauer, J. A., and Ehlers, M. D. (2008) Myosin Vb mobilizes recycling endosomes and AMPA receptors for postsynaptic plasticity. *Cell* **135**, 535-548
80. Mouritsen, O. G. (2005) Life - As a matter of Fat. *The Frontiers Collection* **XIV**, 276
81. Stahelin, R. V. (2009) Lipid binding domains: more than simple lipid effectors. *Journal of lipid research* **50 Suppl**, S299-304
82. Manna, D., Albanese, A., Park, W. S., and Cho, W. (2007) Mechanistic basis of differential cellular responses of

- phosphatidylinositol 3,4-bisphosphate- and phosphatidylinositol 3,4,5-trisphosphate-binding pleckstrin homology domains. *J Biol Chem* **282**, 32093-32105
83. Hurley, J. H., and Misra, S. (2000) Signaling and subcellular targeting by membrane-binding domains. *Annual review of biophysics and biomolecular structure* **29**, 49-79
84. Arumugam, S., Chwastek, G., and Schwille, P. (2011) Protein-membrane interactions: the virtue of minimal systems in systems biology. *Wiley interdisciplinary reviews. Systems biology and medicine* **3**, 269-280
85. Manneville, J. B., Casella, J. F., Ambroggio, E., Gounon, P., Bertherat, J., Bassereau, P., Cartaud, J., Antonny, B., and Goud, B. (2008) COPI coat assembly occurs on liquid-disordered domains and the associated membrane deformations are limited by membrane tension. *Proc Natl Acad Sci U S A* **105**, 16946-16951
86. Anitei, M., Stange, C., Parshina, I., Baust, T., Schenck, A., Raposo, G., Kirchhausen, T., and Hoflack, B. (2010) Protein complexes containing CYFIP/Sra/PIR121 coordinate Arf1 and Rac1 signalling during clathrin-AP-1-coated carrier biogenesis at the TGN. *Nature cell biology* **12**, 330-340
87. Heinemann, F., and Schwille, P. (2011) Preparation of micrometer-sized free-standing membranes. *Chemphyschem : a European journal of chemical physics and physical chemistry* **12**, 2568-2571
88. Bashkirov, P. V., Akimov, S. A., Evseev, A. I., Schmid, S. L., Zimmerberg, J., and Frolov, V. A. (2008) GTPase cycle of dynamin is coupled to membrane squeeze and release, leading to spontaneous fission. *Cell* **135**, 1276-1286
89. Lakowicz, J. R. (1999) Principles of fluorescence spectroscopy. Kluwer Academic-Plenum publishers, New York, Boston, London, Moscow.
90. Schwille, E. P. a. P. (2007) State of the art and novel trends in fluorescence correlation spectroscopy. Springer, Verlag Berlin Heidelberg
91. Bacia, K., and Schwille, P. (2007) Practical guidelines for dual-color fluorescence cross-correlation spectroscopy. *Nature protocols* **2**, 2842-2856 syndrome

92. Lleres, D., Swift, S., and Lamond, A. I. (2007) Detecting protein-protein interactions in vivo with FRET using multiphoton fluorescence lifetime imaging microscopy (FLIM). *Current protocols in cytometry* **Chapter 12**, Unit12.10
93. Franco, M., Chardin, P., Chabre, M., and Paris, S. (1995) Myristoylation of ADP-ribosylation factor 1 facilitates nucleotide exchange at physiological Mg²⁺ levels. *J Biol Chem* **270**, 1337-1341
94. Angelova, M. I., and Dimitrov, D. S. (1986) Liposome Electroformation. *Faraday Discuss* **81**, 303-+
95. Hofer, C. T., Herrmann, A., and Muller, P. (2010) Use of liposomes for studying interactions of soluble proteins with cellular membranes. *Methods in molecular biology* **606**, 69-82
96. Wolny, M., Grzybek, M., Bok, E., Chorzalska, A., Lenoir, M., Czogalla, A., Adamczyk, K., Kolondra, A., Diakowski, W., Overduin, M., and Sikorski, A. F. (2011) Key amino acid residues of ankyrin-sensitive phosphatidylethanolamine/phosphatidylcholine-lipid binding site of betaI-spectrin. *PloS one* **6**, e21538
97. Coskun, U., Grzybek, M., Drechsel, D., and Simons, K. (2011) Regulation of human EGF receptor by lipids. *Proc Natl Acad Sci U S A* **108**, 9044-9048
98. Kolondra, A., Lenoir, M., Wolny, M., Czogalla, A., Overduin, M., Sikorski, A. F., and Grzybek, M. (2010) The role of hydrophobic interactions in ankyrin-spectrin complex formation. *Biochimica et biophysica acta* **1798**, 2084-2089
99. Weidemann, T., and Schwille, P. (2013) Dual-color fluorescence cross-correlation spectroscopy with continuous laser excitation in a confocal setup. *Methods in enzymology* **518**, 43-70
100. Weidemann, T. (2014) Application of fluorescence correlation spectroscopy (FCS) to measure the dynamics of fluorescent proteins in living cells. *Methods in molecular biology* **1076**, 539-555
101. Hayakawa, A., Hayes, S. J., Lawe, D. C., Sudharshan, E., Tuft, R., Fogarty, K., Lambright, D., and Corvera, S. (2004) Structural basis for endosomal targeting by FYVE domains. *J Biol Chem* **279**, 5958-5966
102. Lee, S. A., Eyeson, R., Cheever, M. L., Geng, J., Verkhusha, V. V., Burd, C., Overduin, M., and Kutateladze, T. G. (2005) Targeting of the FYVE domain to endosomal membranes is regulated by a histidine switch. *Proc Natl Acad Sci U S A* **102**, 13052-13057

103. Otto, I. M., Raabe, T., Rennefahrt, U. E., Bork, P., Rapp, U. R., and Kerkhoff, E. (2000) The p150-Spir protein provides a link between c-Jun N-terminal kinase function and actin reorganization. *Curr Biol* **10**, 345-348
104. Weiß, S. (2011) Function of the Spir actin nucleators in intracellular vesicle transport processes. *Dissertation*
105. Narayan, K., and Lemmon, M. A. (2006) Determining selectivity of phosphoinositide-binding domains. *Methods* **39**, 122-133
106. Busse, R. A., Scacioc, A., Hernandez, J. M., Krick, R., Stephan, M., Janshoff, A., Thumm, M., and Kuhnel, K. (2013) Qualitative and quantitative characterization of protein-phosphoinositide interactions with liposome-based methods. *Autophagy* **9**, 770-777
107. Lawe, D. C., Patki, V., Heller-Harrison, R., Lambright, D., and Corvera, S. (2000) The FYVE domain of early endosome antigen 1 is required for both phosphatidylinositol 3-phosphate and Rab5 binding. Critical role of this dual interaction for endosomal localization. *J Biol Chem* **275**, 3699-3705
108. Hayakawa, A., Hayes, S. J., Lawe, D. C., Sudharshan, E., Tuft, R., Fogarty, K., Lambright, D., and Corvera, S. (2004) Structural basis for endosomal targeting by FYVE domains. *J Biol Chem* **279**, 5958-5966
109. Dumas, J. J., Merithew, E., Sudharshan, E., Rajamani, D., Hayes, S., Lawe, D., Corvera, S., and Lambright, D. G. (2001) Multivalent endosome targeting by homodimeric EEA1. *Mol Cell* **8**, 947-958
110. Rosales-Nieves, A. E., Johndrow, J. E., Keller, L. C., Magie, C. R., Pinto-Santini, D. M., and Parkhurst, S. M. (2006) Coordination of microtubule and microfilament dynamics by Drosophila Rho1, Spire and Cappuccino. *Nature cell biology* **8**, 367-376
111. Watanabe, N., Kato, T., Fujita, A., Ishizaki, T., and Narumiya, S. (1999) Cooperation between mDia1 and ROCK in Rho-induced actin reorganization. *Nature cell biology* **1**, 136-143
112. Weidemann, T., Worch, R., Kurgonaite, K., Hintersteiner, M., Bokel, C., and Schwille, P. (2011) Single cell analysis of ligand binding and complex formation of interleukin-4 receptor subunits. *Biophys J* **101**, 2360-2369
113. Cohen, L. A., and Donaldson, J. G. (2010) Analysis of Arf GTP-binding protein function in cells. *Current protocols in cell biology / editorial board, Juan S. Bonifacino ... [et al.]* **Chapter 3**, Unit 14 12 11-17

114. Donaldson, J. G., and Jackson, C. L. (2000) Regulators and effectors of the ARF GTPases. *Current opinion in cell biology* **12**, 475-482
115. Casanova, J. E. (2007) Regulation of Arf activation: the Sec7 family of guanine nucleotide exchange factors. *Traffic* **8**, 1476-1485
116. Anders, N., and Jurgens, G. (2008) Large ARF guanine nucleotide exchange factors in membrane trafficking. *Cellular and molecular life sciences : CMLS* **65**, 3433-3445
117. Alvarez, C., and Sztul, E. S. (1999) Brefeldin A (BFA) disrupts the organization of the microtubule and the actin cytoskeletons. *European journal of cell biology* **78**, 1-14
118. Kahn, R. A., Randazzo, P., Serafini, T., Weiss, O., Rulka, C., Clark, J., Amherdt, M., Roller, P., Orci, L., and Rothman, J. E. (1992) The amino terminus of ADP-ribosylation factor (ARF) is a critical determinant of ARF activities and is a potent and specific inhibitor of protein transport. *J Biol Chem* **267**, 13039-13046
119. Franco, M., Chardin, P., Chabre, M., and Paris, S. (1996) Myristoylation-facilitated binding of the G protein ARF1GDP to membrane phospholipids is required for its activation by a soluble nucleotide exchange factor. *J Biol Chem* **271**, 1573-1578
120. Ambroggio, E., Sorre, B., Bassereau, P., Goud, B., Manneville, J. B., and Antonny, B. (2010) ArfGAP1 generates an Arf1 gradient on continuous lipid membranes displaying flat and curved regions. *The EMBO journal* **29**, 292-303
121. Stamnes, M. (2002) Regulating the actin cytoskeleton during vesicular transport. *Current opinion in cell biology* **14**, 428-433
122. Randazzo, P. A., and Hirsch, D. S. (2004) Arf GAPs: multifunctional proteins that regulate membrane traffic and actin remodelling. *Cellular signalling* **16**, 401-413
123. Myers, K. R., and Casanova, J. E. (2008) Regulation of actin cytoskeleton dynamics by Arf-family GTPases. *Trends in cell biology* **18**, 184-192
124. Pollard, T. D. (2010) A guide to simple and informative binding assays. *Mol Biol Cell* **21**, 4061-4067
125. Antonny, B., Beraud-Dufour, S., Chardin, P., and Chabre, M. (1997) N-terminal hydrophobic residues of the G-protein ADP-ribosylation factor-1 insert into membrane phospholipids upon GDP to GTP exchange. *Biochemistry-Us* **36**, 4675-4684

126. Padilla-Parra, S., Auduge, N., Lalucque, H., Mevel, J. C., Coppey-Moisan, M., and Tramier, M. (2009) Quantitative comparison of different fluorescent protein couples for fast FRET-FLIM acquisition. *Biophys J* **97**, 2368-2376
127. Bissig, C., and Gruenberg, J. (2013) Lipid sorting and multivesicular endosome biogenesis. *Cold Spring Harbor perspectives in biology* **5**, a016816
128. Kutateladze, T. G., Capelluto, D. G., Ferguson, C. G., Cheever, M. L., Kutateladze, A. G., Prestwich, G. D., and Overduin, M. (2004) Multivalent mechanism of membrane insertion by the FYVE domain. *J Biol Chem* **279**, 3050-3057
129. Ding, J., Su, L., and Gao, G. (2011) Hrs inhibits citron kinase-mediated HIV-1 budding via its FYVE domain. *Protein & cell* **2**, 470-476
130. Schonichen, A., Alexander, M., Gasteier, J. E., Cuesta, F. E., Fackler, O. T., and Geyer, M. (2006) Biochemical characterization of the diaphanous autoregulatory interaction in the formin homology protein FHOD1. *J Biol Chem* **281**, 5084-5093
131. Kobiela, A., Pasolli, H. A., and Fuchs, E. (2004) Mammalian formin-1 participates in adherens junctions and polymerization of linear actin cables. *Nature cell biology* **6**, 21-30
132. Bor, B., Vizcarra, C. L., Phillips, M. L., and Quinlan, M. E. (2012) Autoinhibition of the formin Cappuccino in the absence of canonical autoinhibitory domains. *Mol Biol Cell* **23**, 3801-3813
133. Lakshmi, S. (2011) Post-translational modification and regulation of human Spir protein. *Dissertation*
134. Dietrich, S., Weiss, S., Pleiser, S., and Kerkhoff, E. (2013) Structural and functional insights into the Spir/formin actin nucleator complex. *Biological chemistry* **394**, 1649-1660
135. Lei, M., Lu, W., Meng, W., Parrini, M. C., Eck, M. J., Mayer, B. J., and Harrison, S. C. (2000) Structure of PAK1 in an autoinhibited conformation reveals a multistage activation switch. *Cell* **102**, 387-397
136. Niault, T., Sobczak, I., Meissl, K., Weitsman, G., Piazzolla, D., Maurer, G., Kern, F., Ehrenreiter, K., Hamerl, M., Moarefi, I., Leung, T., Carugo, O., Ng, T., and Baccarini, M. (2009) From autoinhibition to inhibition in trans: the Raf-1 regulatory domain inhibits Rho-alpha kinase activity. *The Journal of cell biology* **187**, 335-342

-
137. Nie, Z., Hirsch, D. S., and Randazzo, P. A. (2003) Arf and its many interactors. *Current opinion in cell biology* **15**, 396-404
138. Meierhofer, T. E. (2013) NMR-Spektroskopie und Biochemische Charakterisierung der konformationellen Gleichgewichte des Guaninnukleotid-bindenden Proteins Arf1 *Dissertation*
139. Dominguez, M., Dejgaard, K., Fullekrug, J., Dahan, S., Fazel, A., Paccaud, J. P., Thomas, D. Y., Bergeron, J. J., and Nilsson, T. (1998) gp25L/emp24/p24 protein family members of the cis-Golgi network bind both COP I and II coatomer. *The Journal of cell biology* **140**, 751-765
140. Gommel, D. U., Memon, A. R., Heiss, A., Lottspeich, F., Pfannstiel, J., Lechner, J., Reinhard, C., Helms, J. B., Nickel, W., and Wieland, F. T. (2001) Recruitment to Golgi membranes of ADP-ribosylation factor 1 is mediated by the cytoplasmic domain of p23. *The EMBO journal* **20**, 6751-6760
141. Bui, Q. T., Golinelli-Cohen, M. P., and Jackson, C. L. (2009) Large Arf1 guanine nucleotide exchange factors: evolution, domain structure, and roles in membrane trafficking and human disease. *Molecular genetics and genomics : MGG* **282**, 329-350
142. Nie, Z., and Randazzo, P. A. (2006) Arf GAPs and membrane traffic. *Journal of cell science* **119**, 1203-1211
143. Stenmark, H. (2009) Rab GTPases as coordinators of vesicle traffic. *Nature reviews. Molecular cell biology* **10**, 513-525
144. Pylypenko, O., Attanda, W., Gauquelin, C., Lahmani, M., Coulibaly, D., Baron, B., Hoos, S., Titus, M. A., England, P., and Houdusse, A. M. (2013) Structural basis of myosin V Rab GTPase-dependent cargo recognition. *Proc Natl Acad Sci U S A* **110**, 20443-20448
145. Li, X. D., Jung, H. S., Wang, Q., Ikebe, R., Craig, R., and Ikebe, M. (2008) The globular tail domain puts on the brake to stop the ATPase cycle of myosin Va. *Proc Natl Acad Sci U S A* **105**, 1140-1145
146. Bosch, M., Le, K. H., Bugyi, B., Correia, J. J., Renault, L., and Carlier, M. F. (2007) Analysis of the function of Spire in actin assembly and its synergy with formin and profilin. *Mol Cell* **28**, 555-568
147. Ito, T., Narita, A., Hirayama, T., Taki, M., Iyoshi, S., Yamamoto, Y., Maeda, Y., and Oda, T. (2011) Human spire interacts with the barbed end of the actin filament. *Journal of molecular biology* **408**, 18-25

148. Montaville, P., Jegou, A., Pernier, J., Compper, C., Guichard, B., Mogessie, B., Schuh, M., Romet-Lemonne, G., and Carlier, M. F. (2014) Spire and Formin 2 synergize and antagonize in regulating actin assembly in meiosis by a ping-pong mechanism. *PLoS biology* **12**, e1001795
149. Sitar, T., Gallinger, J., Ducka, A. M., Ikonen, T. P., Wohlhoefer, M., Schmoller, K. M., Bausch, A. R., Joel, P., Trybus, K. M., Noegel, A. A., Schleicher, M., Huber, R., and Holak, T. A. (2011) Molecular architecture of the Spire-actin nucleus and its implication for actin filament assembly. *Proc Natl Acad Sci U S A* **108**, 19575-19580
150. Breitsprecher, D., Jaiswal, R., Bombardier, J. P., Gould, C. J., Gelles, J., and Goode, B. L. (2012) Rocket launcher mechanism of collaborative actin assembly defined by single-molecule imaging. *Science* **336**, 1164-1168
151. Graziano, B. R., DuPage, A. G., Michelot, A., Breitsprecher, D., Moseley, J. B., Sagot, I., Blanchoin, L., and Goode, B. L. (2011) Mechanism and cellular function of Bud6 as an actin nucleation-promoting factor. *Mol Biol Cell* **22**, 4016-4028
152. Ehlers, M. D. (2000) Reinsertion or degradation of AMPA receptors determined by activity-dependent endocytic sorting. *Neuron* **28**, 511-525
153. Perlson, E., and Holzbaaur, E. L. (2008) Myosin learns to recruit AMPA receptors. *Cell* **135**, 414-415

8 Appendix

8.1 List of constructs

Construct	Description (Tag)	Fragment boundaries (Restriction sites)	Purification	Purpose
pProExHTb-Spir-2-KIND	Spir-2-KIND (His ₆ -tag)	aa 18-207 BamHI/XhoI	Ni-NTA, Sephadex G200	FCCS, EIA
pProExHTb-Spir-2-CT	AcGFP-Spir-2-CT (His ₆ -tag)	aa 502-728 BamHI/EcoRI/ HindIII	Ni-NTA HP, Sephadex G200	FCCS, imaging, EIA
pProExHTb-Spir-2-CT-C1,2,7,8S	AcGFP-Spir-2-CT-C1,2,7,8S (His ₆ -tag)	aa 502-728 Quick-Change Template: pProExHTb-Spir-2-CT	Ni-NTA HP, Sephadex G200	imaging
pProExHTb-Spir-2-CT-LAFA	AcGFP-Spir-2-CT-LAFA (His ₆ -tag)	aa 502-728 Quick-Change Template: pProExHTb-Spir-2-CT	Ni-NTA HP, Sephadex G200	imaging
pProExHTb-AcGFP1	AcGFP (His ₆ -tag)	BamHI/KpnI	Ni-NTA HP, Sephadex G200	FCCS, imaging
pRSFDuet-1 Arf1/NMT (provided by Volker Haucke)	myrArf1-Cys	aa 1-181 NdeI/ MfeI	(NH ₄) ₂ SO ₄ Precipitation DEAE-Sepharose	FCCS, imaging
pProEXHtb-hs-Arf1-DHelix	ΔH-Arf1-KCK (His ₆ -tag)	aa 1 - 181 BamHI/KpnI	Ni-NTA HP, Sephadex G200	imaging
pGEX4T1-NTEV-Fmn-2-eFSI	Fmn-2-eFSI (GST-tag)	aa 1523-1578 EcoRI/SalI	GSH Sepharose FF, TEV protease, SP-Sepharose XL	FCCS (without GST-tag) GST-pulldown

Appendix

pGEX4T1-NTEV-Spir-2-KIND	Spir-2-KIND	aa 18-207 BamHI/XhoI	GSH-Sepharose 4B	GST-pulldown
pEGFP-C1-Fmn-2-FSI	eGFP-Fmn-2-FH2-FSI	aa 1134-1578 KpnI/XbaI		GST-pulldown
pEGFP-C1-hs-Spir-2	eGFP-Spir-2	aa 2-728 BamHI/XbaI		Cell imaging
pEGFP-C1-hs-Spir-2-ΔSB	eGFP-Spir-2-ΔSpir-box	aa 2-728		In vivo FCS/FCCS Cell imaging
pEGFP-C1-hs-Spir-2-LAFA	eGFP-Spir-2-LAFA Leu595Ala,Phe506Ala	aa 2-728 Quick-Change Template: pEGFP-C1-hs-Spir-2		In vivo FCS/FCCS Cell imaging
pEGFP-C1-hs-Spir-2-C1,2,7,8S	eGFP-Spir-2-C1,2,7,8S Cys586Ser,Cys589Ser, Cys683Ser, Cys686Ser	aa 2-728 Quick-Change: Template: pEGFP-C1-hs-Spir-2		In vivo FCS/FCCS Cell imaging
pEGFP-C1-Spir-2-CT	eGFP-Spir-2-CT	aa 502-728		In vivo FCS Cell imaging
pEGFP-C1-Spir-2-FYVE	eGFP-Spir-2-FYVE	aa 577-696 XhoI/BamHI		GST-pulldown
pEGFP-C1-Spir-2-ΔKW	eGFP-Spir-2-ΔKW	aa 375-728 EcoRI/XbaI		GST-pulldown, Cell imaging
pEGFP-C1-Spir-2-ΔKW-LAFA	eGFP-Spir-2-ΔKW-LAFA Leu595Ala, Phe506Ala	aa 375-728 Quick-Change Template: pEGFP-C1-Spir-2-ΔKW		GST-pulldown
pEGFP-C1-Spir-2-ΔKW-C1,2,7,8S	eGFP-Spir-2-ΔKW Cys586Ser,Cys589Ser, Cys683Ser, Cys686Ser	aa 375-728 Quick-Change Template: pEGFP-C1-Spir-2-ΔKW		GST-pulldown

pmStrawberry-N3-hs-Arf1	mStrawberry-Arf1	aa 1 - 181 KpnI/BamHI		In vivo FCCS Cell imaging
pmStrawberry-N3-Rab11a	mStrawberry-Rab11	EcoRI/BamHI		In vivo FCCS Cell imaging
pmStrawberry-Myosin Vb-cc-tail	mStrawberry-Myosin Vb-cc-tail	aa 909-1849 HindIII/XbaI		In vivo FCCS Cell imaging
pmStrawberry-Spir-2-KIND	mStrawberry-KIND	aa 18-207 XhoI/BamHI		Cell imaging
pmStrawberry-N3	mStrawberry	BamHI/NotI Template: pEGFP-N3		In vivo FCCS In vivo FLIM-FRET Cell imaging
pEGFP-C1	eGFP	Clontech		In vivo FCCS
pEGFP-linker-Strawberry-C1	eGFP-linker-mStrawberry linker: ASGAG	BspE1/Bgl2		In vivo FCCS In vivo FLIM-FRET
pEGFP-hsMyosin5b aa 1467-Ende	eGFP-Myosin5b-tail	Hind3/Sal1 Template: pEGFP-C1-Vektor		In vivo FLIM-FRET
pmStrawberry-C1-hs-Spir2-375-728	mStrawberry-Spir-2- Δ KW	Template: pEGFP-C1-hs-Spir2-375-728		In vivo FLIM-FRET

9 Abbreviations

°C	Degree Celsius
2D	Two-dimensional
3D	Three-dimensional
aa	Amino acids
AcGFP	Green fluorescent protein from <i>Aequorea coerulea</i>
ADP	Adenosin diphosphate
Arf	ADP ribosylation factor
Arp2/3	Actin-related protein 2 and 3
BFA	Brefeldin A
cc	Coiled-coil region
Cdc42	Cell division cycle 42
Cy5	Cyanine 5
DAAM	Disheveled-associated activator of morphogenesis
DAD	Diaphanous autoregulatory domain
DID	Diaphanous inhibitory domain
DMEM	Dulbecco's modified Eagle's medium
DOPC	1,2-dioleoyl-<i>sn</i>-glycero-3-phosphocholine
<i>E. coli</i>	Escherichia coli
EDTA	Ethylenediaminetetraacetic acid
EEA1	Early endosome antigen 1
EIA	Electrochemiluminescence immunoassay
eGFP	Enhanced Green fluorescent protein
eFSI	Extended Formin/Spir interaction sequence
F-actin	Filamentous actin
FYVE	Fab1p, YOTB, Vac1p, EEA1
FCS	Fluorescence correlation spectroscopy
FCCS	Fluorescence cross-correlation spectroscopy
FH 1	Formin homology 1

FH 2	Formin homology 2
FIP2	Family of interacting proteins
FSI	Formin/Spir interaction sequence
G-actin	Globular actin
GAP	GTPase-Activating protein
GEF	Guanin nucleotid exchange factor
GDB	GTPase binding domain
GDP	Guanosine diphosphate
GTPase	Guanosine triphosphatase
GTP	Guanosine triphosphate
G protein	Guanine nucleotide-binding protein
GST	Glutathione S-transferase
Hrs	Hepatocyte growth factor Regulated tyrosine kinase Substrate
JNK	Jun N-terminal kinase
KIND	Kinase non-catalytic C-lobe domain
LUV	Large unilamella vesicle
mM	Millimolar (10⁻³ mol/l)
µm	Micrometer (10⁻⁶ m)
µM	Micromolar (10⁻⁶ mol/l)
nm	Nanometer (10⁻⁹ m)
nM	Nanomolar (10⁻⁹ mol/l)
Ni-NTA	Nickel-nitrilotriacetic acid
NPF	Nucleation promoting factor
OD	Optical density
PAK	P21-activated kinase
PBS	Phosphate buffered saline
POPC	1-palmitoyl-2-oleoyl-<i>sn</i>-glycero-3-phosphocholine
PA	Phosphatidic acid
PE	Phosphatidylethanolamin
PS	Phosphatidylserine
PI(3,4)P2	Phosphatidylinositol-3,4-bisphosphate

PI(3,5)P ₂	Phosphatidylinositol-3,5-bisphosphate
PI(3)P	Phosphatidylinositol-3-phosphat
PI(4,5)P ₂	Phosphatidylinositol-4,5-bisphosphate
PI(4)P	Phosphatidylinositol-4-phosphat
PI(5)P	Phosphatidylinositol-5-phosphat
Rab	Ras-like proteins in brain
SDS-PAGE	Sodium dodecyl sulfate polyacrylamide gel electrophoresis
TBS	Tris buffered saline
TGN	Trans-Golgi network
WH2	Wiskott-Aldrich protein (WASP) homology 2 domain

10 Symbols

a	fraction of interacting donor molecules
A_{eff}	effective area
b	fraction of non-interacting donor molecules
B	background signal
β	cross-talk
D	diffusion coefficient
E_{FRET}	FRET efficiency
F	fluorescence intensity
$G(\tau)$	correlation curve
$\tilde{G}(\tau)$	background-corrected correlation curve
$\hat{G}(\tau)$	crosstalk-corrected correlation curve
K_d	dissociation constant
S	structural parameter
τ_D	diffusion time
$\tau_{triplet}$	triplet relaxation time
t	time
τ_0	fluorescence lifetime of non-interacting donor molecules
τ_{FRET}	fluorescence lifetime of interacting donor molecules
T	triplet
V_{eff}	effective volume
χ^2	chi-squared goodness-of-fit test
ω_0	lateral radius of detection volume
z_0	half axial extension of detection volume

11 Acknowledgements

My PhD thesis involved the work and support of several people. I would like to express my gratitude to all who made it possible:

First of all, my PhD advisor Prof. Petra Schwille for giving me the opportunity to do my PhD in her group, and especially to complete it in Dresden without losing the group spirit.

Secondly I would like to thank Prof. Eugen Kerkhoff, with whom it was great to collaborate and whom I really enjoyed to listen to talk about the Spir world. This collaboration was very important and fruitful through the help of Annette Samol and Susanne Dietrich. Without this collaboration, this work would not have been possible. It was a great pleasure to work with them and always nice to visit and chat with them. I really enjoyed my visits in Regensburg and could not imagine a better collaboration.

I would like to take the opportunity to thank Thomas Weidemann, Wolfgang Staroske and Markus Burkhardt for all the help and fruitful discussions about FCS and FLIM.

I would like to thank all past and present members of the Schwille lab – Grzesiek, Jakob, Sonal, Jens, Erdinc, Ilaria, Franziska, Hetvi, Senthil, Fabian, Sven, Viktoria, Christoph, Martin, Alena, Katja, Ariadna and Henri, who made my PhD time very enjoyable. I enjoyed the kicker games, the Klosters trips, the Lissabon conference and the coffee breaks with Franziska's cake. In particular, I am very thankful to Sonal for the organization of many things for me in Munich, proof-reading my thesis and being a good friend. I was always looking forward to Munich and meeting her. I also want to thank Grzesiek for showing me his lovely hometown Wroclaw. It was such a beautiful trip, especially the lovely hosting from his grandma and the milonga in Brzeg.

Furthermore, I would like to thank Prof. Jochen Guck and all members of his group for not only hosting me as a guest, but more accepting me as a part of the group, offering feedback and help and a nice retreat to Usedom. I am very thankful to Heike for all the organizational skills and to Elke, Paul, Katrin, Mirjam, Anna and Gilbert for their help in the lab and office. Especially, I would like to thank Christoph Faigle for proof reading my thesis, being the best lindy hop/balboa dancing partner ever, the best company for mensa and the best hiking partner. I cannot imagine a better colleague with whom I would want to start a PhD on the same day.

I would like to thank Christoph Stange for help and discussions during the Arf1 production.

I am also grateful to all the technical and organizational assistance that made my lab work easier. Thanks to Silke, Karin, Sarah, Isabel, Sigrid, Bea and Kerstin.

Above all, I am very grateful to my parents, Margit and Thomas, for all their support. They always stood me by and helped me whenever they could. I am very happy to know that I can always rely on them. I am also grateful to Teresa and Tomasito who made my life much more colorful.

Erklärung entsprechend §5.5 der Promotionsordnung

Hiermit versichere ich, dass ich die vorliegende Arbeit ohne unzulässige Hilfe Dritter und ohne Benutzung anderer als der angegebenen Hilfsmittel angefertigt habe; die aus fremden Quellen direkt oder indirekt übernommenen Gedanken sind als solche kenntlich gemacht. Die Arbeit wurde bisher weder im Inland noch im Ausland in gleicher oder ähnlicher Form einer anderen Prüfungsbehörde vorgelegt.

Die Dissertation wurde im Zeitraum vom **01.10.2010** bis **30.04.2014** verfasst und von **Prof. Dr. Petra Schwille**, Biotechnologisches Zentrum der TU Dresden/Max-Planck-Institut für Biochemie, Martinsried betreut.

Meine Person betreffend erkläre ich hiermit, dass keine früheren erfolglosen Promotionsverfahren stattgefunden haben.

Ich erkenne die Promotionsordnung der Fakultät für Mathematik und Naturwissenschaften, Technische Universität Dresden an.

Declaration according to §5.5 of doctorate regulation

I herewith declare that I have produced this paper without the prohibited assistance of third parties and without making use of aids other than those specified; notions taken over directly or indirectly from other sources have been identified as such. This paper has not previously been presented in identical or similar form to any other German or foreign examination board.

The thesis work was conducted from starting **October 1, 2010** to **April 30, 2014** of finish under the supervision of **Prof. Dr. Petra Schwille**, Biotechnology Center of the TU Dresden/Max Planck Institute for Biochemistry, Martinsried.

I declare that I have not undertaken any previous unsuccessful doctorate proceedings.

I declare that I recognize the doctorate regulations of the Fakultät für Mathematik und Naturwissenschaften of the Technische Universität Dresden

Date: 30.04.2014

Signature: